

Knot Diagrammatics

Louis H. Kauffman

Department of Mathematics, Statistics and Computer Science

University of Illinois at Chicago

851 South Morgan Street

Chicago, IL, 60607-7045

March 29, 2022

Abstract

This paper is a survey of knot theory and invariants of knots and links from the point of view of categories of diagrams. The topics range from foundations of knot theory to virtual knot theory and topological quantum field theory.

1 Introduction

This paper is an exploration of the theme of knot diagrams. I have deliberately focused on basics in a number of interrelated domains. In most cases some fundamentals are done in a new or in a more concise way. Some parts of the paper are expository to fill in the context. This exposition is an outgrowth of the series of lectures [69] that I gave in Tokyo at the *Knots 96* conference in the summer of 1996. The present exposition goes considerably farther than those lectures, and includes material on virtual knot theory and on links that are undetectable by the Jones polynomial.

The paper is divided into seven sections (counting from section 2 onward). Section 2, on the Reidemeister moves, gives a proof of Reidemeister's basic theorem (that the three Reidemeister moves on diagrams generate ambient isotopy of links in three-space). A discussion on graph embeddings extends Reidemeister's theorem to graphs and proves the appropriate moves for topological and rigid vertices. We hope that this subsection fills in some gaps in the literature. Section 3 discusses Vassiliev invariants and invariants of rigid vertex graphs. This section is expository, with discussions of the four-term relations, Lie algebra weights, relationships with the Witten functional integral, and combinatorial constructions for some Vassiliev invariants. The discussion raises some well-known problems about Vassiliev invariants. The section on the functional integral introduces a useful abstract tensor notation that helps in understanding how the Lie algebra weight systems

are related to the functional integral. Sections 4 and 5 are based on a reformulation of the Reidemeister moves so that they work with diagrams arranged generically transverse to a special direction in the plane. We point out how the technique by which we proved Reidemeister's Theorem (it is actually Reidemeister's original technique) generalises to give these moves as well. The moves with respect to a vertical are intimately related to quantum link invariants and to Hopf algebras. Section 4 is a quick exposition of quantum link invariants, their relationship with Vassiliev invariants, classical Yang-Baxter equation and infinitesimal braiding relations. Again, this provides the context to raise many interesting questions. Section 5 is a very concise introduction to the work of the author, David Radford and Steve Sawin on invariants of three-manifolds from finite dimensional Hopf algebras. We touch on the question of the relationship of this work to the Kuperberg invariants. Section 6 is a discussion of the Temperley-Lieb algebra. Here we give a neat proof of the relation structure in the Temperley-Lieb monoid via piecewise linear diagrams. The last part of this section explains the relationship of the Temperley-Lieb monoid to parenthesis structures and shows how this point of view can be used to relate parentheses to the pentagon and the Stasheff polyhedron. Section seven discusses virtual knot theory. Section eight discusses the construction of links that while linked, have the same Jones polynomial as the unlink.

Acknowledgement. Most of this effort was sponsored by the Defense Advanced Research Projects Agency (DARPA) and Air Force Research Laboratory, Air Force Materiel Command, USAF, under agreement F30602-01-2-05022. Some of this effort was also sponsored by the National Institute for Standards and Technology (NIST). The U.S. Government is authorized to reproduce and distribute reprints for Government purposes notwithstanding any copyright annotations thereon. The views and conclusions contained herein are those of the authors and should not be interpreted as necessarily representing the official policies or endorsements, either expressed or implied, of the Defense Advanced Research Projects Agency, the Air Force Research Laboratory, or the U.S. Government. (Copyright 2004.) It gives the author great pleasure to acknowledge support from NSF Grant DMS-0245588.

2 Reidemeister Moves

Reidemeister [131] discovered a simple set of moves on link diagrams that captures the concept of ambient isotopy of knots in three-dimensional space. There are three basic Reidemeister moves. Reidemeister's theorem states that two diagrams represent ambient isotopic knots (or links) if and only if there is a sequence of Reidemeister moves taking one diagram to the other. The Reidemeister moves are illustrated in Figure 1.

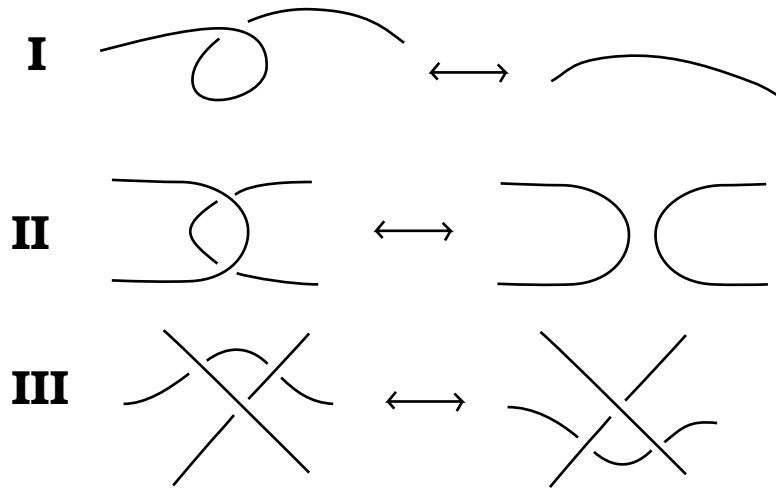


Figure 1 - Reidemeister Moves

Reidemeister's three moves are interpreted as performed on a larger diagram in which the small diagram shown is a literal part. Each move is performed without disturbing the rest of the diagram. Note that this means that each move occurs, up to topological deformation, just as it is shown in the diagrams in Figure 1. There are no extra lines in the local diagrams. For example, the equivalence (A) in Figure 2 is **not** an instance of a single first Reidemeister move. Taken literally, it factors into a move *II* followed by a move *I*.

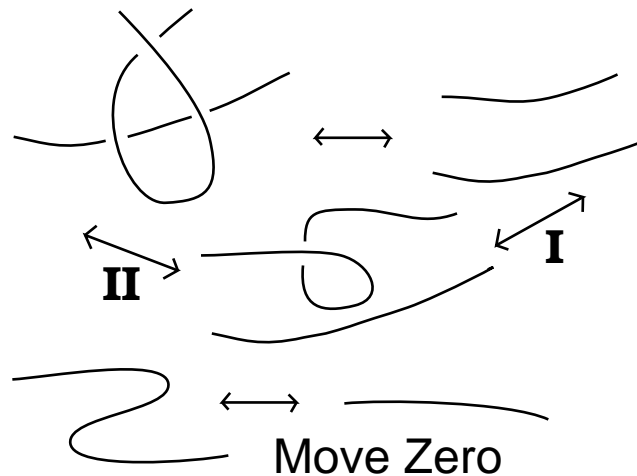


Figure 2 - Factorable Move, Move Zero

Diagrams are always subject to topological deformations in the plane that preserve the structure of the crossings. These deformations could be designated as “Move Zero”. See Figure 2.

A few exercises with the Reidemeister moves are in order. First of all, view the diagram in Figure 3. It is unknotted and you can have a good time finding a sequence of Reidemeister moves that will do the trick. Diagrams of this type are produced by tracing a curve and always producing an undercrossing at each return crossing. This type of knot is called a *standard unknot*. Of course we see clearly that a standard unknot is unknotted by just *pulling* on it, since it has the same structure as a coil of rope that is wound down onto a flat surface.

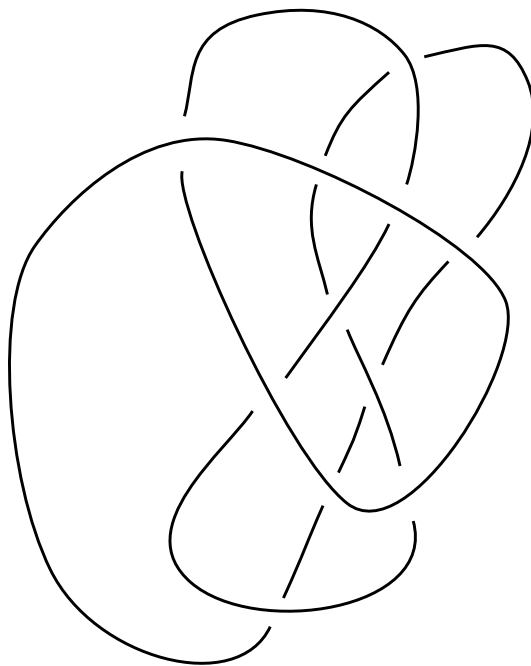


Figure 3 - Standard Unknot

Can one recognise unknots by simply looking for sequences of Reidemeister moves that undo them? This would be easy if it were not for the case that there are examples of unknots that require some moves that increase the number of crossings before they can be subsequently decreased. Such an demonic example is illustrated in Figure 4.

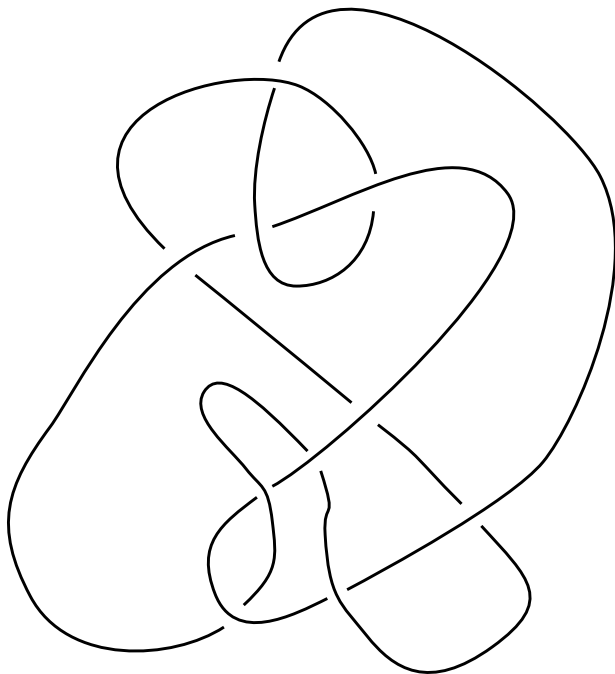


Figure 4 - A Demon

It is generally not so easy to recognise unknots. However, here is a tip: Look for *macro moves* of the type shown in Figure 5. In a macro move, we identify an arc that passes entirely under some piece of the diagram (or entirely over) and shift this part of the arc, keeping it under (or over) during the shift. In Figure 5, we illustrate a macro move on an arc that passes under a piece of the diagram that is indicated by arcs going into a circular region. A more general macro move is possible where the moving arc moves underneath one layer of diagram, and at the same time, over another layer of diagram. Macro moves often allow a reduction in the number of crossings even though the number of crossings will increase during a sequence of Reidemeister moves that generates the macro move.

As shown in Figure 5, the macro-move includes as a special case both the second and the third Reidemeister moves, and it is not hard to verify that a macro move can be generated by a sequence of type II and type III Reidemeister moves. It is easy to see that the type I moves can be left to the end of any deformation. The demon of Figure 4 is easily demolished by macro moves, and from the point of view of macro moves the diagram never gets more complicated.

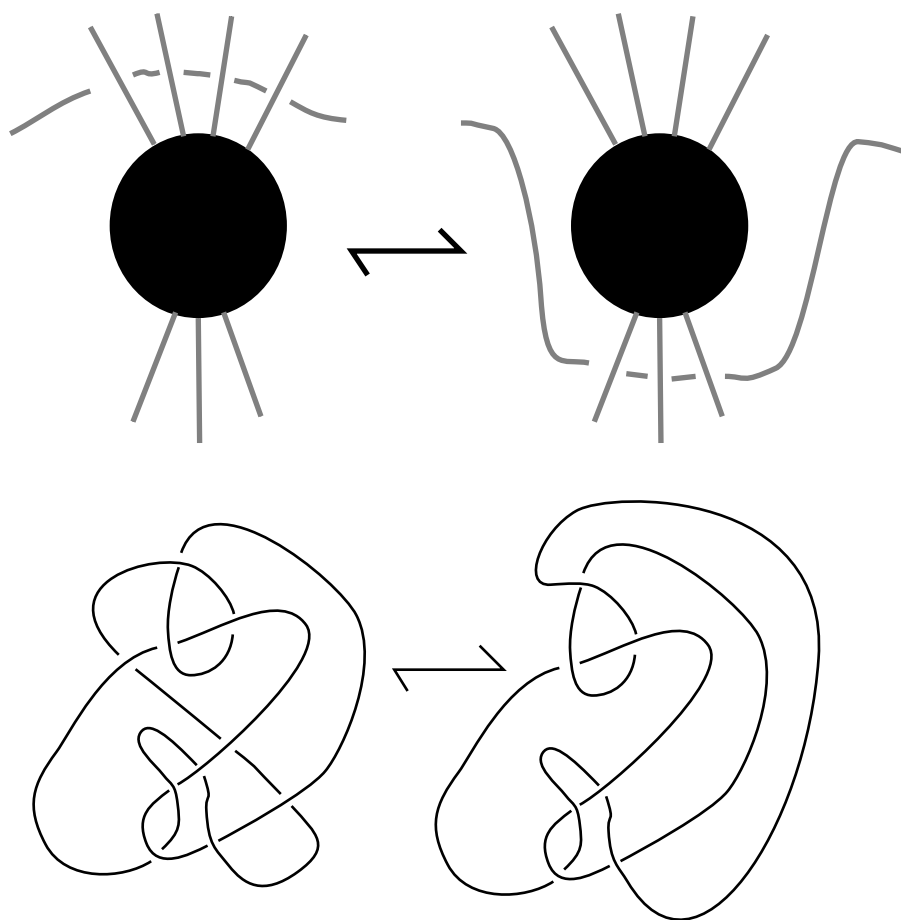


Figure 5 - Macro Move

Let's say that a knot can be *reduced* by a set of moves if it can be transformed by these moves to the unknotted circle diagram through diagrams that never have more crossings than the original diagram. Then we have shown that there are diagrams representing the unknot that cannot be reduced by the Reidemeister moves. On the other hand, I do not know whether unknotted diagrams can always be reduced by the macro moves in conjunction with the first Reidemeister move. If this were true it would give a combinatorial way to recognise the unknot.

Remark. In fact, there is a combinatorial way to recognise the unknot based on a diagrams and moves. In [32] I. A. Dynnikov finds just such a result, using piecewise linear knot diagrams with all ninety degree angles in the diagrams, and all arcs in the diagram either horizontal or vertical. The interested reader should consult his lucid paper.

2.1 Reidemeister's Theorem

We now indicate how Reidemeister proved his Theorem.

An embedding of a knot or link in three-dimensional space is said to be *piecewise linear* if it consists in a collection of straight line segments joined end to end. Reidemeister started with a *single* move in three-dimensional space for piecewise linear knots and links. Consider a point in the complement of the link, and an edge in the link such that the surface of the triangle formed by the end points of that edge and the new point is not pierced by any other edge in the link. Then one can replace the given edge on the link by the other two edges of the triangle, obtaining a new link that is ambient isotopic to the original link. Conversely, one can remove two consecutive edges in the link and replace them by a new edge that goes directly from initial to final points, whenever the triangle spanned by the two consecutive edges is not pierced by any other edge of the link. This triangle replacement constitutes Reidemeister's three-dimensional move. See Figure 6. It can be shown that two piecewise linear knots or links are ambient isotopic in three-dimensional space if and only if there is a sequence of Reidemeister triangle moves from one to the other. This will not be proved here. At the time when Reidemeister wrote his book, equivalence via three-dimensional triangle moves was taken as the definition of topological equivalence of links.

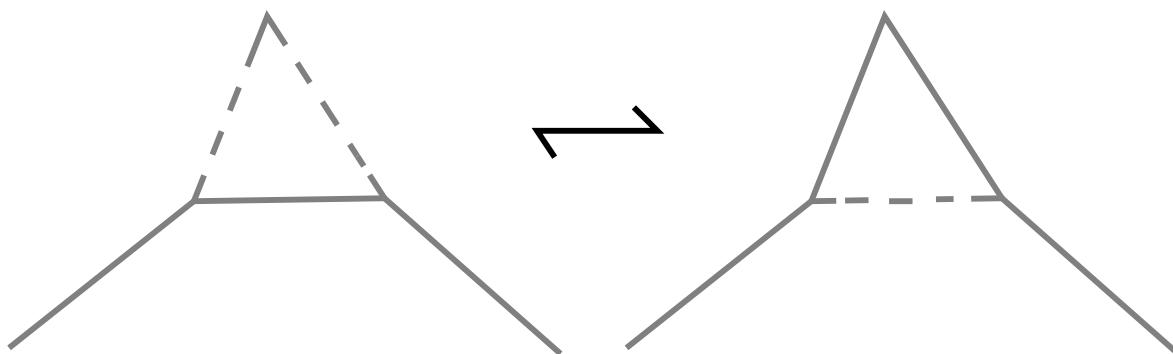


Figure 6 - Triangle Move

It can also be shown that tame knots and links have piecewise linear representatives in their ambient isotopy class. It is sufficient for our purposes to work with piecewise linear knots and links. Reidemeister's planar moves then follow from an analysis of the shadows projected into the plane by Reidemeister triangle moves in space. Figure 7 gives a hint of this analysis. The result is a reformulation of the three-dimensional problems of knot theory to a combinatorial game in the plane.

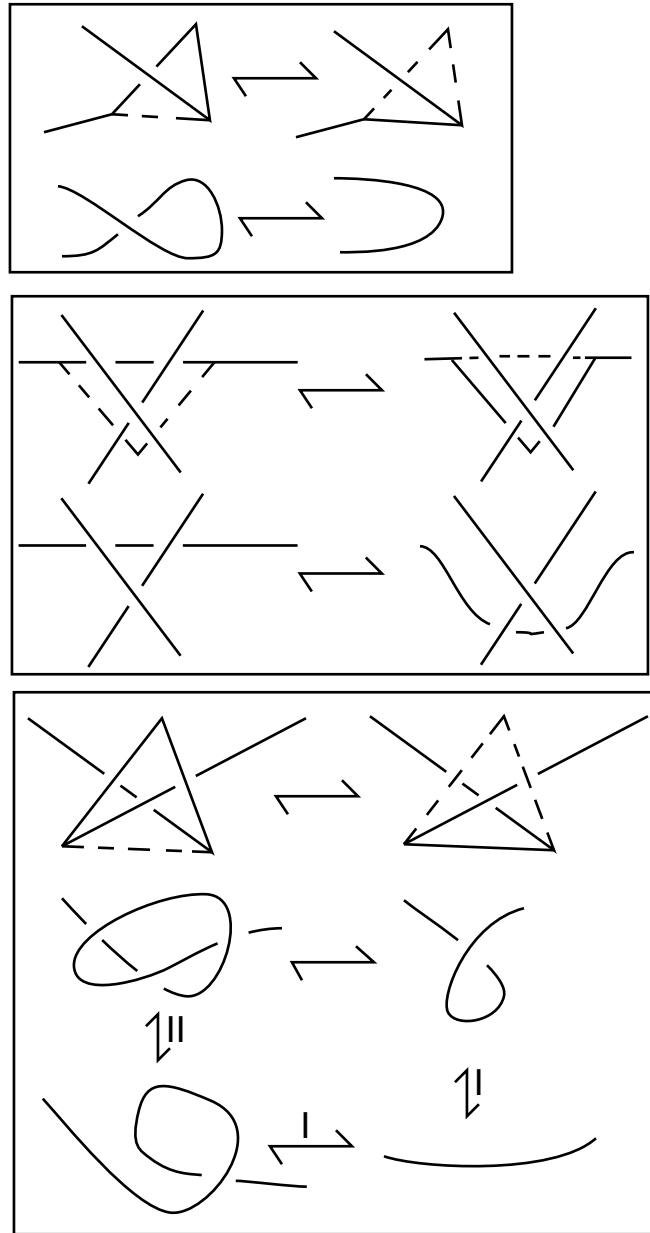


Figure 7 - Shadows

To go beyond the hint in Figure 7 to a complete proof that Reidemeister's planar moves suffice involves preliminary remarks about subdivision. The simplest subdivision that one wants to be able to perform on a piecewise linear link is the placement of a new vertex at an interior point of an edge - so that that edge becomes two edges in the subdivided link. Figure 8 shows how to accomplish this subdivision via triangle moves.

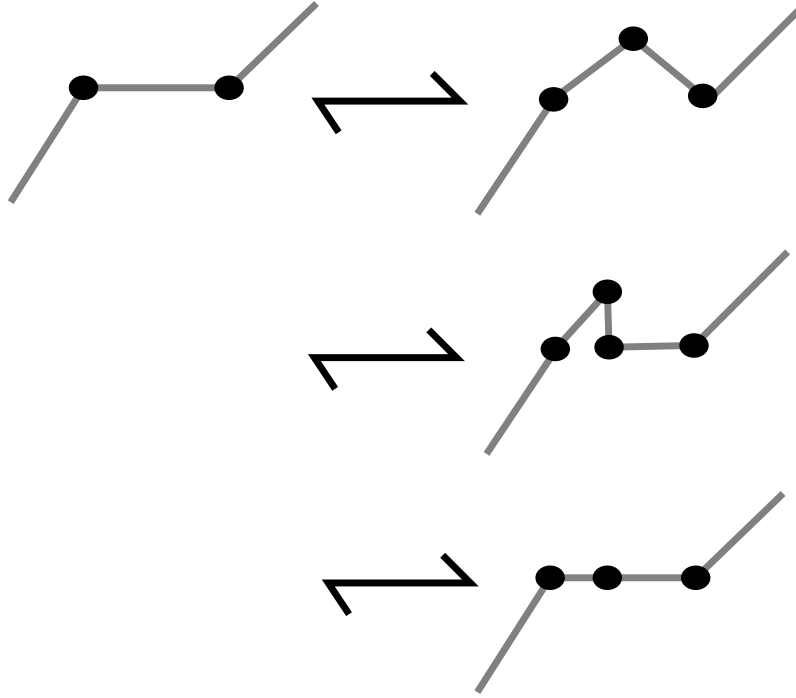


Figure 8 - Subdivision of an Edge

Any triangle move can be factored into a sequence of smaller triangle moves corresponding to a simplicial subdivision of that triangle. This is obvious, since the triangles in the subdivision of the large triangle that is unpierced by the link are themselves unpierced by the link.

To understand how the Reidemeister triangle move behaves on diagrams it is sufficient to consider a projection of the link in which the triangle is projected to a non-singular triangle in the plane. Of course, there may be many arcs of the link also projected upon the interior of the projected triangle. However, by using subdivision, we can assume that the cases of the extra arcs are as shown in Figure 9. In Figure 9 we have also shown how each of these cases can be accomplished by (combinations of) the three Reidemeister moves. This proves that a projection of a single triangle move can be accomplished by a sequence of Reidemeister diagram moves.

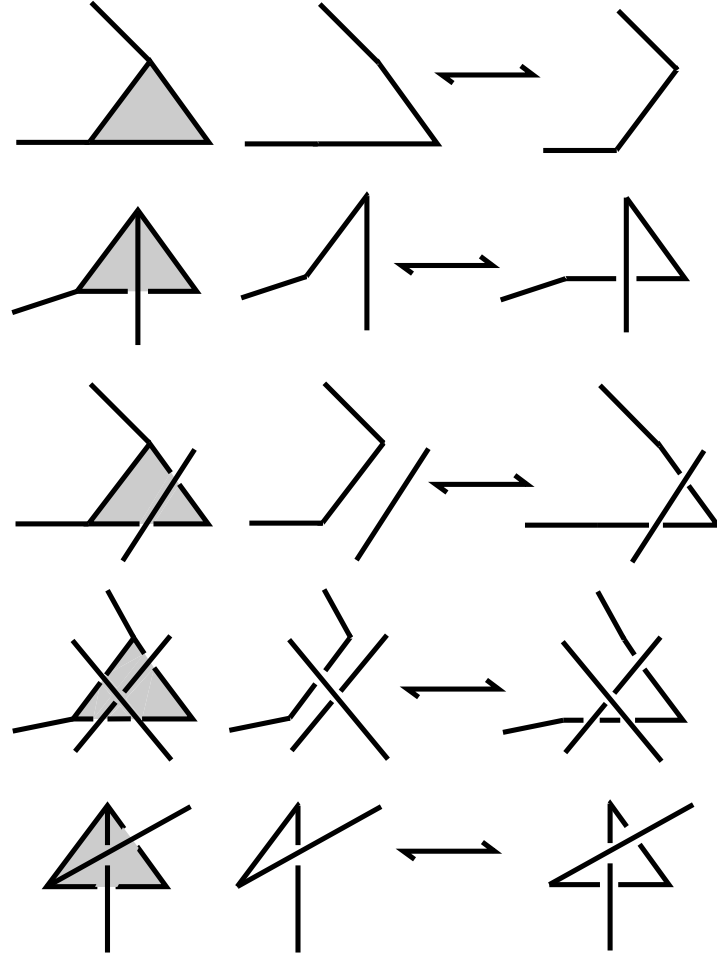


Figure 9 - Projections of Triangle Moves

A piecewise linear isotopy consists in a finite sequence of triangle moves. There exists a direction in three-dimensional space that makes a non-zero angle with each of these triangles and is in general position with the link diagram. Projecting to the plane along this direction makes it possible to perform the entire ambient isotopy in the language of projected triangle moves. Now apply the results of the previous paragraph and we conclude

Reidemeister's Theorem. If two links are piecewise linearly equivalent (ambient isotopic), then there is a sequence of Reidemeister diagram moves taking a projection of one link to a projection of the other.

Note that the proof tells us that the two diagrams can be obtained from one spatial projection direction for the entire spatial isotopy. It is obvious that diagrams related by Reidemeister moves represent ambient isotopic links. Reidemeister's Theorem gives a complete combinatorial description of the topology of knots and links in three-dimensional space.

2.2 Graph Embeddings

Let G be a (multi-)graph. That is, G is a finite abstract graph with, possibly, a multiplicity of edges between any two of its vertices. Now consider the embeddings of G in Euclidean three-space R^3 . In the category of topological embeddings, any edge of G can acquire local knotting as shown in Figure 10. On top of this there is the possibility of global knotting that results from the structure of the graph as a whole.

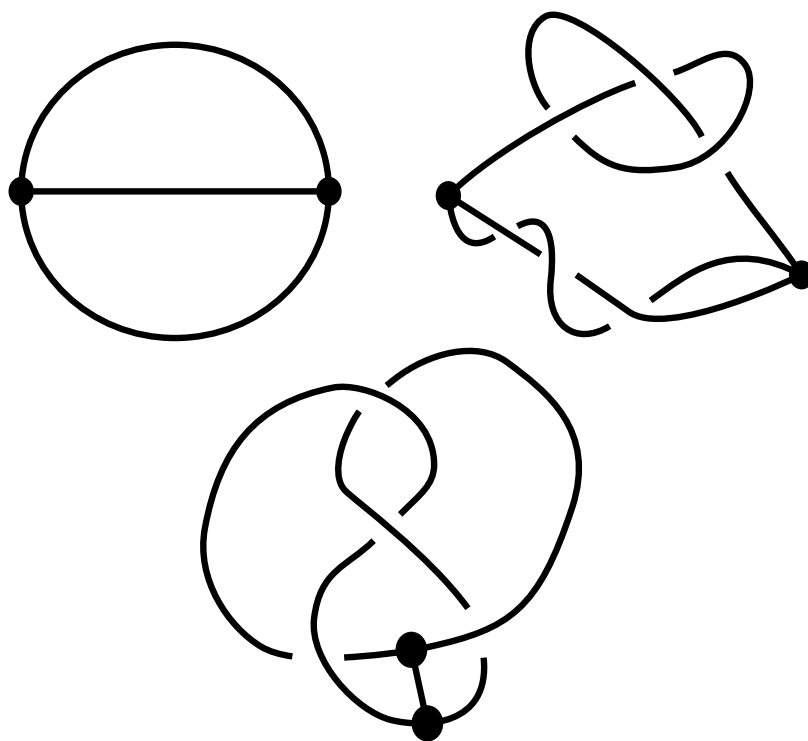


Figure 10 - Graph Embedding

Topological or piecewise linear ambient isotopy of graph embeddings is complicated by the fact that arbitrary braiding can be created or destroyed at a vertex, as illustrated in Figure 11.

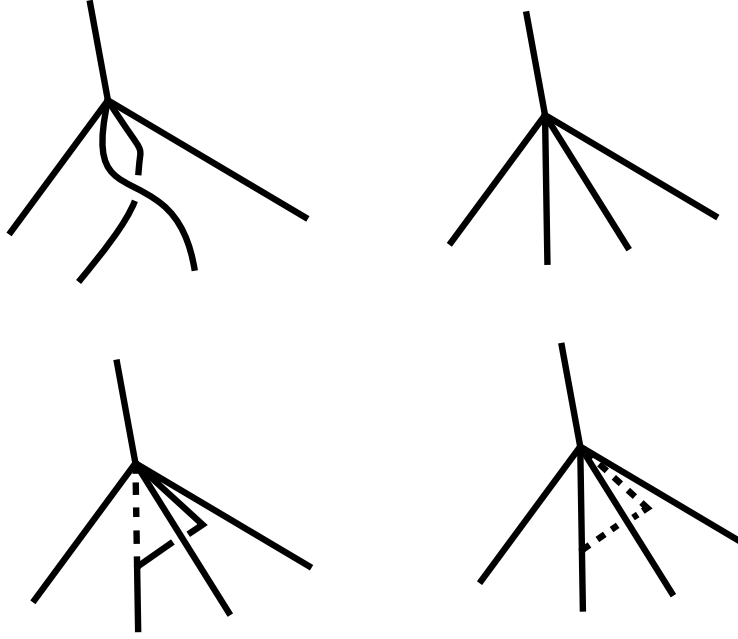


Figure 11 - Braiding at a Vertex

For this reason, it is useful to consider ways to restrict the allowed movement in the neighborhood of a vertex. One way to accomplish this is to decree that each vertex will come equipped with a specific cyclic order of the edges meeting the vertex. This cyclic order can be instantiated on the boundary of a disk, and the graph replaced by a configuration of disks with cyclic orders of marked points along their boundaries. The edges of the original graph are replaced by edges that go from one disk to another terminating in the marked points. Call such an arrangement a *rigid vertex graph* G . If G is a rigid vertex graph, then we consider embeddings of G where the disks are embedded metrically while the (graphical) edges are embedded topologically. A *rigid vertex isotopy* of one RV (RV will stand for rigid vertex) embedding G to another G' is a combination of ambient isotopies of the embedded edges of the graph (the *strings* of the graph) relative to their endpoints on the disks, coupled with affine motions of the disks (carrying along the strings in ambient isotopy). An affine motion of a disk is a combination of parallel translations of the disk along a given direction in three-space and rotations of the disk about an axis through its center. We can think of a given disk as embedded inside a standard three-ball with the strings from the disk emanating straight to the boundary of the three-ball. Each basic affine motion is assumed to leave the points on the boundary of the containing three-ball fixed. Thus the types of affine motion are as illustrated in Figure 12.

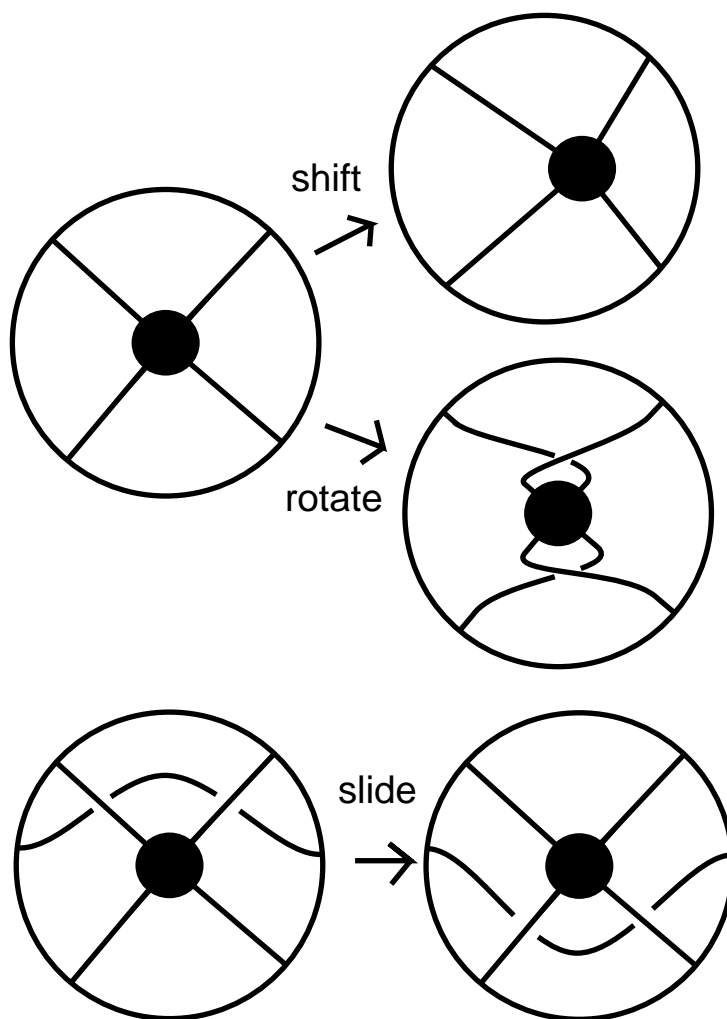


Figure 12 - Rigid Vertex Graphs and Affine Motions

We will give versions of the Reidemeister moves for both topological isotopy and rigid vertex isotopy of embedded graphs. In the topological case the extra moves are illustrated in Figure 13. Here we have indicated the elementary braiding at a vertex and slide moves that take an edge underneath a vertex. The proof that these moves suffice is a generalisation of our original proof of the Reidemeister moves. That is, we model the graph embeddings by piecewise linear embeddings. This may entail subdividing the edges of the original graph so that those edges can have enough flexibility to sustain a given topological conformation. Thus, when we speak of a piecewise linear embedding of a given graph, we mean a piecewise linear embedding of a graph that is obtained from the given graph by subdividing some of its edges.

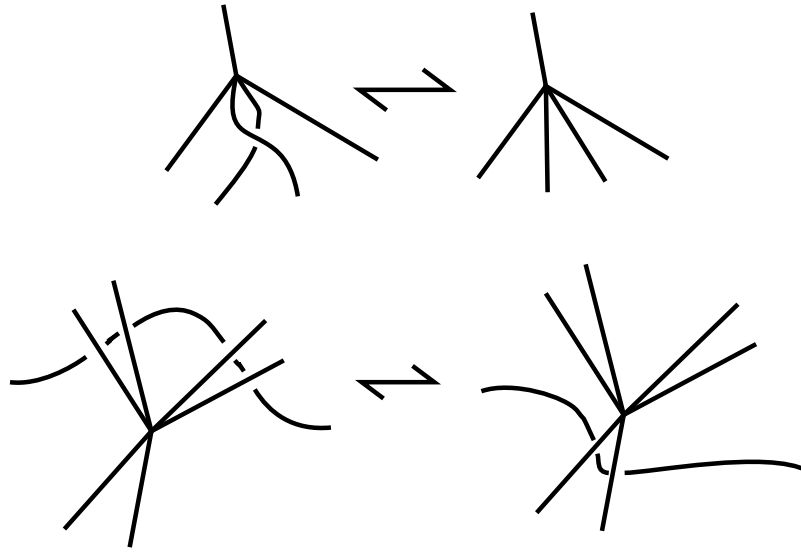


Figure 13 - Extra Moves For Topological Isotopy of Graphs

Piecewise ambient isotopy of graph embeddings is defined exactly as in the case of piecewise linear isotopy for knots and links. The same projection arguments apply and the extra moves are obtained from the three-dimensional triangle move as illustrated in Figure 14. This completes the proof of our assertion about the topological Reidemeister moves for graphs.

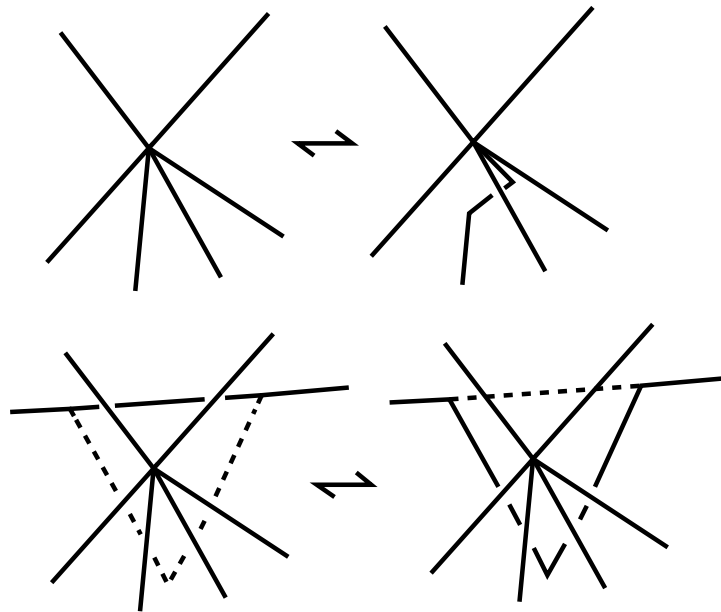


Figure 14 - PL Isotopy Inducing Topological Graphical Moves

Consider rigid vertex isotopy of rigid vertex (*RV*) graphs. We will assume that the topological moves are performed in the piecewise linear setting. Thus subdivisions of the edges of the graph can be produced. Basic translational affine moves of the embedded disks can have piecewise linear starting and ending states by drawing straight lines from the marked points on the disk boundaries to the corresponding points in the containing balls. Rotatory moves with the center of a disk as axis can also have piecewise linear starting and ending states by taking the braiding that is induced by the rotation and suitably subdividing it. These remarks show that *RV* isotopy can be achieved in the *PL* category.

The next point to consider is the result of projection of an *RV* isotopy on the corresponding diagrams. A sequence of elementary *RV* isotopies from a graph G to a graph G' has associated with it a direction of projection so that each *PL* triangle move has its triangle projected to a non-singular triangle in the plane and each affine move has its disk projected to a non-singular disk in the plane. In the case of the affine moves we can assume that the before to after appearance of the disk and its corresponding containing ball will represent either a topological identity map (albeit an affine shift) or a rotation about the disk axis by π radians. (Higher multiples of π can be regarded as iterates of a π rotation.) Therefore the basic π rotation can be schematized as shown in Figure 15. Figure 15 illustrates the moves that we need to add to the Reidemeister moves to obtain a planar diagram version of *RV* isotopy. The remaining moves in Figure 15 follow from the same projection arguments that we have used earlier in this section. This completes the construction of the diagrammatic calculus for *RV* isotopy.

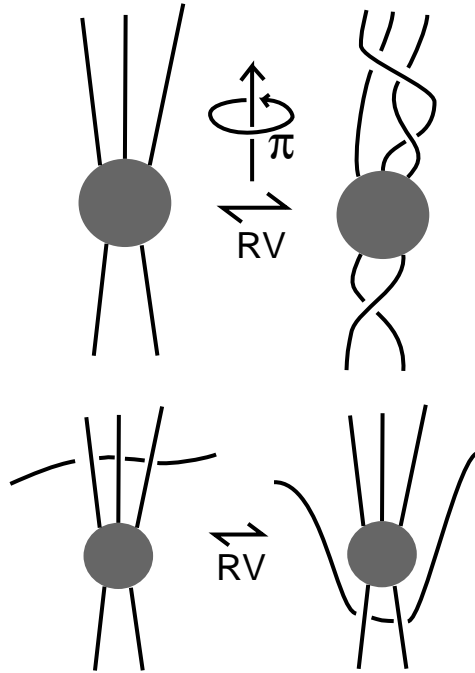


Figure 15 - Diagrammatic Rigid Vertex Isotopy

Note that the generating moves for rigid vertex graph isotopy are almost the same as the generating moves for topological graph isotopy, except that the braiding at the vertex in the rigid vertex case comes from the twisting the disk as a whole. This circumstance makes the construction of invariants of rigid vertex graphs much easier. We will discuss constructions of such invariants in the next section. In section 4 we will return to the Reidemeister moves and reformulate them once again for the sake of quantum link invariants.

3 Vassiliev Invariants and Invariants of Rigid Vertex Graphs

If $V(K)$ is a (Laurent polynomial valued, or more generally - commutative ring valued) invariant of knots, then it can be naturally extended to an invariant of rigid vertex graphs by defining the invariant of graphs in terms of the knot invariant via an “unfolding” of the vertex. That is, we can regard the vertex as a “black box” and replace it by any tangle of our choice. Rigid vertex motions of the graph preserve the contents of the black box, and hence entail ambient isotopies of the link obtained by replacing the black box by its contents. Invariants of knots and links that are evaluated on these replacements are then automatically rigid vertex invariants of the corresponding graphs. If we set up a collection of multiple replacements at the vertices with standard conventions for the insertions of the tangles, then a summation over all possible replacements can lead to a graph invariant with new coefficients corresponding to the different replacements. In this way each invariant of knots and links implicates a large collection of graph invariants. See [62], [63].

$$\begin{aligned}
V \begin{array}{c} \nearrow \\ \bullet \\ \searrow \end{array} &= a V \begin{array}{c} \nearrow \\ \diagdown \\ \nearrow \end{array} + b V \begin{array}{c} \nearrow \\ \diagup \\ \searrow \end{array} + c V \begin{array}{c} \nearrow \\ \searrow \end{array} \\
V \begin{array}{c} \nearrow \\ \bullet \\ \searrow \end{array} &= V \begin{array}{c} \nearrow \\ \diagdown \\ \nearrow \end{array} - V \begin{array}{c} \nearrow \\ \diagup \\ \searrow \end{array} \\
V \begin{array}{c} \nearrow \\ \bullet \\ \text{loop} \end{array} &= V \begin{array}{c} \nearrow \\ \text{loop} \end{array} - V \begin{array}{c} \nearrow \\ \text{loop} \end{array} = 0 \\
V \begin{array}{c} \text{loop} \end{array} &= 0 \\
V \begin{array}{c} \text{loop} \\ \bullet \end{array} &= V \begin{array}{c} \text{loop} \\ \diagdown \end{array} - V \begin{array}{c} \text{loop} \\ \diagup \end{array} = - V \begin{array}{c} \text{loop} \\ \diagup \end{array}
\end{aligned}$$

Figure 16 - Graphical Vertex Formulas

The simplest tangle replacements for a 4-valent vertex are the two crossings, positive and negative, and the oriented smoothing. Let $V(K)$ be any invariant of knots and links. Extend V to the category of rigid vertex embeddings of 4-valent graphs by the formula (See Figure 16)

$$V(K_*) = aV(K_+) + bV(K_-) + cV(K_0)$$

Here K_* indicates an embedding with a transversal 4-valent vertex. This formula means that we define $V(G)$ for an embedded 4-valent graph G by taking the sum

$$V(G) = \sum_S a^{i_+(S)} b^{i_-(S)} c^{i_0(S)} V(S)$$

with the summation over all knots and links S obtained from G by replacing a node of G with either a crossing of positive or negative type, or with a smoothing (denoted 0). Here $i_+(S)$ denotes the number of positive crossings in the replacement, $i_-(S)$ the number of negative crossings in the replacement, and $i_0(S)$ the number of smoothings in the replacement. It is not hard to see that if $V(K)$ is an ambient isotopy invariant of knots, then, this extension is a rigid vertex isotopy invariant of graphs. In rigid vertex isotopy the cyclic order at the vertex is preserved, so that the vertex behaves like a rigid disk with flexible strings attached to it at specific points. See the previous section.

There is a rich class of graph invariants that can be studied in this manner. The Vassiliev Invariants [152], [11], [4] constitute the important special case of these graph invariants where $a = +1$, $b = -1$ and $c = 0$. Thus $V(G)$ is a Vassiliev invariant if

$$V(K_*) = V(K_+) - V(K_-).$$

Call this formula the *exchange identity* for the Vassiliev invariant V . V is said to be of finite type k if $V(G) = 0$ whenever $|G| > k$ where $|G|$ denotes the number of 4-valent nodes in the graph G . The notion of finite type is of paramount significance in studying these invariants. One reason for this is the following basic Lemma.

Lemma. If a graph G has exactly k nodes, then the value of a Vassiliev invariant v_k of type k on G , $v_k(G)$, is independent of the embedding of G .

Proof. The different embeddings of G can be represented by link diagrams with some of the 4-valent vertices in the diagram corresponding to the nodes of G . It suffices to show that the value of $v_k(G)$ is unchanged under switching of a crossing. However, the exchange identity for v_k shows that this difference is equal to the evaluation of v_k on a graph with $k + 1$ nodes and hence is equal to zero. This completes the proof.

The upshot of this Lemma is that Vassiliev invariants of type k are intimately involved with certain abstract evaluations of graphs with k nodes. In fact, there are restrictions (the four-term relations) on these evaluations demanded by the topology (we shall articulate these restrictions shortly) and it follows from results of Kontsevich [4] that such abstract

evaluations actually determine the invariants. The invariants derived from classical Lie algebras are all built from Vassiliev invariants of finite type. All this is directly related to Witten's functional integral [156].

Definition. Let v_k be a Vassiliev invariant of type k . The *top row* of v_k is the set of values that v_k assigns to the set of (abstract) 4-valent graphs with k nodes. If we concentrate on Vassiliev invariants of knots, then these graphs are all obtained by marking $2k$ points on a circle, and choosing a pairing of the $2k$ points. The pairing can be indicated by drawing a circle and connecting the paired points with arcs. Such a diagram is called a *chord diagram*. Some examples are indicated in Figure 17.

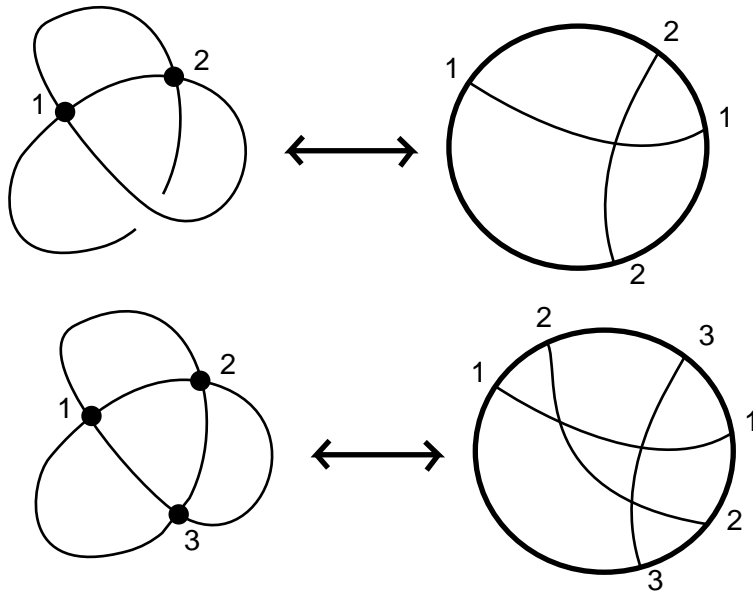


Figure 17 - Chord Diagrams

Note that a top row diagram cannot contain any isolated pairings since this would correspond to a difference of local curls on the corresponding knot diagram (and these curls, being isotopic, yield the same Vassiliev invariants).

The Four-Term Relation. (Compare [142].) Consider a single embedded graphical node in relation to another embedded arc, as illustrated in Figure 18. The arc underlies the lines incident to the node at four points and can be slid out and isotoped over the top so that it overlies the four nodes. One can also switch the crossings one-by-one to exchange the arc until it overlies the node. Each of these four switchings gives rise to an equation, and the left-hand sides of these equations will add up to zero, producing a relation corresponding to the right-hand sides. Each term in the right-hand side refers to the value of the Vassiliev invariant on a graph with two nodes that are neighbors to each other. See Figure 18.

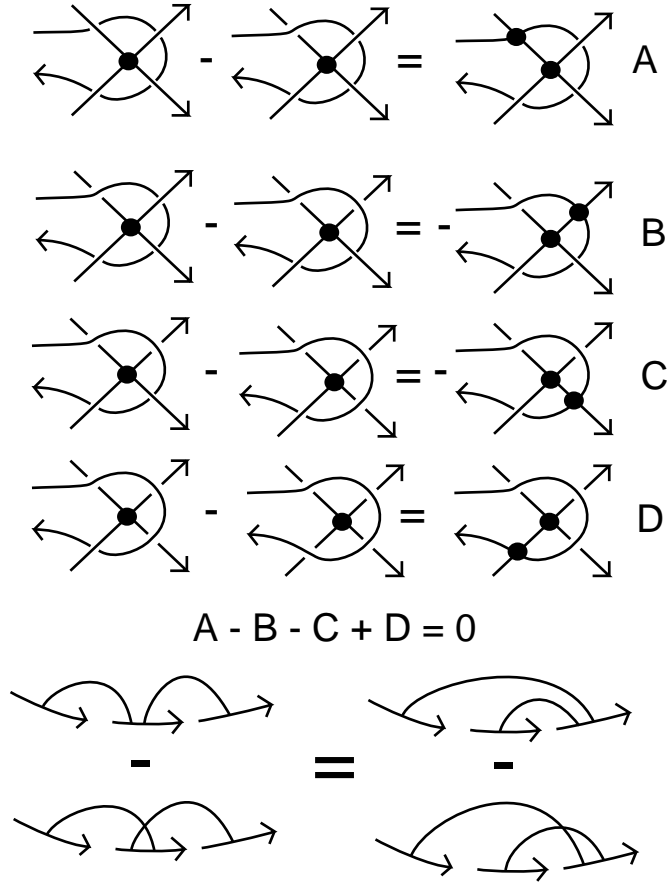


Figure 18 - The Four Term Relation

There is a corresponding 4-term relation for chord diagrams. This is the 4-term relation for the top row. In chord diagrams the relation takes the form shown at the bottom of Figure 18. Here we have illustrated only those parts of the chord diagram that are relevant to the two nodes in question (indicated by two pairs of points on the circle of the chord diagram). The form of the relation shows the points on the chord diagram that are immediate neighbors. These are actually neighbors on any chord diagram that realizes this form. Otherwise there can be many other pairings present in the situation.

As an example, consider the possible chord diagrams for a Vassiliev invariant of type 3. There are two possible diagrams as shown in Figure 19. One of these has the projected pattern of the trefoil knot and we shall call it the *trefoil graph*. These diagrams satisfy the 4-term relation. This shows that one diagram must have twice the evaluation of the other. Hence it suffices to know the evaluation of one of these two diagrams to know the top row of a Vassiliev invariant of type 3. We can take this generator to be the trefoil graph

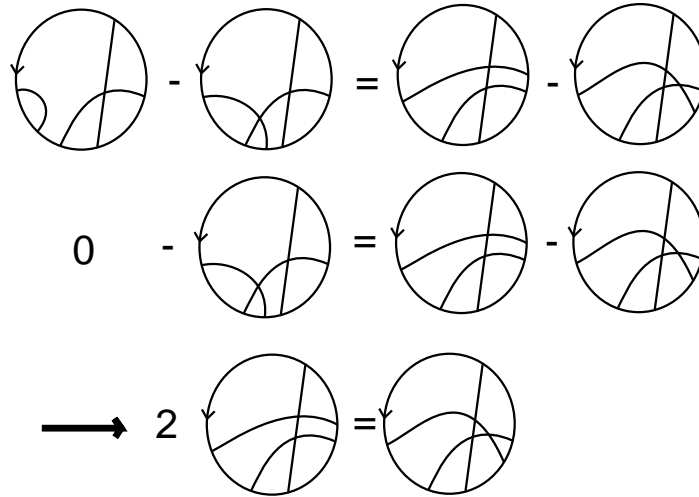


Figure 19 - Four Term Relation For Type Three Invariant

Now one more exercise: Consider any Vassiliev invariant v and let's determine its value on the trefoil graph as in Figure 20.

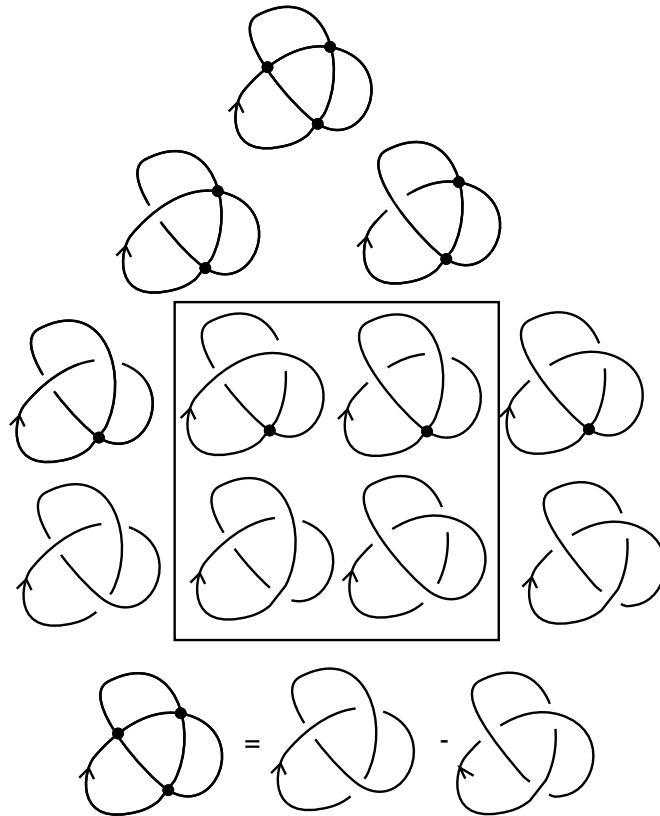


Figure 20 - Trefoil Graph

The value of this invariant on the trefoil graph is equal to the difference between its values on the trefoil knot and its mirror image. Therefore any Vassiliev invariant that assigns a non-zero value to the trefoil graph can tell the difference between the trefoil knot and its mirror image.

Example. This example shows how the original Jones polynomial is composed of Vassiliev invariants of finite type. Let $V_K(t)$ denote the original Jones polynomial [50]. Recall the oriented state expansion for the Jones polynomial [64] with the basic formulas (δ is the loop value.)

$$\begin{aligned} V_{K_+} &= -t^{1/2}V_{K_0} - tV_{K_\infty} \\ V_{K_-} &= -t^{-1/2}V_{K_0} - t^{-1}V_{K_\infty}. \\ \delta &= -(t^{1/2} + t^{-1/2}). \end{aligned}$$

Let $t = e^x$. Then

$$\begin{aligned} V_{K_+} &= -e^{x/2}V_{K_0} - e^xV_{K_\infty} \\ V_{K_-} &= -e^{-x/2}V_{K_0} - e^{-x}V_{K_\infty}. \\ \delta &= -(e^{x/2} + e^{-x/2}). \end{aligned}$$

Thus

$$V_{K_*} = V_{K_+} - V_{K_-} = -2\sinh(x/2)V_{K_0} - 2\sinh(x)V_{K_\infty}.$$

Thus x divides V_{K_*} , and therefore x^k divides V_G whenever G is a graph with at least k nodes. Letting

$$V_G(e^x) = \sum_{k=0}^{\infty} v_k(G)x^k,$$

we see that this condition implies that $v_k(G)$ vanishes whenever G has more than k nodes. Hence *the coefficients of the powers of x in the expansion of $V_K(e^x)$ are Vassiliev invariants of finite type!* This result was first observed by Birman and Lin [11] by a different argument.

Let's look a little deeper and see the structure of the top row for the Vassiliev invariants related to the Jones polynomial. By our previous remarks the top row evaluations correspond to the leading terms in the power series expansion. Since

$$\begin{aligned} \delta &= -(e^{x/2} + e^{-x/2}) = -2 + [higher], \\ -e^{x/2} + e^{-x/2} &= -x + [higher], \\ -e^x + e^{-x} &= -2x + [higher], \end{aligned}$$

it follows that the top rows for the Jones polynomial are computed by the recursion formulas

$$v(K_*) = -v(K_0) - 2V(K_\infty)$$

$$v([loop]) = -2.$$

The reader can easily check that this recursion formula for the top rows of the Jones polynomial implies that v_3 takes the value 24 on the trefoil graph and hence it is the Vassiliev invariant of type 3 in the Jones polynomial that first detects the difference between the trefoil knot and its mirror image.

This example gives a good picture of the general phenomenon of how the Vassiliev invariants become building blocks for other invariants. In the case of the Jones polynomial, we already know how to construct the invariant and so it is possible to get a lot of information about these particular Vassiliev invariants by looking directly at the Jones polynomial. This, in turn, gives insight into the structure of the Jones polynomial itself.

3.1 Lie Algebra Weights

Consider the diagrammatic relation shown in Figure 21 . Call it (after Bar-Natan [4]) the *STU* relation.

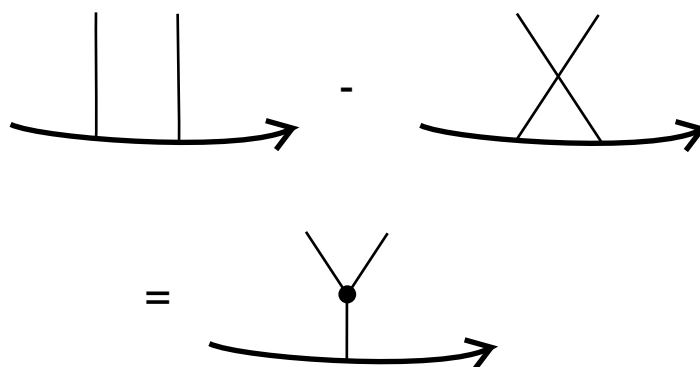


Figure 21 - The *STU* Relation

Lemma. *STU* implies the 4-term relation.

Proof. View Figure 22.

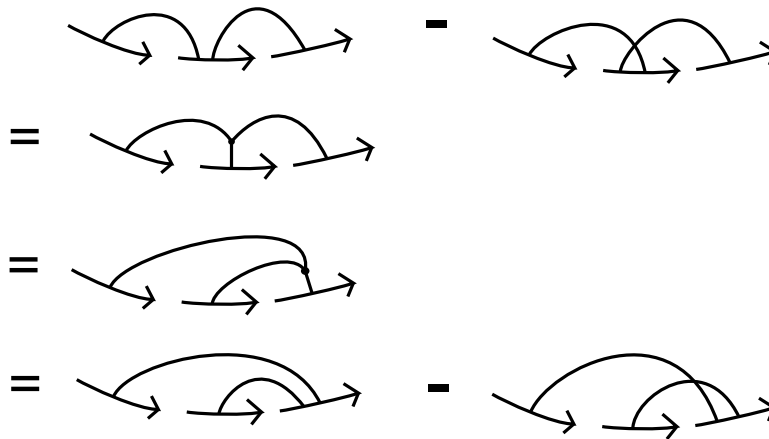


Figure 22 - A Diagrammatic Proof

STU is the smile of the Cheshire cat. That smile generalizes the idea of a Lie algebra. Take a (matrix) Lie algebra with generators T^a . Then

$$T^a T^b - T^b T^a = if_{abc} T^c$$

expresses the closure of the Lie algebra under commutators. Translate this equation into diagrams as shown in Figure 23, and see that this translation is STU with Lie algebraic clothing!

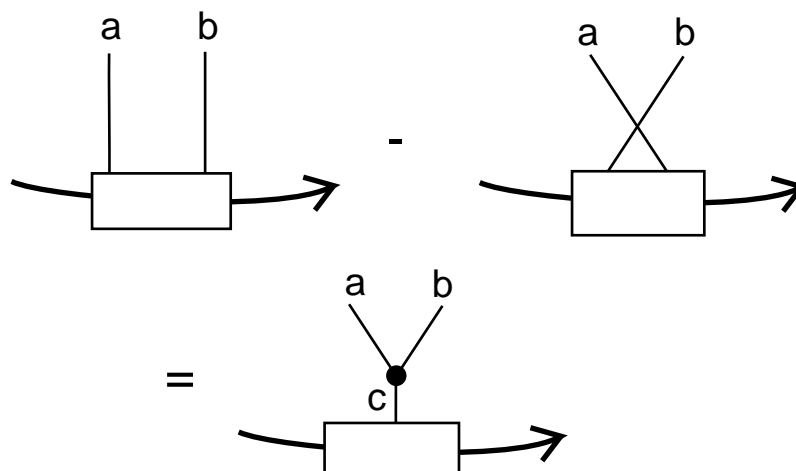


Figure 23 - Algebraic Clothing

Here the structure tensor of the Lie algebra has been assumed (for simplicity) to be invariant under cyclic permutation of the indices. This invariance means that our last Lemma applies to this Lie algebraic interpretation of STU . The upshot is that we can manufacture weight systems for graphs that satisfy the 4-term relation by replacing paired points on the chord diagram by an insertion of T^a in one point of the pair and a corresponding insertion of T^a at the other point in the pair and summing over all a . The result of all such insertions on a given chord diagram is a big sum of specific matrix products along the circle of the diagram, each of which (being a circular product) is interpreted as a trace.

Let's say this last matter more precisely: Regard a graph with k nodes as obtained by identifying k pairs of points on a circle. Thus a code such as 1212 taken in cyclic order specifies such a graph by regarding the points 1, 2, 1, 2 as arrayed along a circle with the first and second 1's and 2's identified to form the graph. Define, for a code $a_1 a_2 \dots a_m$

$$wt(a_1 a_2 \dots a_m) = trace(T^{a_1} T^{a_2} T^{a_1} \dots T^{a_m})$$

where the Einstein summation convention is in place for the double appearances of indices on the right-hand side. This gives the weight system.

The weight system described by the above procedure satisfies the 4-term relation, but does not necessarily satisfy the vanishing condition for isolated pairings. This is because the framing compensation for converting an invariant of regular isotopy to ambient isotopy has not yet been introduced. We will show how to do this in the course of the discussion in the next paragraph. The main point to make here is that by starting with the idea of extending an invariant of knots to a Vassiliev invariant of embedded graphs and searching out the conditions on graph evaluation demanded by the topology, we have inevitably entered the domain of relations between Lie algebras and link invariants. Since the STU relation does not demand Lie algebras for its satisfaction we see that the landscape is wider than the Lie algebra context, but it is not yet understood how big is the class of link invariants derived from Lie algebras.

In fact, we can line up this weight system with the formalism related to the knot diagram by writing the Lie algebra insertions back on the 4-valent graph. We then get a Casimir insertion at the node.

To get the framing compensation, note that an isolated pairing corresponds to the trace of the Casimir. Let γ denote this trace. See Figure 24.

$$\gamma = tr\left(\sum_a T^a T^a\right)$$

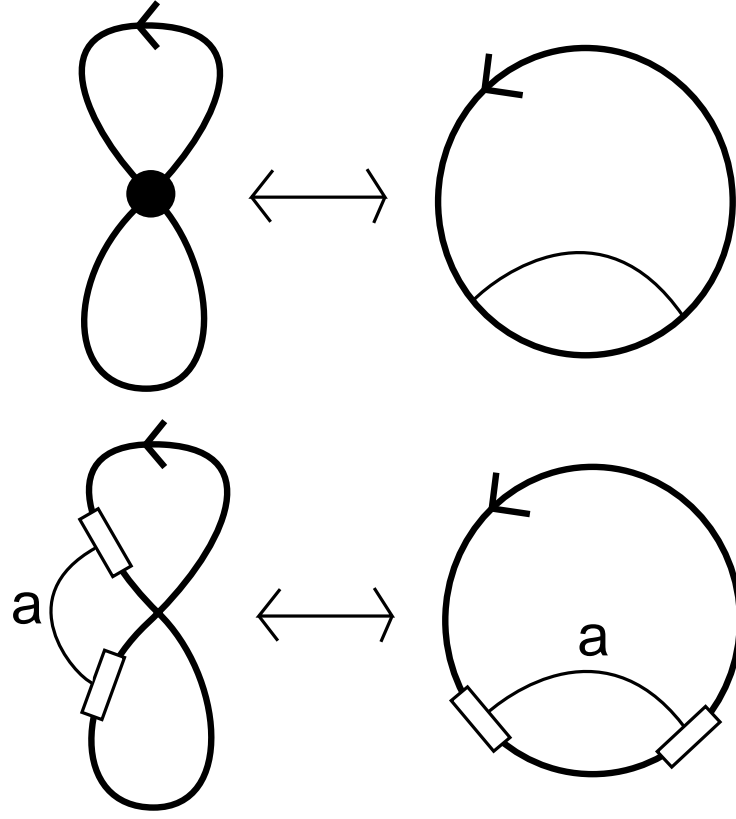


Figure 24 - Weight System and Casimir Insertion

Let D be the trace of the identity. Then it is easy to see that we must compensate the given weight system by subtracting (γ/D) multiplied by the result of dropping the identification of the two given points. We can diagram this by drawing two crossed arcs without a node drawn to bind them. Then the modified recursion formula becomes as shown in Figure 25.

For example, in the case of $SU(N)$ we have $D = N$, $\gamma = (N^2 - 1)/2$ so that we get the transformation shown in Figure 25, including the use of the Fierz identity.

For $N = 2$ the final formula of Figure 25 is, up to a multiple, exactly the top row formula that we deduced for the Jones polynomial from its combinatorial structure.

$$\text{Circle with } C = \text{Zigzag line } a \times \text{Box } a$$

$$V \text{ (black dot)} = V \text{ (C)} - (\gamma/D) V \text{ (black dot)}$$

$SU(N): D=N, \quad \gamma = (N^2 - 1)/2$

$$V \text{ (black dot)} = V \text{ (C)} - (N^2 - 1)/(2N) V \text{ (black dot)}$$

$$V \text{ (C)} = (1/2) \text{ (curved lines)} - (1/2N) V \text{ (black dot)}$$

(Fierz Identity)

$$V \text{ (black dot)} = (1/2) \text{ (curved lines)} - (N/2) V \text{ (black dot)}$$

Figure 25 - Modified Recursion Formula

3.2 Vassiliev Invariants and Witten's Functional Integral

In [156] Edward Witten proposed a formulation of a class of 3-manifold invariants as generalized Feynman integrals taking the form $Z(M)$ where

$$Z(M) = \int dA \exp[(ik/4\pi)S(M, A)].$$

Here M denotes a 3-manifold without boundary and A is a gauge field (also called a gauge potential or gauge connection) defined on M . The gauge field is a one-form on a trivial G -bundle over M with values in a representation of the Lie algebra of G . The group G corresponding to this Lie algebra is said to be the gauge group. In this integral the “action” $S(M, A)$ is taken to be the integral over M of the trace of the Chern-Simons three-form $CS = AdA + (2/3)AAA$. (The product is the wedge product of differential forms.)

$Z(M)$ integrates over all gauge fields modulo gauge equivalence (See [2] for a discussion of the definition and meaning of gauge equivalence.)

The formalism and internal logic of Witten's integral supports the existence of a large class of topological invariants of 3-manifolds and associated invariants of knots and links in these manifolds.

The invariants associated with this integral have been given rigorous combinatorial descriptions [133], [150], [93], [105], [153], [73], but questions and conjectures arising from the integral formulation are still outstanding. (See for example [3], [41], [43], [49], [134].) Specific conjectures about this integral take the form of just how it involves invariants of links and 3-manifolds, and how these invariants behave in certain limits of the coupling constant k in the integral. Many conjectures of this sort can be verified through the combinatorial models. On the other hand, the really outstanding conjecture about the integral is that it exists! At the present time there is no measure theory or generalization of measure theory that supports it. It is a fascinating exercise to take the speculation seriously, suppose that it does really work like an integral and explore the formal consequences. Here is a formal structure of great beauty. It is also a structure whose consequences can be verified by a remarkable variety of alternative means. Perhaps in the course of the exploration there will appear a hint of the true nature of this form of integration.

We now look at the formalism of the Witten integral in more detail and see how it involves invariants of knots and links corresponding to each classical Lie algebra. In order to accomplish this task, we need to introduce the Wilson loop. The Wilson loop is an exponentiated version of integrating the gauge field along a loop K in three-space that we take to be an embedding (knot) or a curve with transversal self-intersections. For this discussion, the Wilson loop will be denoted by the notation $W_K(A) = \langle K|A \rangle$ to denote the dependence on the loop K and the field A . It is usually indicated by the symbolism

$tr(Pexp(\int_K A))$. Thus

$$W_K(A) = \langle K|A \rangle = tr(Pexp(\int_K A)).$$

Here the P denotes path ordered integration - we are integrating and exponentiating matrix valued functions, and so must keep track of the order of the operations. The symbol tr denotes the trace of the resulting matrix.

With the help of the Wilson loop functional on knots and links, Witten writes down a functional integral for link invariants in a 3-manifold M :

$$\begin{aligned} Z(M, K) &= \int dA exp[(ik/4\pi)S(M, A)] tr(Pexp(\int_K A)) \\ &= \int dA exp[(ik/4\pi)S] \langle K|A \rangle . \end{aligned}$$

Here $S(M, A)$ is the Chern-Simons Lagrangian, as in the previous discussion.

We abbreviate $S(M, A)$ as S and write $\langle K|A \rangle$ for the Wilson loop. Unless otherwise mentioned, the manifold M will be the three-dimensional sphere S^3

An analysis of the formalism of this functional integral reveals quite a bit about its role in knot theory. This analysis depends upon key facts relating the curvature of the gauge field to both the Wilson loop and the Chern-Simons Lagrangian. The idea for using the curvature in this way is due to Lee Smolin [140, 141] (See also [129]). To this end, let us recall the local coordinate structure of the gauge field $A(x)$, where x is a point in three-space. We can write $A(x) = A_a^k(x)T^a dx_k$ where the index a ranges from 1 to m with the Lie algebra basis $\{T^1, T^2, T^3, \dots, T^m\}$. The index k goes from 1 to 3. For each choice of a and k , $A_a^k(x)$ is a smooth function defined on three-space. In $A(x)$ we sum over the values of repeated indices. The Lie algebra generators T^a are matrices corresponding to a given representation of the Lie algebra of the gauge group G . We assume some properties of these matrices as follows:

1. $[T^a, T^b] = if_{abc}T^c$ where $[x, y] = xy - yx$, and f_{abc} (the matrix of structure constants) is totally antisymmetric. There is summation over repeated indices.
2. $tr(T^a T^b) = \delta^{ab}/2$ where δ^{ab} is the Kronecker delta ($\delta^{ab} = 1$ if $a = b$ and zero otherwise).

We also assume some facts about curvature. (The reader may enjoy comparing with the exposition in [64]. But note the difference of conventions on the use of i in the Wilson loops and curvature definitions.) The first fact is the relation of Wilson loops and curvature for small loops:

Fact 1. The result of evaluating a Wilson loop about a very small planar circle around a point x is proportional to the area enclosed by this circle times the corresponding value of

the curvature tensor of the gauge field evaluated at x . The curvature tensor is written

$$F_a^{rs}(x)T^a dx_r dy_s.$$

It is the local coordinate expression of $AdA + AA$.

Application of Fact 1. Consider a given Wilson line $\langle K|S \rangle$. Ask how its value will change if it is deformed infinitesimally in the neighborhood of a point x on the line. Approximate the change according to Fact 1, and regard the point x as the place of curvature evaluation. Let $\delta \langle K|A \rangle$ denote the change in the value of the line. $\delta \langle K|A \rangle$ is given by the formula

$$\delta \langle K|A \rangle = dx_r dx_s F_a^{rs}(x) T^a \langle K|A \rangle.$$

This is the first order approximation to the change in the Wilson line.

In this formula it is understood that the Lie algebra matrices T^a are to be inserted into the Wilson line at the point x , and that we are summing over repeated indices. This means that each $T^a \langle K|A \rangle$ is a new Wilson line obtained from the original line $\langle K|A \rangle$ by leaving the form of the loop unchanged, but inserting the matrix T^a into that loop at the point x . A Lie algebra generator is diagrammed by a little box with a single index line and two input/output lines which correspond to its role as a matrix (hence as mappings of a vector space to itself). See Figure 26.

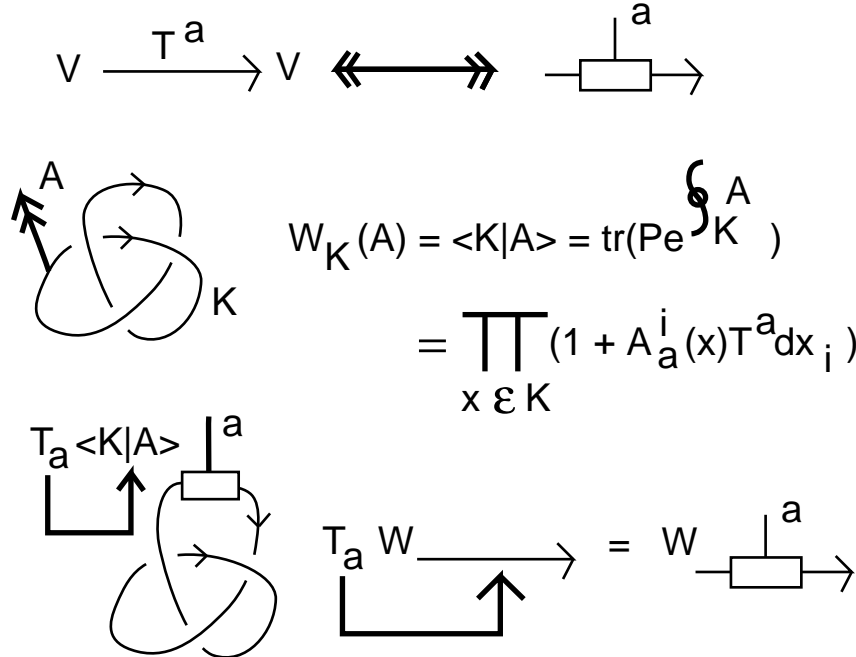


Figure 26 - Wilson Loop Insertion

Remark. In thinking about the Wilson line $\langle K|A \rangle = \text{tr}(P \exp(\int_K A))$, it is helpful to recall Euler's formula for the exponential:

$$e^x = \lim_{n \rightarrow \infty} (1 + x/n)^n.$$

The Wilson line is the limit, over partitions of the loop K , of products of the matrices $(1 + A(x))$ where x runs over the partition. Thus we can write symbolically,

$$\langle K|A \rangle = \prod_{x \in K} (1 + A(x)) = \prod_{x \in K} (1 + A_a^k(x) T^a dx_k).$$

It is understood that a product of matrices around a closed loop connotes the trace of the product. The ordering is forced by the one-dimensional nature of the loop. Insertion of a given matrix into this product at a point on the loop is then a well-defined concept. If T is a given matrix then it is understood that $T \langle K|A \rangle$ denotes the insertion of T into some point of the loop. In the case above, it is understood from context in the formula

$$dx_r dx_s F_a^{rs}(x) T^a \langle K|A \rangle$$

that the insertion is to be performed at the point x indicated in the argument of the curvature.

Remark. The previous remark implies the following formula for the variation of the Wilson loop with respect to the gauge field:

$$\delta \langle K|A \rangle / \delta(A_a^k(x)) = dx_k T^a \langle K|A \rangle.$$

Varying the Wilson loop with respect to the gauge field results in the insertion of an infinitesimal Lie algebra element into the loop.

Proof.

$$\begin{aligned} & \delta \langle K|A \rangle / \delta(A_a^k(x)) \\ &= \delta \prod_{y \in K} (1 + A_a^k(y) T^a dy_k) / \delta(A_a^k(x)) \\ &= \prod_{y < x \in K} (1 + A_a^k(y) T^a dy_k) [T^a dx_k] \prod_{y > x \in K} (1 + A_a^k(y) T^a dy_k) \\ &= dx_k T^a \langle K|A \rangle. \end{aligned}$$

Fact 2. The variation of the Chern-Simons Lagrangian S with respect to the gauge potential at a given point in three-space is related to the values of the curvature tensor at that point by the following formula:

$$F_a^{rs}(x) = \epsilon_{rst} \delta S / \delta(A_a^t(x)).$$

Here ϵ_{abc} is the epsilon symbol for three indices, i.e. it is $+1$ for positive permutations of 123 and -1 for negative permutations of 123 and zero if any two indices are repeated.

With these facts at hand we are prepared to determine how the Witten integral behaves under a small deformation of the loop K .

In accord with the theme of this paper, we shall use a system of abstract tensor diagrams to look at the differential algebra related to the functional integral. The translation to diagrams is accomplished with the aid of Figure 27 and Figure 28. In Figure 27 we give diagrammatic equivalents for the component parts of our machinery. Tensors become labelled boxes. Indices become lines emanating from the boxes. Repeated indices that we intend to sum over become lines from one box to another. (The eye can immediately apprehend the repeated indices and the tensors where they are repeated.) Note that we use a capital D with lines extending from the top and the bottom for the partial derivative with respect to the gauge field, a capital W with a link diagrammatic subscript for the Wilson loop, a cubic vertex for the three-index epsilon, little triangles with emanating arcs for the differentials of the space variables.

The Lie algebra generators are little boxes with single index lines and two input/output lines which correspond to their roles as matrices (hence as mappings of a vector space to itself). The Lie algebra generators are, in all cases of our calculation, inserted into the Wilson line either through the curvature tensor or through insertions related to differentiating the Wilson line.

In Figure 28 we give the diagrammatic calculation of the change of the functional integral corresponding to a tiny change in the Wilson loop. The result is a double insertion of Lie Algebra generators into the line, coupled with the presence of a volume form that will vanish if the deformation does not twist in three independent directions. This shows that the functional integral is formally invariant under regular isotopy since the regular isotopy moves are changes in the Wilson line that happen entirely in a plane. One does not expect the integral to be invariant under a Reidemeister move of type one, and it is not. This framing compensation can be determined by the methods that we are discussing [74], but we will not go into the details of those calculations here.

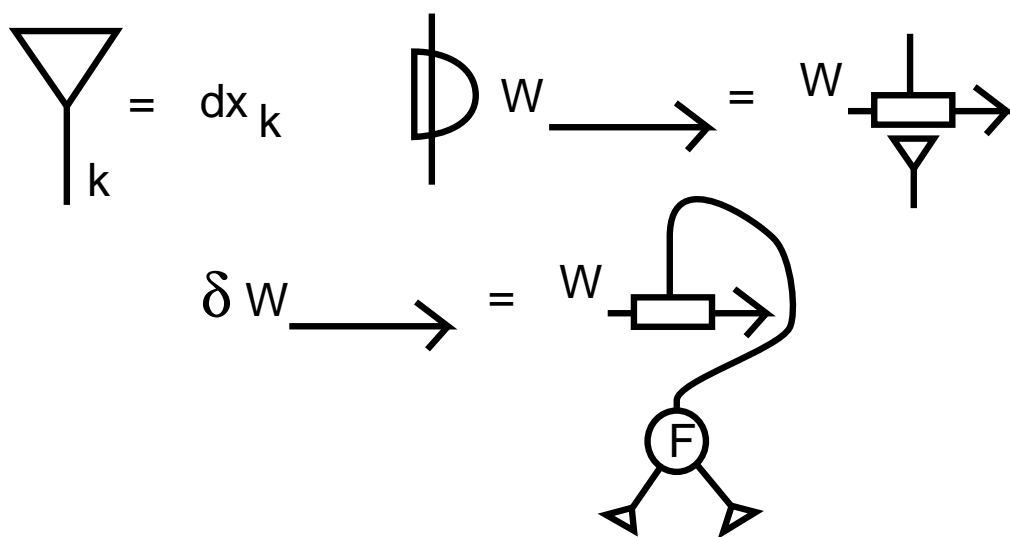
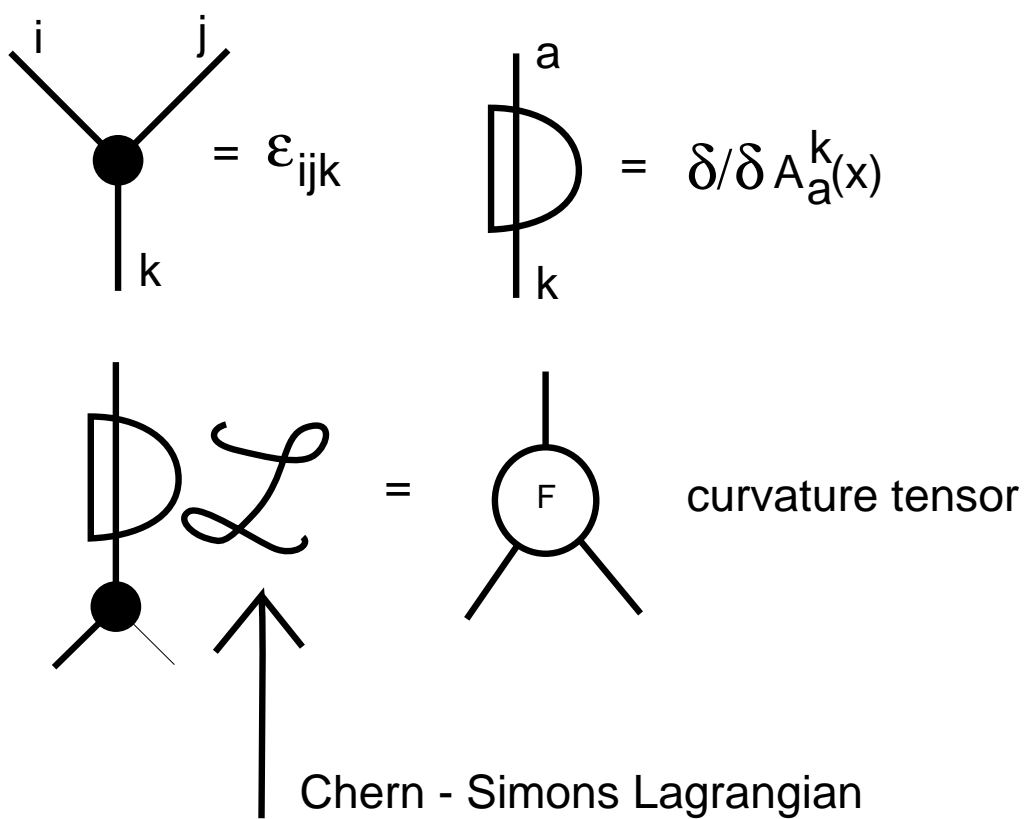


Figure 27 - Notation

$$\begin{aligned}
\delta Z_K &= \int e^{k\mathcal{L}} \delta W \longrightarrow = \int e^{k\mathcal{L}} \text{ (Diagram: a circle with 'F' inside, connected to a box with an arrow) } \\
&= \int e^{k\mathcal{L}} \text{ (Diagram: a loop with a box and arrow, and a vertex with two arrows) } \\
&= (1/k) \int \text{ (Diagram: a loop with a box and arrow, and a vertex with two arrows) } \\
&= - (1/k) \int e^{k\mathcal{L}} \text{ (Diagram: a loop with a box and arrow, and a vertex with two arrows) } \\
&= - (1/k) \int e^{k\mathcal{L}} \text{ (Diagram: a loop with a box and arrow, and a vertex with two arrows) } \\
&= - (1/k) \int e^{k\mathcal{L}} \text{ (Diagram: a loop with a box and arrow, and a vertex with two arrows) }
\end{aligned}$$

Figure 28 - Derivation

In Figure 29 we show the application of the calculation in Figure 28 to the case of switching a crossing. The same formula applies, with a different interpretation, to the case where x is a double point of transversal self-intersection of a loop K , and the deformation consists in shifting one of the crossing segments perpendicularly to the plane of intersection so that the self-intersection point disappears. In this case, one T^a is inserted into each of the transversal crossing segments so that $T^a T^a < K|A >$ denotes a Wilson loop with a

self-intersection at x and insertions of T^a at $x + \epsilon_1$ and $x + \epsilon_2$ where ϵ_1 and ϵ_2 denote small displacements along the two arcs of K that intersect at x . In this case, the volume form is nonzero, with two directions coming from the plane of movement of one arc, and the perpendicular direction is the direction of the other arc. The reason for the insertion into the two lines is a direct consequence of the calculational form of Figure 28: The first insertion is in the moving line, due to curvature. The second insertion is the consequence of differentiating the self-touching Wilson line. Since this line can be regarded as a product, the differentiation occurs twice at the point of intersection, and it is the second direction that produces the non-vanishing volume form.

$$\begin{aligned}
\delta Z_K &= Z \text{ (crossing) } - Z \text{ (crossing with moving line) } \\
&= - (1/k) \int e^{k\mathcal{L}} \text{ (diagram with Wilson line and vertex) } \\
&= - (1/k) \int e^{k\mathcal{L}} \text{ (diagram with Wilson line and vertex) } \\
&= Z \text{ (crossing) } - Z \text{ (crossing) } = 4\pi i/k Z \text{ (circle with c) } \\
Z_{K_+} - Z_{K_-} &= 4\pi i/k Z_T^a T^a K_{**}
\end{aligned}$$

Figure 29 - Crossing Switch

Up to the choice of our conventions for constants, the switching formula is, as shown in Figure 29,

$$\begin{aligned} Z(K_+) - Z(K_-) &= (4\pi i/k) \int dA \exp[(ik/4\pi)S] T^a T^a < K_{**} | A > \\ &= (4\pi i/k) Z(T^a T^a K_{**}). \end{aligned}$$

The key point is to notice that the Lie algebra insertion for this difference is exactly what we did to make the weight systems for Vassiliev invariants (without the framing compensation). Thus the formalism of the Witten functional integral takes us directly to these weight systems in the case of the classical Lie algebras. The functional integral is central to the structure of the Vassiliev invariants.

3.3 Combinatorial Constructions for Vassiliev Invariants

Perhaps the most remarkable thing about this story of the structure of the Vassiliev invariants is the way that Lie algebras are so naturally involved in the structure of the weight systems. This shows the remarkably close nature of the combinatorial structure of Lie algebras and the combinatorics of knots and links via the Reidemeister moves. A really complete story about the Vassiliev invariants at this combinatorial level would produce their existence on the basis of the weight systems with entirely elementary arguments.

As we have already mentioned, one can prove that a given set of weights for the top row, satisfying the abstract four-term relation does imply that there exists a Vassiliev invariant of finite type n realizing these weights for graphs with n nodes. Proofs of this result either use analysis [4], [1] or non-trivial algebra [13], [4]. There is no known elementary combinatorial proof of the existence of Vassiliev invariants for given top rows.

Of course quantum link invariants (See section 4 of these lectures.) do give combinatorial constructions for large classes of link invariants. These constructions rest on solutions to the Yang-Baxter equations, and it is not known how to describe the subset of finite type Vassiliev invariants that are so produced.

It is certainly helpful to look at the structure of Vassiliev invariants that arise from already-defined knot invariants. If $V(K)$ is an already defined invariant of knots (and possibly links), then its extension to a Vassiliev invariant is calculated on embedded graphs G by expanding each graphical vertex into a difference by resolving the vertex into a positive crossing and a negative crossing. If we know that $V(K)$ is of finite type n and G has n nodes then we can take any embedding of G that is convenient, and calculate $V(G)$ in terms of all the knots that arise in resolving the nodes of this chosen embedding. This is a finite collection of knots. Since there is a finite collection of 4-valent graphs with n nodes, it follows that the top row evaluation for the invariant $V(K)$ is determined by the values of $V(K)$ on a finite collection of knots. Instead of asking for the values of the Vassiliev

invariant on a top row, we can ask for this set of knots and the values of the invariant on this set of knots. A minimal set of knots that can be used to generate a given Vassiliev invariant will be called a *knots basis* for the invariant. Thus we have shown that the set consisting of the unknot, the right-handed trefoil and the left handed-trefoil is a knots basis for a Vassiliev invariant of type 3. See [122] for more information about this point of view.

A tantalizing combinatorial approach to Vassiliev invariants is due to Michael Polyak and Oleg Viro [127]. They give explicit formulas for the second, third and fourth Vassiliev invariants and conjecture that their method will work for Vassiliev invariants of all orders. The method is as follows.

First one makes a new representation for oriented knots by taking *Gauss diagrams*. A Gauss diagram is a diagrammatic representation of the classical *Gauss code* of the knot. The Gauss code is obtained from the oriented knot diagram by first labelling each crossing with a naming label (such as 1,2,...) and also indicating the crossing type (+1 or -1). Then choose a basepoint on the knot diagram and begin walking along the diagram, recording the name of the crossings encountered, their sign and whether the walk takes you over or under that crossing. For example, if you go under crossing 1 whose sign is + then you will record $o+1$. Thus the Gauss code of the positive trefoil diagram is

$$(o1+)(u2+)(o3+)(u1+)(o2+)(u3+).$$

For prime knots the Gauss code is sufficient information to reconstruct the knot diagram. See [67] for a sketch of the proof of this result and for other references.

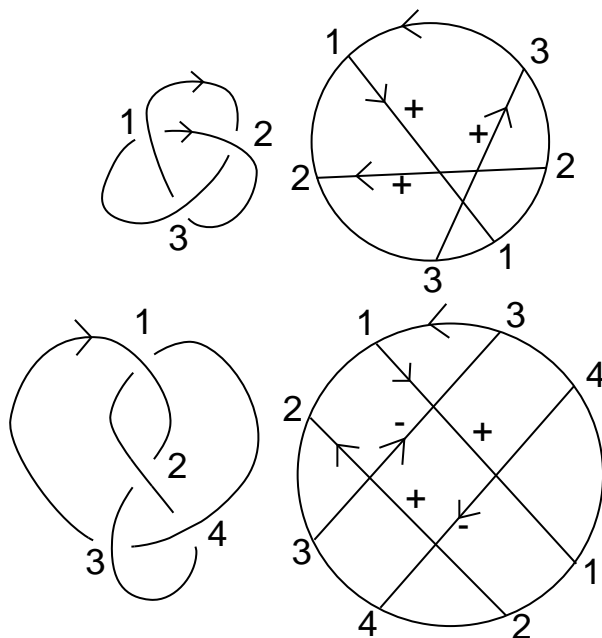


Figure 30 - Gauss Diagrams

To form a Gauss diagram from a Gauss code, take an oriented circle with a basepoint chosen on the circle. Walk along the circle marking it with the labels for the crossings in the order of the Gauss code. Now draw chords between the points on the circle that have the same label. Orient each chord from overcrossing site to undercrossing site. Mark each chord with $+1$ or -1 according to the sign of the corresponding crossing in the Gauss code. The resulting labelled and basepointed graph is the Gauss diagram for the knot. See Figure 30 for examples.

The Gauss diagram is deliberately formulated to have the structure of a chord diagram (as we have discussed for the weight systems for Vassiliev invariants). If $G(K)$ is the Gauss diagram for a knot K , and D is an oriented (i.e. the chords as well as the circle in the diagram are oriented) chord diagram, let $|G(K)|$ denote the number of chords in $G(K)$ and $|D|$ denote the number of chords in D . If $|D| \leq |G(K)|$ then we may consider oriented embeddings of D in $G(K)$. For a given embedding $i : D \rightarrow G(K)$ define

$$\langle i(D) | G(K) \rangle = \text{sign}(i)$$

where $\text{sign}(i)$ denotes the product of the signs of the chords in $G(K) \cap i(D)$. Now suppose that C is a collection of *oriented* chord diagrams, each with n chords, and that

$$\text{eval} : C \rightarrow R$$

is an evaluation mapping on these diagrams that satisfies the four-term relation at level n . Then we can define

$$\langle D | K \rangle = \sum_{i: D \rightarrow G(K)} \langle i(D) | G(K) \rangle$$

and

$$v(K) = \sum_{D \in C} \langle D | K \rangle \text{eval}(D).$$

For appropriate oriented chord subsets this definition can produce Vassiliev invariants $v(K)$ of type n . For example, in the case of the Vassiliev invariant of type three taking value 0 on the unknot and value 1 on the right-handed trefoil, -1 on the left-handed trefoil, Polyak and Viro give the specific formula

$$v_3(K) = \langle A | K \rangle + (1/2) \langle B | K \rangle$$

where A denotes the trefoil chord diagram as we described it in section 3 and B denotes the three-chord diagram consisting of two parallel chords pierced by a third chord. In Figure 31 we show the specific orientations for the chord diagrams A and B . The key to this construction is in the choice of orientations for the chord diagrams in $C = \{A, B\}$. It is a nice exercise in translation of the Reidemeister moves to Gauss diagrams to see that $v_3(K)$ is indeed a knot invariant.

It is possible that all Vassiliev invariants can be constructed by a method similar to the formula $v(K) = \sum_{D \in C} \langle D | K \rangle \text{eval}(D)$. This remains to be seen.

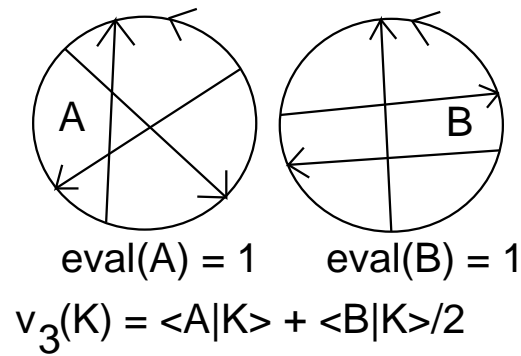


Figure 31 - Oriented Chord Diagrams for v_3 .

3.4 8_{17}

It is an open problem whether there are Vassiliev invariants that can detect the difference between a knot and its reverse (The reverse of an oriented knot is obtained by flipping the orientation.). The smallest instance of a non-invertible knot is the knot 8_{17} depicted in Figure 32.

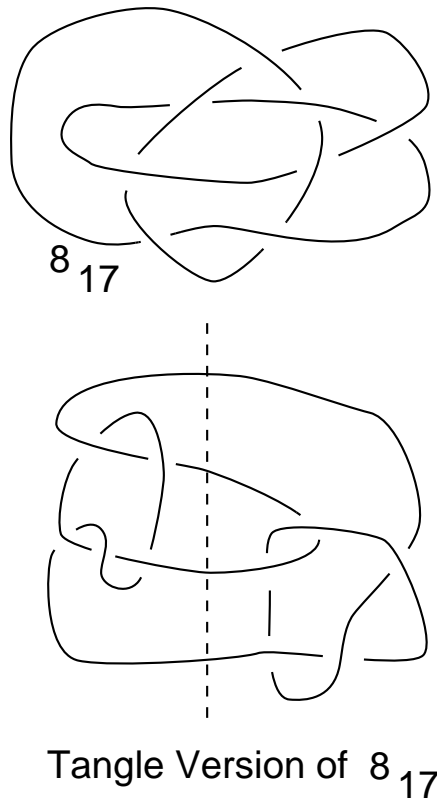


Figure 32 - Tangle Decomposition of 8_{17} .

Thus, at the time of this writing there is no known Vassiliev invariant that can detect the non-invertibility of 8_{17} . On the other hand, the tangle decomposition shown in Figure 32 can be used in conjunction with the results of Siebenmann and Bonahon [138] and the formulations of John Conway [23] to show this non-invertibility. These tangle decomposition methods use higher level information about the diagrams than is easy to encode in Vassiliev invariants. The purpose of this section is to underline this discrepancy between different levels in the combinatorial topology.

4 Quantum Link Invariants

In this section we describe the construction of quantum link invariants from knot and link diagrams that are arranged with respect to a given direction in the plane. This special direction will be called “time”. Arrangement with respect to the special direction means that perpendiculars to this direction meet the diagram transversely (at edges or at crossings) or tangentially (at maxima and minima). The designation of the special direction as time allows the interpretation of the consequent evaluation of the diagram as a generalized scattering amplitude.

In the course of this discussion we find the need to reformulate the Reidemeister moves for knot and link diagrams that are arranged to be transverse (except for a finite collection of standard critical points) to the specific special direction introduced in the previous paragraph. This brings us back to our theme of diagrams and related structures. This particular reformulation of the Reidemeister moves is quite far-reaching. It encompasses the relationship of link invariants with solutions to the Yang-Baxter equation and the relationship with Hopf algebras (to be dealt with in Section 5).

4.1 Knot Amplitudes

Consider first a circle in a spacetime plane with time represented vertically and space horizontally as in Figure 33.

The circle represents a vacuum to vacuum process that includes the creation of two “particles” and their subsequent annihilation. We could divide the circle into these two parts (creation “cup” and annihilation “cap”) and consider the amplitude $\langle cap|cup \rangle$. Since the diagram for the creation of the two particles ends in two separate points, it is natural to take a vector space of the form $V \otimes V$ as the target for the bra and as the domain of the ket. We imagine at least one particle property being catalogued by each factor of the tensor product. For example, a basis of V could enumerate the spins of the created particles.

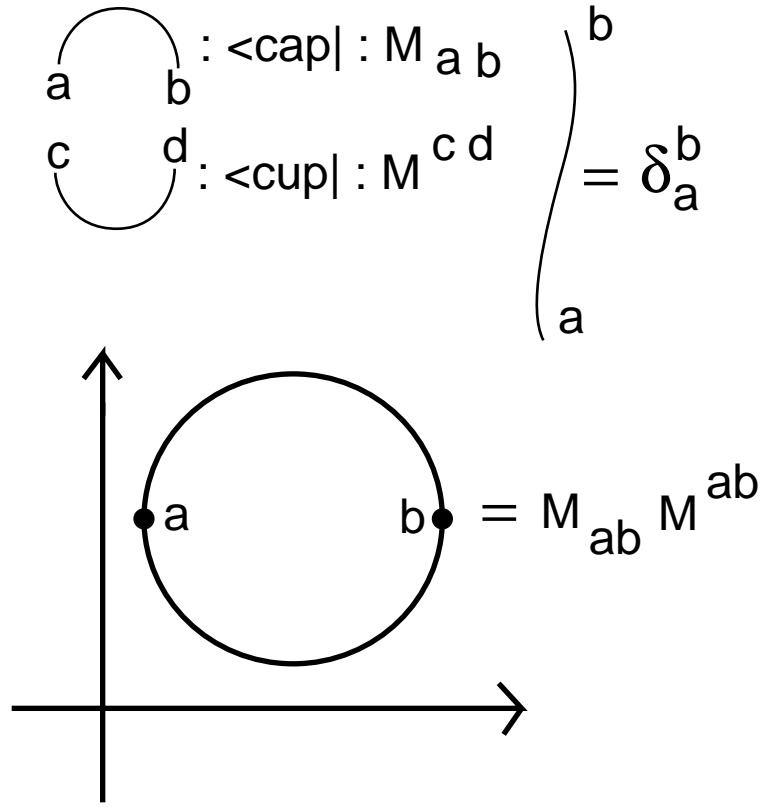


Figure 33 - Spacetime Circle

Any non-self-intersecting differentiable curve can be rigidly rotated until it is in general position with respect to the vertical. It will then be seen to be decomposed into an interconnection of minima and maxima. We can evaluate an amplitude for any curve in general position with respect to a vertical direction. Any simple closed curve in the plane is isotopic to a circle, by the Jordan Curve Theorem. If these are topological amplitudes, then the value for any simple closed curve should be equal to the original amplitude for the circle. What condition on creation (cup) and annihilation (cap) will insure topological amplitudes? The answer derives from the fact that isotopies of the simple closed curves are generated by the cancellation of adjacent maxima and minima as illustrated in Figure 34.

This condition is articulated by taking a matrix representation for the corresponding operators. Specifically, let $\{e_1, e_2, \dots, e_n\}$ be a basis for V . Let $e_{ab} = e_a \otimes e_b$ denote the elements of the tensor basis for $V \otimes V$. Then there are matrices M_{ab} and M^{ab} such that

$$|cup\rangle(1) = \sum M^{ab} e_{ab}$$

with the summation taken over all values of a and b from 1 to n . Similarly, $\langle cap|$ is described by

$$\langle cap|(e_{ab}) = M_{ab}.$$

Thus the amplitude for the circle is

$$\begin{aligned} \langle cap|cup \rangle (1) &= \langle cap| \sum M^{ab} e_{ab} \\ &= \sum M^{ab} \langle cap|(e_{ab}) = \sum M^{ab} M_{ab}. \end{aligned}$$

In general, the value of the amplitude on a simple closed curve is obtained by translating it into an “abstract tensor expression” in the M^{ab} and M_{ab} , and then summing over these products for all cases of repeated indices. Note that here the value “1” corresponds to the vacuum.

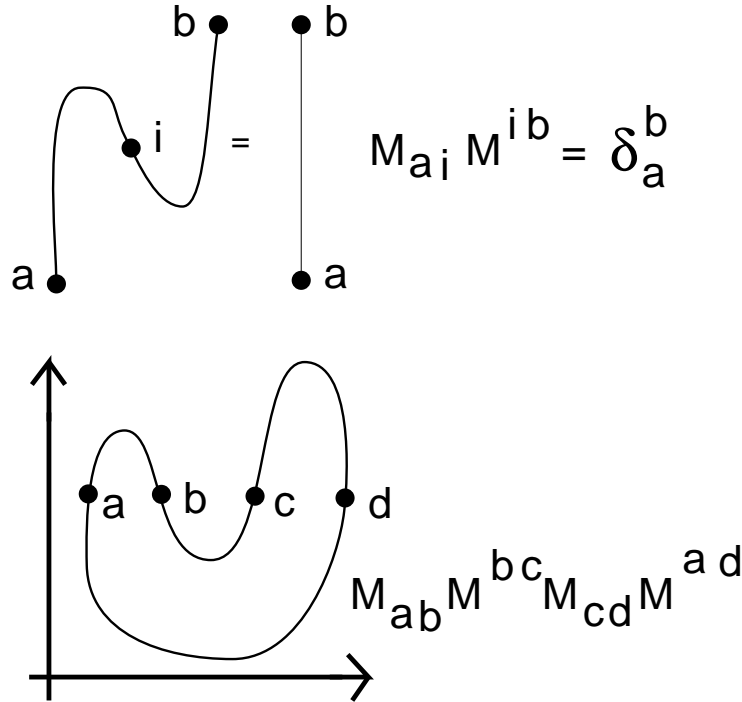


Figure 34- Spacetime Jordan Curve

Returning to the topological conditions we see that they are just that the matrices M^{ab} and M_{cd} are inverses in the sense that

$$\sum_i M^{ai} M_{ib} = \delta_b^a$$

where δ_b^a denotes the identity matrix. See Figure 34.

One of the simplest choices is to take a 2 x 2 matrix M such that $M^2 = I$ where I is the identity matrix. Then the entries of M can be used for both the cup and the cap. The value for a loop is then equal to the sum of the squares of the entries of M :

$$\langle cap|cup \rangle (1) = \sum M^{ab} M_{ab} = \sum M_{ab} M_{ab} = \sum M_{ab}^2.$$

In particular, consider the following choice for M . It has square equal to the identity matrix and yields a loop value of $d = -A^2 - A^{-2}$, just the right loop value for the bracket polynomial model for the Jones polynomial [59], [58].

$$M = \begin{bmatrix} 0 & iA \\ -iA^{-1} & 0 \end{bmatrix}$$

Any knot or link can be represented by a picture that is configured with respect to a vertical direction in the plane. The picture will decompose into minima (creations), maxima (annihilations) and crossings of the two types shown in Figure 35. Here the knots and links are unoriented. These models generalize easily to include orientation.

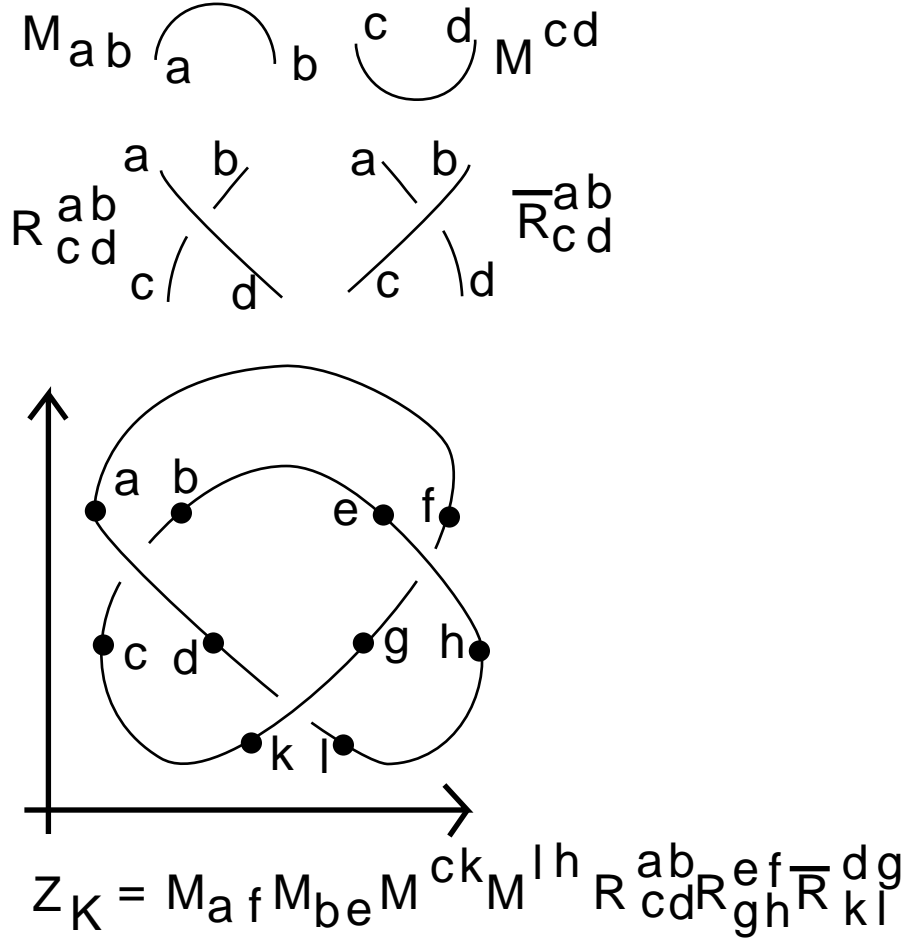


Figure 35 - Cups, Caps and Crossings

Next to each of the crossings we have indicated mappings of $V \otimes V$ to itself, called R and R^{-1} respectively. These mappings represent the transitions corresponding to elementary braiding. We now have the vocabulary of *cup*, *cap*, R and R^{-1} . Any knot or link can be written as a composition of these fragments, and consequently a choice of such mappings determines an amplitude for knots and links. In order for such an amplitude to be topological (i.e. an invariant of regular isotopy the equivalence relation generated by the second and third of the classical Reidemeister moves) we want it to be invariant under a list of local moves on the diagrams as shown in Figure 36. These moves are an augmented list of Reidemeister moves, adjusted to take care of the fact that the diagrams are arranged with respect to a given direction in the plane. The proof that these moves generate regular isotopy is composed in exact parallel to the proof that we gave for the classical Reidemeister moves in section 2. In the piecewise linear setting, maxima and minima are replaced by upward and downward pointing angles. The fact that the triangle, in the Reidemeister piecewise linear triangle move, must be projected so that it is generically transverse to the vertical direction in the plane introduces the extra restriction that expands the move set.

In this context, the algebraic translation of Move *III* is the Yang-Baxter equation that occurred for the first time in problems of exactly solved models in statistical mechanics [10].

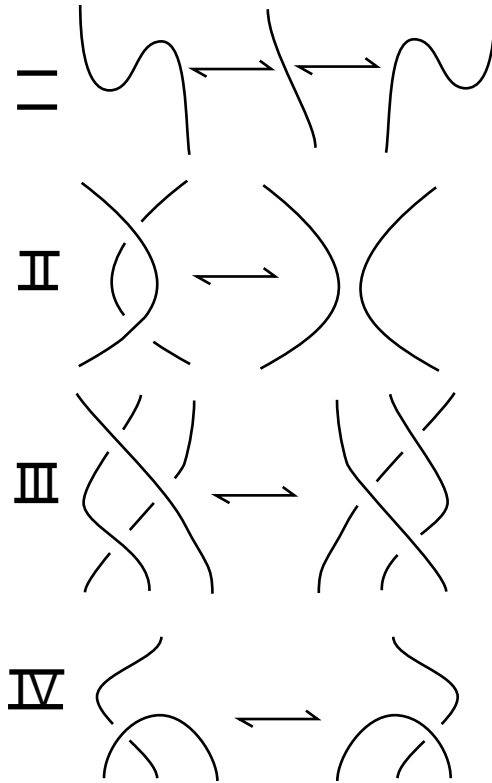


Figure 36 - Regular Isotopy with respect to a Vertical Direction

All the moves taken together are directly related to the axioms for a quasi-triangular Hopf algebra (aka quantum group). Many seeds of the structure of Hopf algebras are prefigured in the patterns of link diagrams and the structure of the category of tangles. The interested reader can consult [133], [157], [67] and [64], [68], [71] and section 5 of this paper for more information on this point.

Here is the list of the algebraic versions of the topological moves. Move 0 is the cancellation of maxima and minima. Move *II* corresponds to the second Reidemeister move. Move *III* is the Yang-Baxter equation. Move *IV* expresses the relationship of switching a line across a maximum. (There is a corresponding version of *IV* where the line is switched across a minimum.)

$$0. \quad M^{ai} M_{ib} = \delta_b^a$$

$$II. \quad R_{ij}^{ab} \overline{R_{cd}^{ij}} = \delta_c^a \delta_d^b$$

$$III. \quad R_{ij}^{ab} R_{kf}^{jc} R_{de}^{ik} = R_{ij}^{bc} R_{dk}^{ai} R_{ef}^{kj}$$

$$IV. \quad R_{bc}^{ai} M_{id} = M_{bi} R_{cd}^{ia}$$

In the case of the Jones polynomial we have all the algebra present to make the model. It is easiest to indicate the model for the bracket polynomial: Let *cup* and *cap* be given by the 2×2 matrix M , described above so that $M_{ij} = M^{ij}$. Let R and R^{-1} be given by the equations

$$R_{cd}^{ab} = AM^{ab}M_{cd} + A^{-1}\delta_c^a\delta_d^b,$$

$$(R^{-1})_{cd}^{ab} = A^{-1}M^{ab}M_{cd} + A\delta_c^a\delta_d^b.$$

This definition of the R -matrices exactly parallels the diagrammatic expansion of the bracket, and it is not hard to see, either by algebra or diagrams, that all the conditions of the model are met.

4.2 Oriented Amplitudes

Slight but significant modifications are needed to write the oriented version of the models we have discussed in the previous section. See [64], [148], [132], [46]. In this section we sketch the construction of oriented topological amplitudes.

The generalization to oriented link diagrams naturally involves the introduction of right and left oriented caps and cups. These are drawn as shown in Figure 37 below.

$$\begin{aligned}
\overrightarrow{M}_{ab} &= \begin{array}{c} \text{a} \quad \text{b} \\ \text{---} \text{---} \end{array} = \lambda^{a/2} \delta_{ab} \\
\overleftarrow{M}_{ab} &= \begin{array}{c} \text{a} \quad \text{b} \\ \text{---} \text{---} \end{array} = \lambda^{-a/2} \delta_{ab} \\
\overrightarrow{M}^{ab} &= \begin{array}{c} \text{a} \quad \text{b} \\ \text{---} \text{---} \end{array} = \overrightarrow{M}_{ab} \\
\overleftarrow{M}^{ab} &= \begin{array}{c} \text{a} \quad \text{b} \\ \text{---} \text{---} \end{array} = \overleftarrow{M}_{ab}
\end{aligned}$$

$$\begin{array}{c} \text{a} \quad \text{a} \\ \text{---} \text{---} \end{array} = \begin{array}{c} \text{a} \quad \text{a} \\ \text{---} \text{---} \end{array} = \delta_b^a$$

Figure 37 - Right and Left Cups and Caps

A right cup cancels with a right cap to produce an upward pointing identity line. A left cup cancels with a left cap to produce a downward pointing identity line.

Just as we considered the simplifications that occur in the unoriented model by taking the cup and cap matrices to be identical, let's assume here that right caps are identical with left cups and that consequently left caps are identical with right cups. In fact, let us assume that the right cap and left cup are given by the matrix

$$M_{ab} = \lambda^{a/2} \delta_{ab}$$

where λ is a constant to be determined by the situation, and δ_{ab} denotes the Kronecker delta. Then the left cap and right cup are given by the inverse of M :

$$M_{ab}^{-1} = \lambda^{-a/2} \delta_{ab}.$$

We assume that along with M we are given a solution R to the Yang-Baxter equation, and that in an oriented diagram the specific choice of R_{cd}^{ab} is governed by the local orientation of the crossing in the diagram. Thus a and b are the labels on the lines going into the crossing and c and d are the labels on the lines emanating from the crossing.

Note that with respect to the vertical direction for the amplitude, the crossings can assume the aspects: both lines pointing upward, both lines pointing downward, one line up and one line down (two cases). See Figure 38.

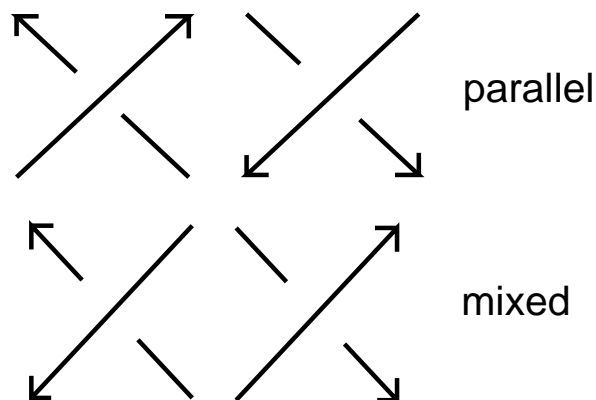


Figure 38 - Oriented Crossings

Call the cases of one line up and one line down the *mixed* cases and the upward and downward cases the *parallel* cases. A given mixed crossing can be converted, in two ways, into a combination of a parallel crossing of the same sign plus a cup and a cap. See Figure 39.

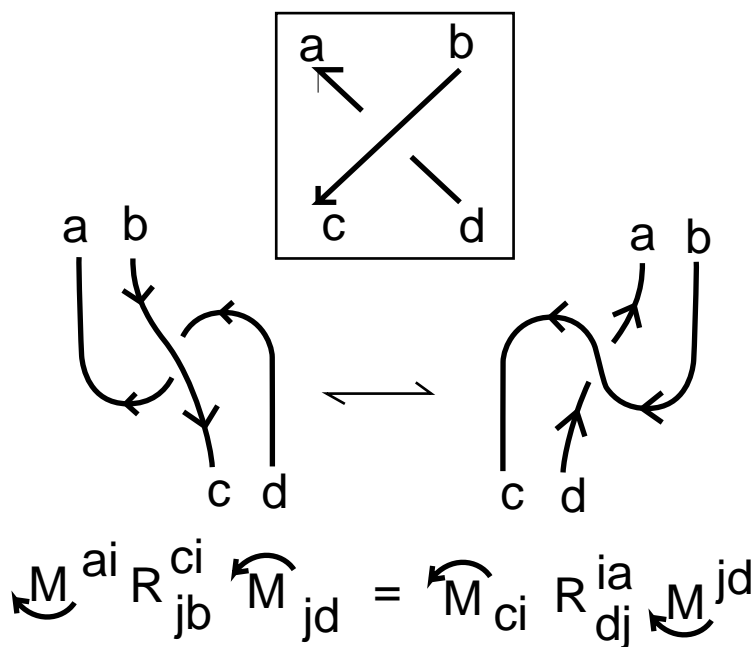


Figure 39 - Conversion

This leads to an equation that must be satisfied by the R matrix in relation to powers of λ (again we use the Einstein summation convention):

$$\lambda^{a/2} \delta^{ai} R_{jb}^{ci} \lambda^{-d/2} \delta_{jd} = \lambda^{-c/2} \delta_{ic} R_{dj}^{ia} \lambda^{b/2} \delta^{jb}.$$

This simplifies to the equation

$$\lambda^{a/2} R_{db}^{ca} \lambda^{-d/2} = \lambda^{-c/2} R_{db}^{ca} \lambda^{b/2},$$

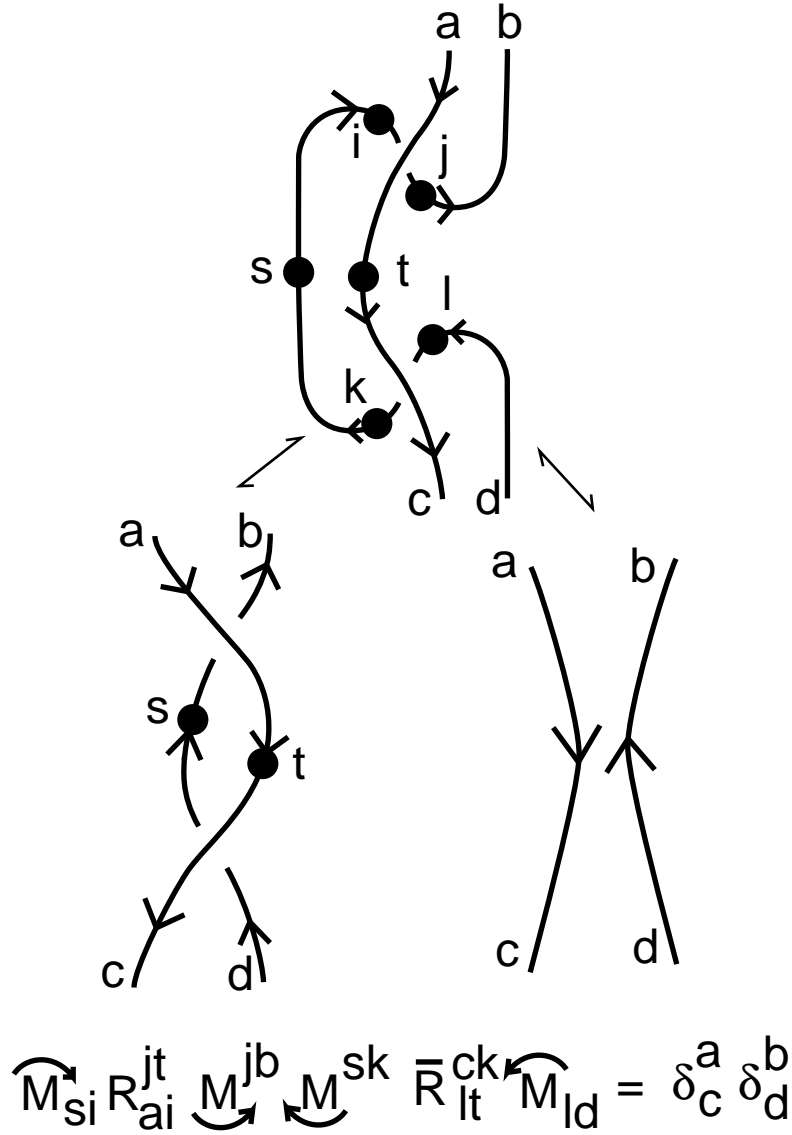


Figure 40 - Antiparallel Second Move

from which we see that R_{db}^{ca} is necessarily equal to zero unless $b + d = a + c$. We say that the R matrix is *spin preserving* when it satisfies this condition. Assuming that the R matrix is spin preserving, the model will be invariant under all orientations of the second and third Reidemeister moves just so long as it is invariant under the anti-parallel version of the second Reidemeister move as shown in Figure 40.

This antiparallel version of the second Reidemeister move places the following demand on the relation between λ and R :

$$\sum_{st} \lambda^{(s-b)/2} \lambda^{(t-c)/2} R_{as}^{bt} \overline{R_{dt}^{cs}} = \delta_c^a \delta_d^b.$$

Call this the $R - \lambda$ equation. The reader familiar with [50] or with the piecewise linear version as described in [64] will recognise this equation as the requirement for regular homotopy invariance in these models.

4.3 Quantum Link Invariants and Vassiliev Invariants

Vassiliev invariants can be used as building blocks for all the presently known quantum link invariants.

It is this result that we can now make clear in the context of the models given in our section on quantum link invariants. Suppose that λ is written as a power series in a variable h , say $\lambda = \exp(h)$ to be specific. Suppose also, that the R -matrices can be written as power series in h with matrix coefficients so that $PR = I + r_+h + O(h^2)$ and $PR^{-1} = I + r_-h + O(h^2)$ where P denotes the map of $V \otimes V$ that interchanges the tensor factors. Let $Z(K)$ denote the value of the oriented amplitude described by this choice of λ and R . Then we can write

$$Z(K) = Z_0(K) + Z_1(K)h + Z_2(K)h^2 + \dots$$

where each $Z_n(K)$ is an invariant of regular isotopy of the link K . Furthermore, we see at once that h divides the series for $Z(K_+) - Z(K_-)$. By the definition of the Vassiliev invariants this implies that h^k divides $Z(G)$ if G is a graph with k nodes. Therefore $Z_n(G)$ vanishes if n is less than the number of nodes of G . Therefore Z_n is a Vassiliev invariant of finite type n . Hence the quantum link invariant is built from an infinite sequence of interlocked Vassiliev invariants.

It is an open problem whether the class of finite type Vassiliev invariants is greater than those generated from quantum link invariants. It is also possible that there are quantum link invariants that cannot be generated by Vassiliev invariants.

4.4 Vassiliev Invariants and Infinitesimal Braiding

Kontsevich [98], [4] proved that a weight assignment for a Vassiliev top row that satisfies the 4-term relation and the framing condition (that the weights vanish for graphs with isolated double points) actually extends to a Vassiliev invariant defined on all knots. His method is motivated by the perturbative expansion of the Witten integral and by Witten's interpretation of the integral in terms of conformal field theory. This section will give a brief description of the Kontsevich approach and the questions that it raises about the functional integral itself.

The key to this approach is to see that the 4-term relations are a kind of “infinitesimal braid relations”. That is, we can re-write the 4-term relations in the form of tangle operators as shown in Figure 41.

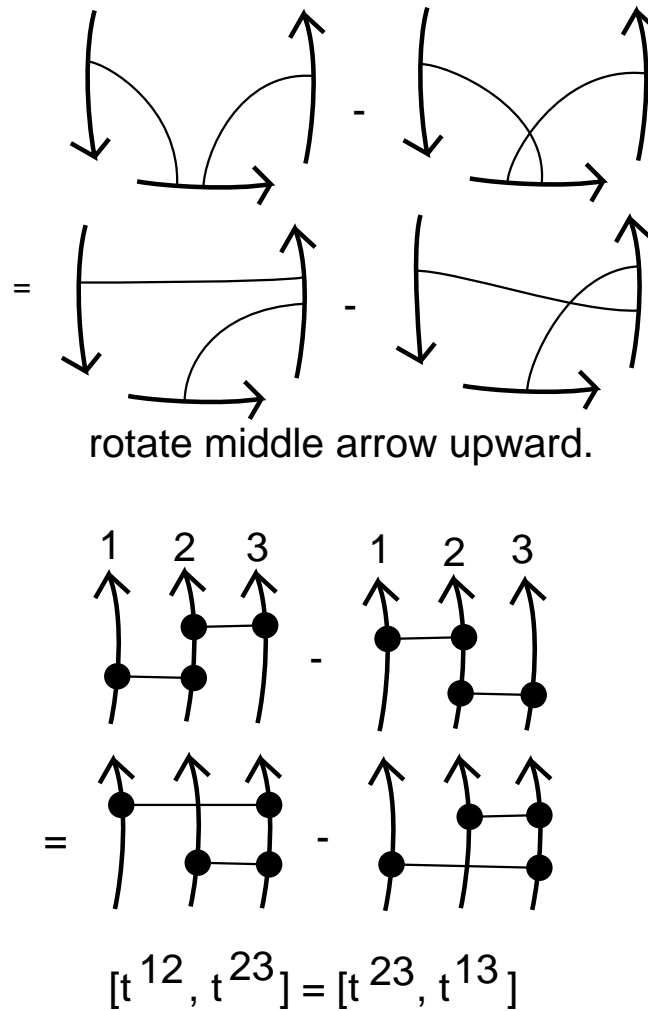


Figure 41 - Infinitesimal Braiding

This shows that the commutator equation

$$[t^{12}, t^{13}] + [t^{13}, t^{23}] = 0$$

is an algebraic form of the 4-term relation. The 4-term relations translate exactly into these infinitesimal braid relations studied by Kohno [99]. Kohno showed that his version of infinitesimal braid relations corresponded to a flatness condition for a certain connection (the Knizhnik-Zamolodchikov connection) and that this meant that these relations constituted an integrability condition for making representations of the braid group via monodromy. Others have verified that the braid group representations related to the Chern-Simons form and the Witten integral arise in this same way from the Knizhnik-Zamolodchikov equations. In the case of Chern-Simons theory the weights in the K-Z equations come from the Casimir of a classical Lie algebra, just as we have discussed. Kontsevich observed that since the arbitrary 4-term relations could also be regarded as an integrability condition it was possible to use them in a generalization of Kohno's ideas to produce braid group representations via iterated integration. He then generalized the process of producing these braid group representations to the production of knot invariants and these become realizations of Vassiliev invariants that have given admissible weight systems for their top rows.

The upshot of the Kontsevich work is a very specific integral formula for the Vassiliev invariants. See [4] for the specifics. It is clear from the nature of the construction that the Kontsevich formula captures the various orders of perturbative terms in the Witten integral. At this writing there is no complete published description of this correspondence.

4.5 Weight Systems and the Classical Yang Baxter Equation

Lets return momentarily to the series form of the solution to the Yang-Baxter equation, as we had indicated it in the previous subsection.

$$\begin{aligned} PR &= I + r_+ h + O(h^2) \\ PR^{-1} &= I + r_- h + O(h^2). \end{aligned}$$

Since $RR^{-1} = P$, it follows that $r_- = -r'_+$ where a' denotes the transpose of a . In the case that R satisfies the $R - \lambda$ equation, it follows that

$$t = r_+ - r_- = r + r'$$

(letting r denote r_+) satisfies the infinitesimal braiding relations

$$[t^{12}, t^{13}] + [t^{13}, t^{23}] = 0.$$

It is interesting to contemplate this fact, since r , being the coefficient of h in the series for R , necessarily satisfies the *classical Yang Baxter Equation*

$$[r^{13}, r^{23}] + [r^{12}, r^{23}] + [r^{12}, r^{13}] = 0.$$

(The classical Yang-Baxter equation for r is a direct consequence of the fact that R is a solution of the (quantum) Yang-Baxter equation.)

Via the quantum link invariants, we have provided a special condition (the assumption that r is the coefficient of \hbar in a power series solution of the quantum Yang-Baxter equation R , and that R satisfies the $R - \lambda$ equation) ensuring that a solution r of the classical Yang-Baxter equation will produce a solution $t = r + r'$ of the infinitesimal braiding relation, whence a weight system for Vassiliev invariants. More work needs to be done to fully understand the relationship between solutions of the classical Yang-Baxter equation and the construction of Vassiliev invariants.

5 Hopf Algebras and Invariants of Three-Manifolds

This section is a rapid sketch of the relationship between the description of regular isotopy with respect to a vertical direction (as described in our discussion of quantum link invariants) and the way that this formulation of the Reidemeister moves is related to Hopf algebras and to the construction of link invariants and invariants of three-manifolds via Hopf algebras. More detailed presentations of this material can be found in [46], [67], [68], [70], [71].

Let's begin by recalling the Kirby calculus [92]. In the context of link diagrams the Kirby calculus has an elegant formulation in terms of (blackboard) framed links represented by link diagrams up to *ribbon equivalence*. Ribbon equivalence consists in diagrams up to regular isotopy coupled with the equivalence of a positive (negative) curl of Whitney degree 1 with a positive (negative) curl of Whitney degree -1 . See Figure 42.

Here we refer informally to the Whitney degree of a plane curve. The Whitney degree is the total turn of the tangent vector. If the curve is not closed, then it is assumed that the tangent direction of the initial point is the same as the tangent vector of the endpoint. In Figure 42 we illustrate how curls encode framings and how ribbon equivalent curls correspond to identical framings. A link is said to be *framed* if it is endowed with a smooth choice of normal vector field. Framing a link is equivalent to specifying an embedded band(s) of which it is the core. The *core* of a band is the center curve. Thus $S^1 \times \{.5\}$ is the core of $S^1 \times [0, 1]$.

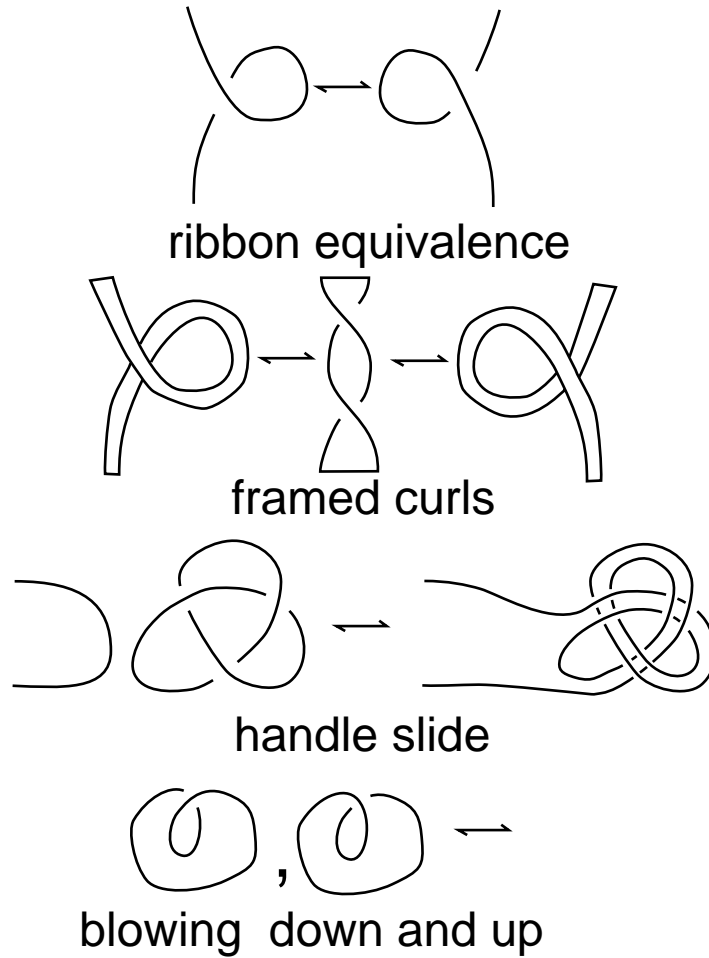


Figure 42 - Framing and Kirby Calculus

Now introduce two new moves on link diagrams called *handle sliding* and *blowing up and down*. These moves are illustrated in Figure 42. Handle sliding consists in duplicating a parallel copy of one link component and then band connect summing it with another component. Blowing up consists in adding an isolated unknotted component with a single curl. Blowing down consists in deleting such a component. These are the basic moves of the Kirby Calculus. Two link diagrams are said to be *KC-equivalent* if there is a combination of ribbon equivalence, handle-sliding and blowing up and blowing down that takes one diagram to the other.

The invariants of three-manifolds described herein are based on the representation of closed three-manifolds via surgery on framed links. Let $M^3(K)$ denote the three-manifold obtained by surgery on the blackboard framed link corresponding to the diagram K . In $M^3(K)$ the longitude associated with the diagram, as shown in Figure 43, bounds the meridian disk of the solid torus attached via the surgery.

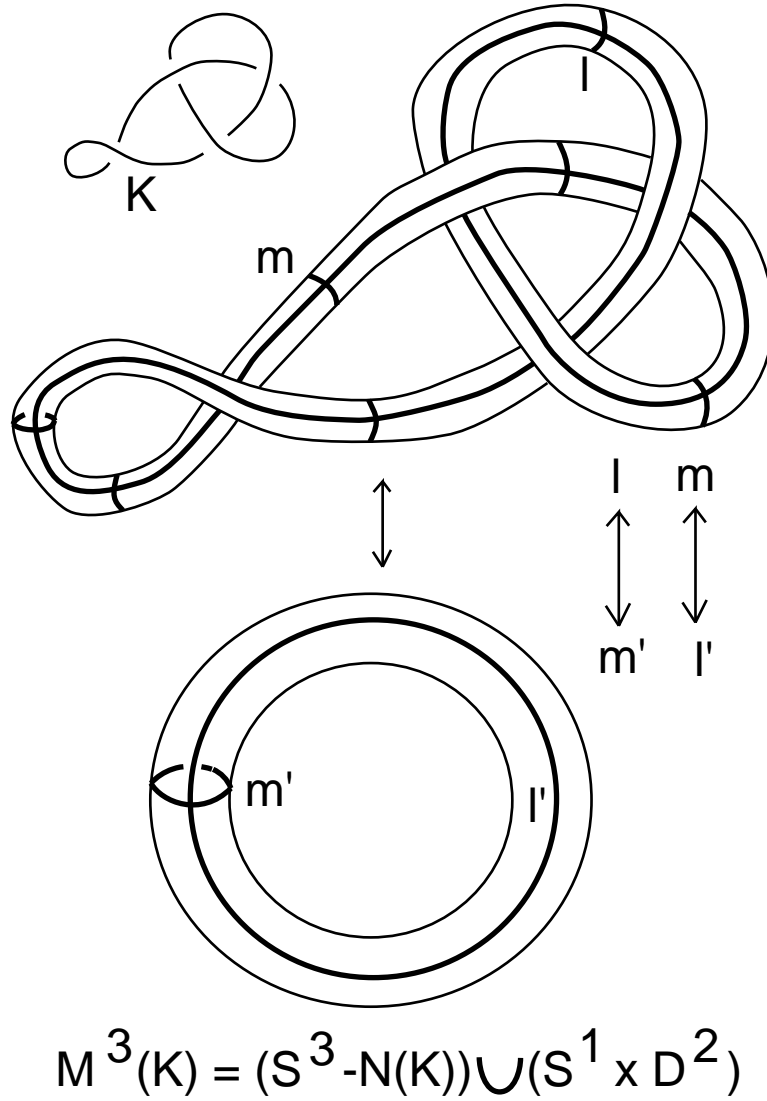


Figure 43 - Surgery on a Blackboard Framed Link

The basic result about Kirby Calculus is that $M^3(K)$ is homeomorphic to $M^3(L)$ if and only if K and L are KC equivalent. Thus invariants of links that are also invariant under Kirby moves will produce invariants of three-manifolds. It is the purpose of this section to sketch one of the approaches to constructing such invariants.

The ideas behind this approach are quite simple. We are given a finite dimensional quasitriangular Hopf algebra A . We associate to A a tensor category $Cat(A)$. The objects in this category are the base field k of the Hopf algebra, and tensor powers of a formal object V . It is assumed that the tensor powers of V are canonically associative and that the tensor product of V with k on either side is canonically isomorphic to V . The morphisms in

$Cat(A)$ are represented by Hopf algebra decorated immersed curves arranged with respect to a vertical direction.

An *immersed curve diagram* is a link diagram where there is no distinction between undercrossings and overcrossings. Segments of the diagram can cross one another transversely as in a standard link diagram, and we can arrange such a diagram with respect to a vertical direction just as we did for link diagrams. A *vertical place* on such a diagram is a point that is not critical with respect to the vertical direction, and is not a crossing. A *decoration* of such an immersed curve diagram consists in a subset of vertical places labelled by elements of the Hopf algebra A . The diagrams can have endpoints and these are either at the bottom of the diagram or at the top (with respect to the vertical). The simplest decorated diagram is a vertical line segment with a label a (corresponding to a element a of the Hopf algebra) in its interior. In the category $Cat(A)$ this segment is regarded as a morphism $[a] : V \longrightarrow V$ where V is the formal object alluded to above. Composition of these morphisms corresponds to multiplication in the algebra: $[a][b] = [ab]$. By convention, we take the order of multiplication from bottom to top with respect to the vertical direction.

A tensor product $a \otimes b$ in $A \otimes A$ is represented by two parallel segments, one decorated by a , the other decorated by b . It is our custom to place the decorations for a and for b at the same level in the diagram. In the Hopf algebra we have the coproduct $\Delta : A \longrightarrow A \otimes A$. We shall write

$$\Delta(a) = \Sigma a_1 \otimes a_2$$

where it is understood that this means that the coproduct of a is a sum over elements of the form $a_1 \otimes a_2$. It is also useful to use a version of the Einstein summation convention and just write

$$\Delta(a) = a_1 \otimes a_2$$

where it is understood that the right hand side is a summation. In diagrams, application of the antipode makes parallel lines with doubled decorations according to the two factors of the coproduct. See Figure 44.

A crossing of two undecorated segments is regarded as a morphism $P : V \otimes V \longrightarrow V \otimes V$. Since the lines interchange, we expect P to behave as the permutation of the two tensor factors. That is, we take the following formula to be axiomatic:

$$P \circ ([a] \otimes [b]) = ([b] \otimes [a]) \circ P.$$

A cap (see Figure 44) is regarded as a morphism from $V \otimes V$ to k , while a cup is regarded as a morphism from k to $V \otimes V$. As in the case of the crossing the relevance of these morphisms to the category is entirely encoded in their properties. The basic property of the cup and the cap is that *if you “slide” a decoration across the maximum or minimum in a counterclockwise turn, then the antipode S of the Hopf algebra is applied to the decoration*. In categorical terms this property says

$$Cup \circ ([a] \otimes 1) = Cup \circ (1 \otimes [Sa])$$

and

$$([Sa] \otimes 1) \circ Cap = (1 \otimes [a]) \circ Cap.$$

These properties and some other naturality properties of the cups and the caps are illustrated in Figure 44. These naturality properties of the flat diagrams include regular homotopy of immersions, as illustrated in Figure 44.

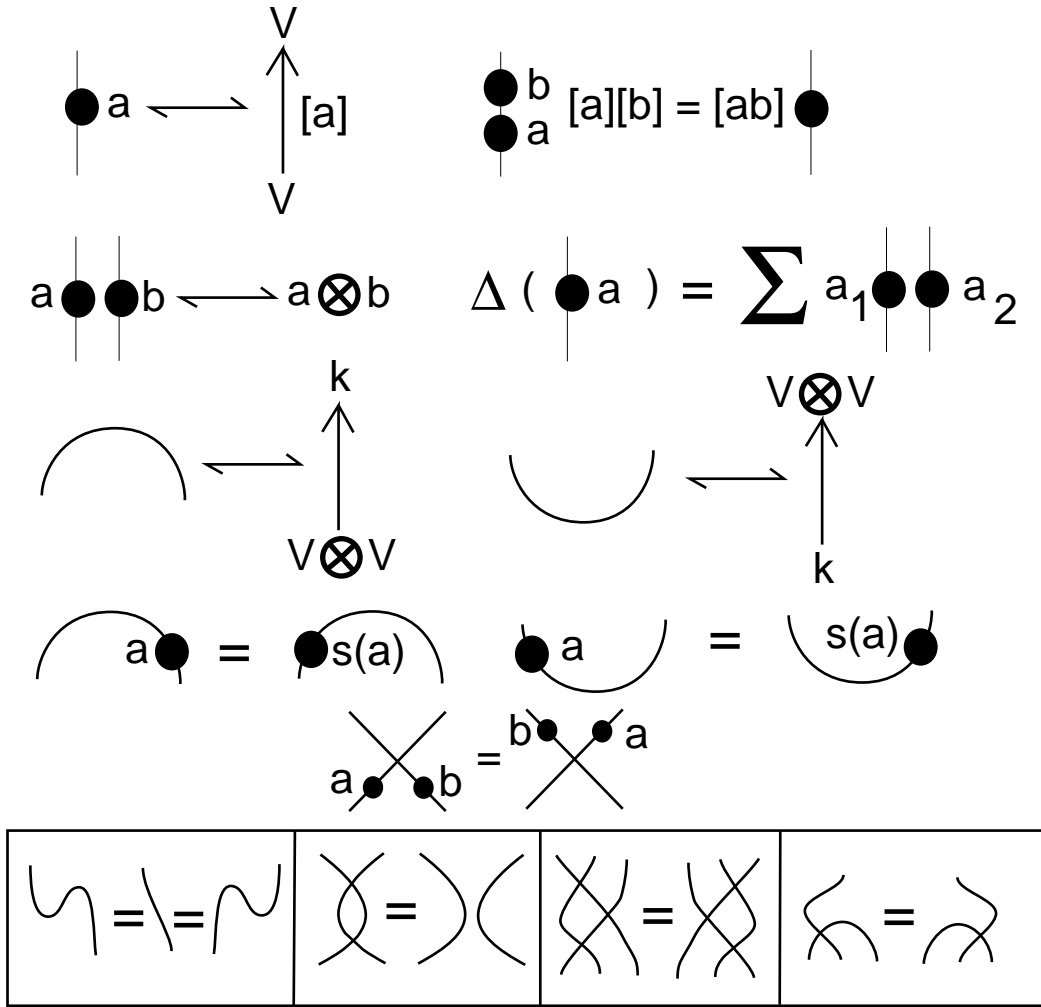


Figure 44 - Morphisms in $Cat(A)$

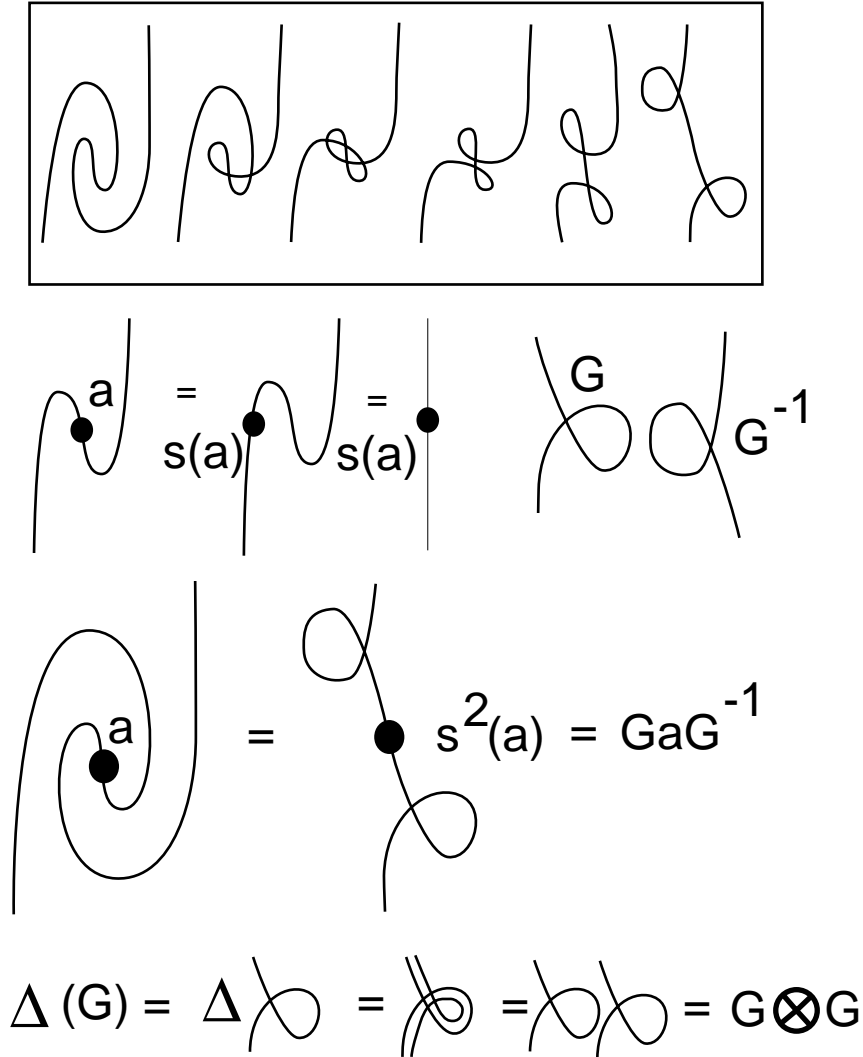


Figure 45 - Diagrammatics of the Antipode

In Figure 45 we see how this property of the cups and the caps leads to a diagrammatic interpretation of the antipode. This, in turn, leads to the interpretation of the flat curl as a grouplike element G in A such that $S^2(a) = GaG^{-1}$ for all a in A . G is a flat curl diagram interpreted as a morphism in the category. We see that formally it is natural to interpret G as an element of A and that $\Delta(G) = G \otimes G$ is a direct consequence of the diagrams for $Cat(A)$. In a so-called *ribbon Hopf algebra* there is such a grouplike already in the algebra. In the general case it is natural to extend the algebra to contain such an element.

We are now in a position to describe a functor F from the tangle category T to $Cat(A)$. (The tangle category is defined for link diagrams without decorations. It has the same objects as $Cat(A)$. The morphisms in the tangle category have relations corresponding to

the augmented Reidemeister moves described in the section on quantum link invariants.) F simply decorates each positive (with respect to the vertical - see Figure 45) crossing of the tangle with the Yang-Baxter element (given by the quasi-triangular Hopf algebra A) $\rho = \Sigma e \otimes e'$ and each negative crossing (with respect to the vertical) with $\rho^{-1} = \Sigma S(e) \otimes e'$. The form of the decoration is indicated in Figure 46.

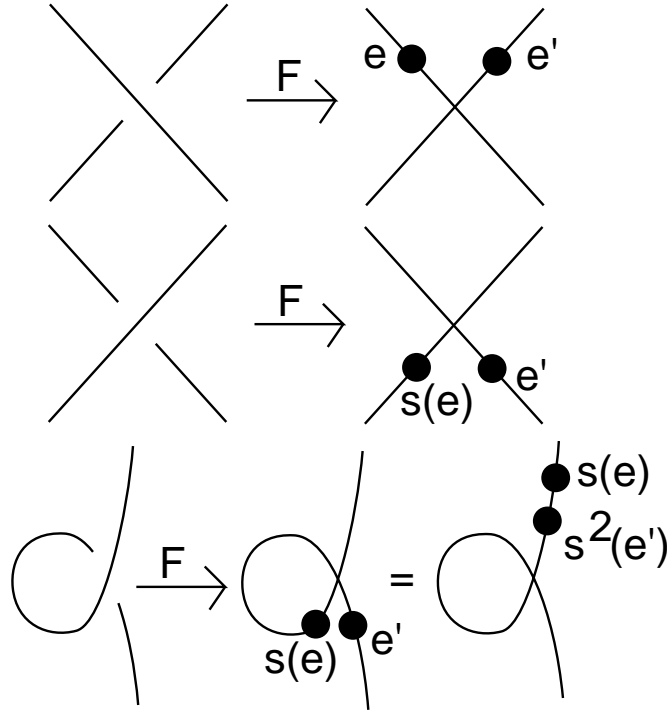


Figure 46 - The Functor $F : T \longrightarrow Cat(A)$.

The key point about this category is that because Hopf algebra elements can be moved around the diagram, we can concentrate all the algebra in one place. Because the flat curls are identified with either G or G^{-1} , we can use regular homotopy of immersions to bring each component of a link diagram to the form of a circle with a single concentrated decoration (involving a sum over many products). An example is shown in Figure 46. Let us denote by $\lambda(a) : k \longrightarrow k$ the morphism that corresponds to decorating the right hand side of a standard circle with a . That is, $\lambda(a) = Cap \circ (1 \otimes [a]) \circ Cup$. We can regard λ as a linear functional defined on A as a vector space over k .

We wish to find out what properties of λ will be appropriate for constructing invariants of three-manifolds. View Figure 47. Handle sliding is accomplished by doubling a component and then band summing. The doubling corresponds to applying the antipode. As a result, we have that in order for λ to be invariant under handle-sliding it is sufficient that it have the property $\lambda(x)1 = \Sigma \lambda(x_1)x_2$. This is the formal defining property of a *right integral*

on the Hopf algebra A . Finite dimensional Hopf algebras have such functionals and suitable normalizations lead to well-defined three-manifold invariants. For more information see the references cited at the beginning of this section. This completes our capsule summary of Hopf algebras and invariants of three-manifolds.

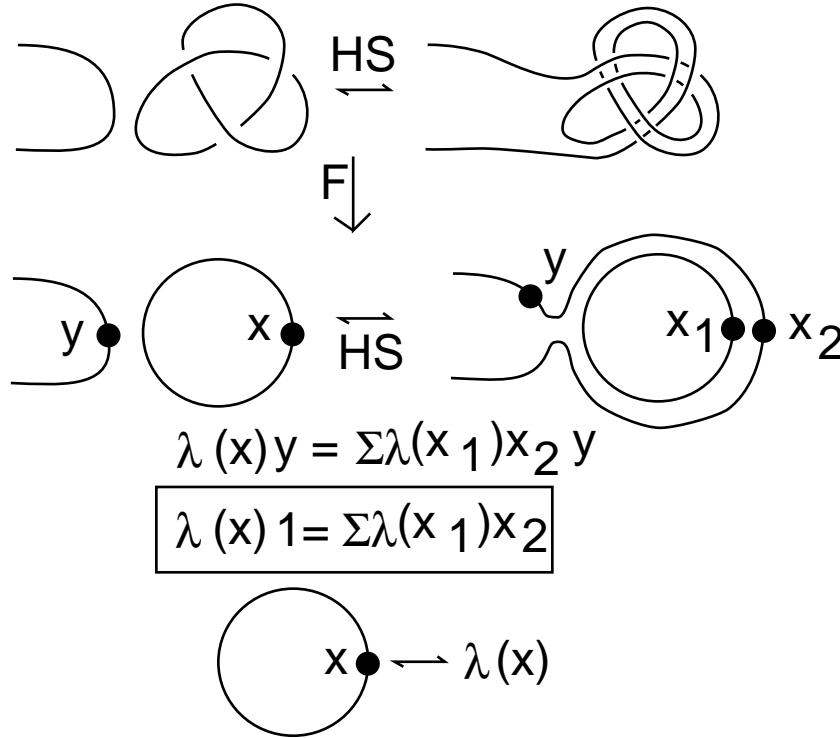


Figure 47 - Handle Sliding and Right Integral

There are a number of problems related to this formulation of invariants of three-manifolds. First of all, while it is the case that the invariants that come from integrals can be different from invariants defined through representations of Hopf algebras as in [133] it is quite difficult to compute them and consequently little is known. Another beautiful problem is related to the work of Greg Kuperberg [100], [101]. Kuperberg defines invariants of three-manifolds associated via Hopf diagrams associated with a Heegard splitting of the three-manifold. Does our invariant on the Drinfeld double of a Hopf algebra H give the same result as Kuperberg's invariant for H ? This conjecture is verified in the (easy) case where H is the group ring of a finite group. Finally, it should be mentioned that the way in which handle-sliding invariance is proven for the universal three-manifold invariant of finite type of Le and Murakami [103] is directly analogous to our method of relating handle sliding, coproduct and right integral. It remains to be seen what is the relationship between three-manifold invariants of finite type and the formulations discussed here.

6 Temperley-Lieb Algebra

This section is devoted to the structure of the Temperley-Lieb algebra as revealed by its diagrammatic interpretation. We begin with a combinatorial description of this algebra. It is customary, in referring to the Temperley-Lieb algebra to refer to a certain free algebra over an appropriate ring. This free algebra is the analog of the group ring of the symmetric group S_n on n letters. It is natural therefore to first describe that multiplicative structure that is analogous to S_n . We shall call this structure the *Temperley-Lieb Monoid* M_n . We shall describe the Temperley-Lieb algebra itself after first defining this monoid.

There is one Temperley-Lieb monoid, M_n , for each natural number n . The *connection elements* of M_n consist in diagrams in the plane that make connections involving two rows of n points. These rows will be referred to as the *top* and *bottom* rows. Each point in a row is paired with a unique point different from itself in either the top or the bottom row (it can be paired with a point in its own row). These pairings are made by arcs drawn in the space between the two rows. *No two arcs are allowed to intersect one another*. Such a connection element will be denoted by U , with subscripts to indicate specific elements. If the top row is the set $Top = \{1, 2, 3, \dots, n\}$ and the bottom row is $Bot = \{1', 2', \dots, n'\}$, then we can regard U as a function from $Top \cup Bot$ to itself such that $U(x)$ is never equal to x , $U(U(x)) = x$ for all x , and satisfying the planar non-intersection property described above. In topological terms U is an n -tangle with no crossings, taken up to regular isotopy of tangles in the plane.

If U and V are two elements of M_n as described above, then their product UV is the tangle product obtained by attaching the bottom row of U to the top row of V . Note that the result of taking such a product will produce a new connection structure plus some loops in the plane. Each loop is regarded as an instance of the *loop element* δ of the Temperley-Lieb monoid M_n . The loop element commutes with all other elements of the monoid and has no other relations with these elements. Thus $UV = \delta^k W$ for some non-negative integer k , and some connection element W of the monoid.

The Temperley-Lieb algebra T_n is the free additive module on M_n modulo the identification

$$\delta = -A^2 - A^{-2},$$

over the ring $Z[A, A^{-1}]$ of Laurent polynomials in the variable A . Products are defined on the connection elements and extended linearly to the algebra. The reason for this loop identification is the application of the Temperley-Lieb algebra for the bracket polynomial and for representations of the braid group [50], [58], [73].

The Temperley-Lieb monoid M_n is generated by the elements $1, U_1, U_2, \dots, U_{n-1}$ where the identity element 1 connects each i in the top row with its corresponding member i' in the bottom row. Here U_k connects i to i' for i not equal to $k, k+1, k', (k+1)'$. U_k connects k to $k+1$ and k' to $(k+1)'$. It is easy to see that

$$U_k^2 = \delta U_k,$$

$$U_k U_{k\pm 1} U_k = U_k,$$

$$U_i U_j = U_j U_i, \quad |i - j| > 1.$$

See Figure 48.

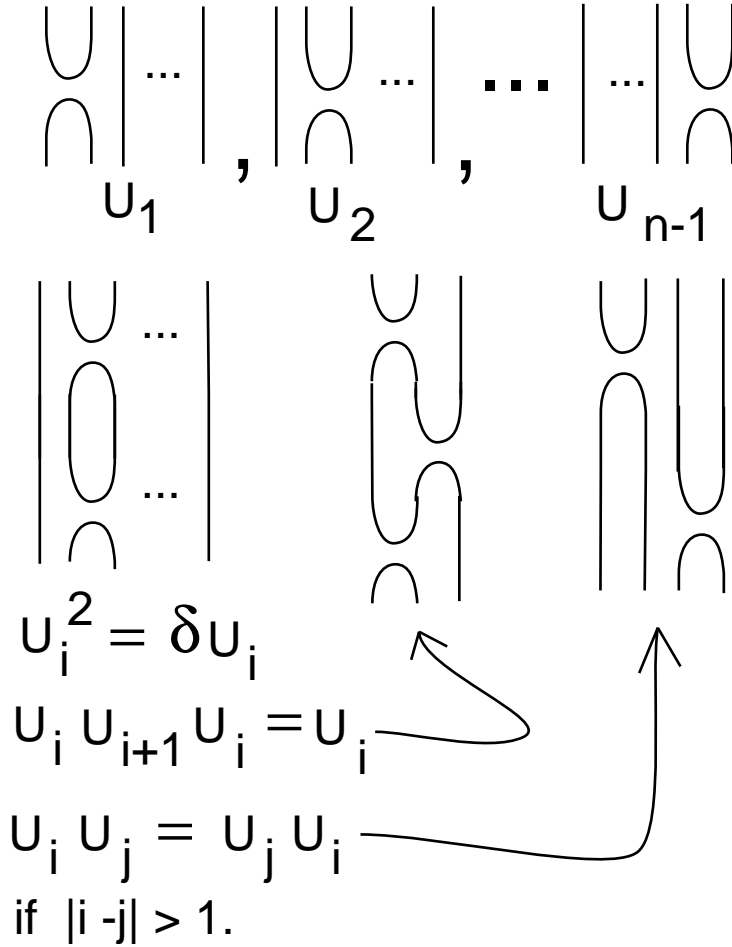


Figure 48 - Relations in the Temperley-Lieb Monoid

We shall prove that the Temperley-Lieb Monoid is the universal monoid on $G_n = \{1, U_1, U_2, \dots, U_{n-1}\}$ modulo these relations. In order to accomplish this end we give a direct diagrammatic method for writing any connection element of the monoid as a certain canonical product of elements of G_n . This method is illustrated in Figure 49.

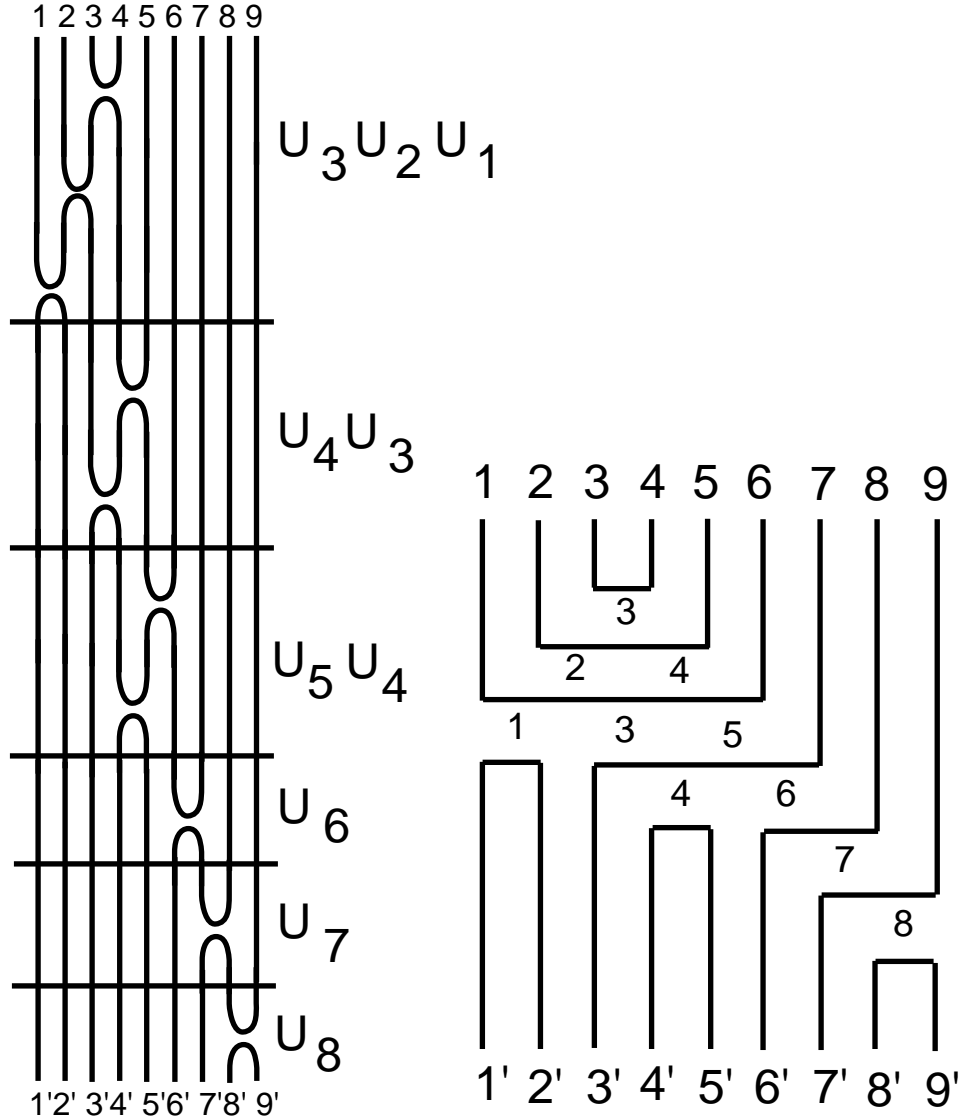


Figure 1 - Figure 49 - Canonical Factorization in the Temperley-Lieb Monoid

As shown in Figure 49, we represent the connection diagram with vertical and horizontal straight arcs such that except for the height of the straight arcs, the form of the connection between any two points is unique - consisting in two vertical arcs and one horizontal arc. The horizontal arc has its endpoints on the vertical lines that go through the row points that are being connected. (Diagram is drawn so that each pair in the set $\{(i, i') : 1 \leq n\}$ determines such a vertical line. The vertical arcs in the connection are chosen as segments from these vertical lines. All connections are chosen so that the connections do not intersect. It is from this diagram that we shall read out a factorization into a product of elements of G_n .

The factorization is achieved via a decoration of the straight arc diagram by dotted vertical arcs, as shown in Figure 49. Each dotted arc connects midpoints of the restrictions of horizontal arcs to the *columns* of the diagram, where a column of the diagram is the space between two consecutive vertical lines (vertical lines described as in the previous paragraph). The *index* of a column is the row number associated to the left vertical boundary of the column. The dotted lines in a given column are uniquely determined by starting at the bottom of the column and pairing up the horizontal arcs in that column in vertical succession. Each dotted arc is labelled by the index of the column in which it stands.

In a given diagram a *sequence* of dotted arcs is a maximal set of dotted arcs (with consecutive indices) that are interconnected by horizontal segments such that one can begin at the top of the dotted arc (in that sequence) of highest index, go down the arc and left to the top of the next arc along a horizontal segment, continuing in this manner until the whole sequence is traversed. It is clear from the construction of the diagram that the dotted segments in the diagram collect into a disjoint union of sequences $\{s^1, s^2, \dots, s^k\}$ where each s^i denotes the corresponding descending sequence of consecutive indices:

$$s^i = (m_i, m_i - 1, m_i - 2, \dots, n_i + 1, n_i).$$

These indices satisfy the inequalities:

$$m_1 < m_2 < m_3 < \dots < m_k$$

and

$$n_1 < n_2 < n_3 < \dots < n_k.$$

The sequences $\{s^1, s^2, \dots, s^k\}$ occur in that order on the diagram read from left to right. Of course the descent of each sequence goes from right to left. If D is a diagram with sequence structure $s(D)$ as we have just described, let $U(s(D))$ be the following product of generators of the Temperley-Lieb monoid:

$$U(D) = U(s^1)U(s^2)U(s^3)\dots U(s^k)$$

where

$$U(s^i) = U_{m_i}U_{m_i-1}\dots U_{n_i+1}U_{n_i}.$$

By looking carefully at the combinatorics of these diagrams, as illustrated in Figure 49, one sees that D and $U(D)$ represent the same connection structure in the Temperley-Lieb monoid. Furthermore, any sequence structure s satisfying the inequalities given above (call these the canonical inequalities) will produce a standard diagram from the product $U(s)$. Thus the sequence structure of a Temperley-Lieb diagram completely classifies this diagram as a connection structure in the monoid.

We must now prove that any product of elements of $G_n = \{1, U_1, U_2, \dots, U_{n-1}\}$ can be written, up to a loop factor, as $U(s(D))$ for some diagram D , or equivalently as $U(s)$ for a sequence structure satisfying the canonical inequalities. This is a simple exercise in using the relations we have already given for the products of elements of G_n . We leave the details to the reader. This completes the proof that the relations in Figure 48 are a complete set of relations for the Temperley-Lieb monoid.

6.1 Parentheses

Elements of the Temperley-Lieb monoid M_n are in one to one correspondence with well-formed parenthesis expressions using n pairs of parentheses. The proof of this statement is shown in Figure 50.

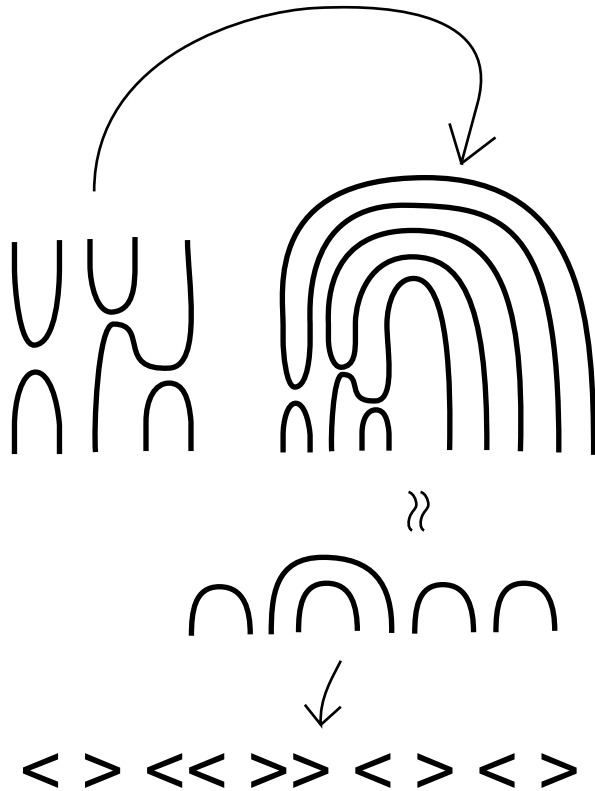


Figure 50 - Creating Parentheses

One result of this reformulation of the Temperley-Lieb monoid is that one can rewrite the product structure in terms of operations on parentheses, getting an interesting formal algebra that encodes properties of the topology of plane curves [72], [60]. In this section we

will take the relationship with parentheses as an excuse to indicate a further relationship with non-associative products.

First consider the abstract structure of non-associative products. They are usually written in the forms:

$$\begin{aligned}
&(a * b) * c \\
&a * (b * c) \\
&((a * b) * c) * d \\
&(a * (b * c)) * d \\
&a * ((b * c) * d) \\
&a * (b * (c * d)) \\
&(a * b) * (c * d)
\end{aligned}$$

In writing products in this standard manner, one sees the same structure of parentheses occurring in different products, as in $((a * b) * c) * d$ and $(a * (b * c)) * d$. In each of these cases if we eliminated the algebraic literals and the operation symbol $*$, we would be left with the parenthetical: $((()))$.

There is another way to write the products so that different products correspond to different arrangements of parentheses. To do this, rewrite the products in the operator notation shown below:

$$\begin{aligned}
a * b &= a(b) \rightsquigarrow () \\
(a * b) * c &= a(b)(c) \rightsquigarrow ()() \\
a * (b * c) &= a(b(c)) \rightsquigarrow (() \\
((a * b) * c) * d &= a(b)(c)(d) \rightsquigarrow ()()() \\
(a * (b * c)) * d &= a(b(c))(d) \rightsquigarrow (()()) \\
a * ((b * c) * d) &= a(b(c)(d)) \rightsquigarrow (()()) \\
a * (b * (c * d)) &= a(b(c(d))) \rightsquigarrow (((())) \\
(a * b) * (c * d) &= a(b)(c(d)) \rightsquigarrow ()(())
\end{aligned}$$

In the operator notation, each product of $n + 1$ terms is uniquely associated with an expression using n pairs of parentheses.

Of course we can replace the expressions in parentheses in terms of nested caps as we did in Figure 50. Once this is done, we notice the very interesting fact that *re-associations* can be visualized in terms of “handle-sliding” at the cap level. The meaning of this remark should be apparent to the reader from Figure 51.

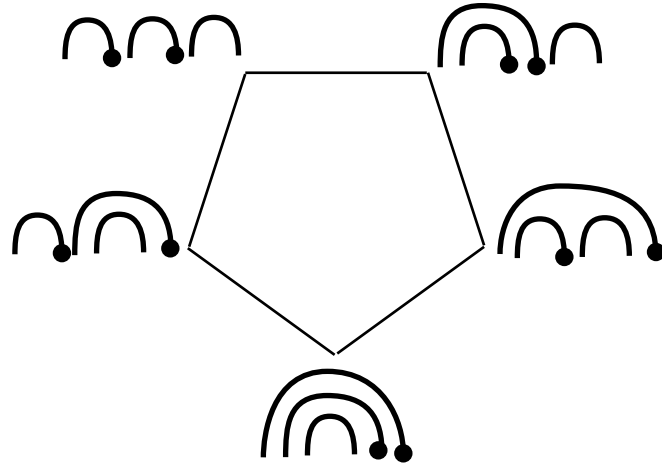
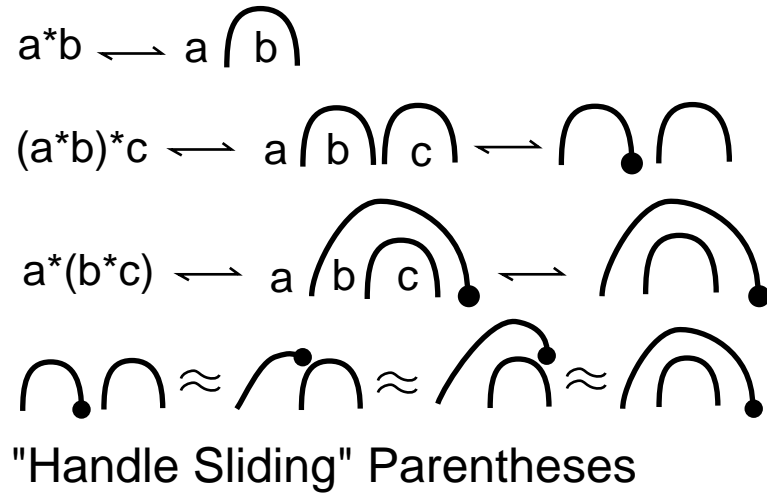


Figure 51 - Pentagon

In Figure 51 we illustrate the pentagon of re-associations of a product of four terms in terms of sliding caps. Notice that we can do this sliding without writing any algebraic literals by labelling the “active” right feet of the caps that do the sliding. In Figure 52 we show the structure of the Stasheff polyhedron with re-associations of five literals in the cap sliding formalism.

Cap sliding is a new formulation of a continuous background for these re-association moves. There is a related continuous background in terms of recoupling formalisms for trees. This formalism is intimately related to many topics in topological quantum field theory. The interested reader will find more about these points of view in [60], [25], [26], in the author’s lecture notes with Scott Carter and Masahico Saito [15] and in his book with Sostenes Lins [73].

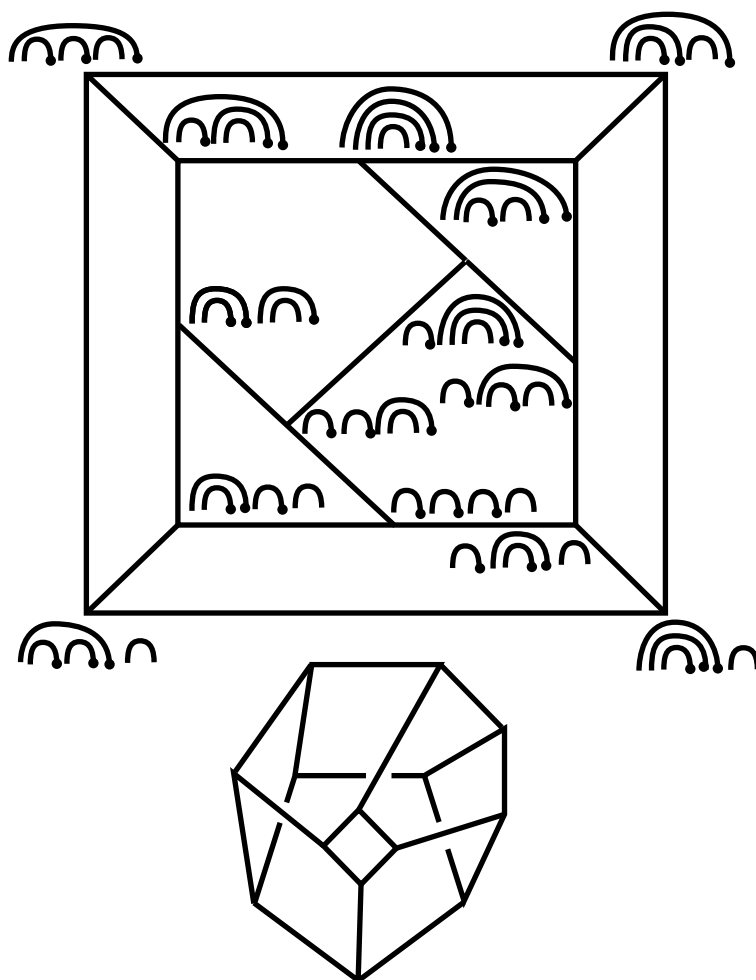


Figure 52 - The Stasheff Polyhedron

7 Virtual Knot Theory

Knot theory studies the embeddings of curves in three-dimensional space. Virtual knot theory studies the embeddings of curves in thickened surfaces of arbitrary genus, up to the addition and removal of empty handles from the surface. Virtual knots have a special diagrammatic theory that makes handling them very similar to the handling of classical knot diagrams. In fact, this diagrammatic theory simply involves adding a new type of crossing to the knot diagrams, a *virtual crossing* that is neither under nor over. From a combinatorial point of view, the virtual crossings are artifacts of the representation of the virtual knot or link in the plane. The extension of the Reidemeister moves that takes care of them respects this viewpoint. A virtual crossing (See Figure 53) is represented by two crossing arcs with a small circle placed around the crossing point.

Moves on virtual diagrams generalize the Reidemeister moves for classical knot and link diagrams. See Figure 53. One can summarize the moves on virtual diagrams by saying that the classical crossings interact with one another according to the usual Reidemeister moves. One adds the detour moves for consecutive sequences of virtual crossings and this completes the description of the moves on virtual diagrams. It is a consequence of moves (B) and (C) in Figure 53 that an arc going through any consecutive sequence of virtual crossings can be moved anywhere in the diagram keeping the endpoints fixed; the places where the moved arc crosses the diagram become new virtual crossings. This replacement is the *detour move*. See Figure 53.1.

One can generalize many structures in classical knot theory to the virtual domain, and use the virtual knots to test the limits of classical problems such as the question whether the Jones polynomial detects knots and the classical Poincaré conjecture. Counterexamples to these conjectures exist in the virtual domain, and it is an open problem whether any of these counterexamples are equivalent (by addition and subtraction of empty handles) to classical knots and links. Virtual knot theory is a significant domain to be investigated for its own sake and for a deeper understanding of classical knot theory.

Another way to understand the meaning of virtual diagrams is to regard them as representatives for oriented Gauss codes (Gauss diagrams) [78, 128]. Such codes do not always have planar realizations and an attempt to embed such a code in the plane leads to the production of the virtual crossings. The detour move makes the particular choice of virtual crossings irrelevant. Virtual equivalence is the same as the equivalence relation generated on the collection of oriented Gauss codes modulo an abstract set of Reidemeister moves on the codes.

One can consider *virtual braids*, generalizing the classical Artin Braid group. We shall not discuss this topic here, but refer the reader to [79, 80, 87, 97, 107].

One intuition for virtual knot theory is the idea of a particle moving in three-dimensional space in a trajectory that occasionally disappears, and then reappears elsewhere. By connecting the disappearance points and the reappearance points with detour lines in the ambient space we get a picture of the motion, but the detours, being artificial, must be treated as subject to replacements.

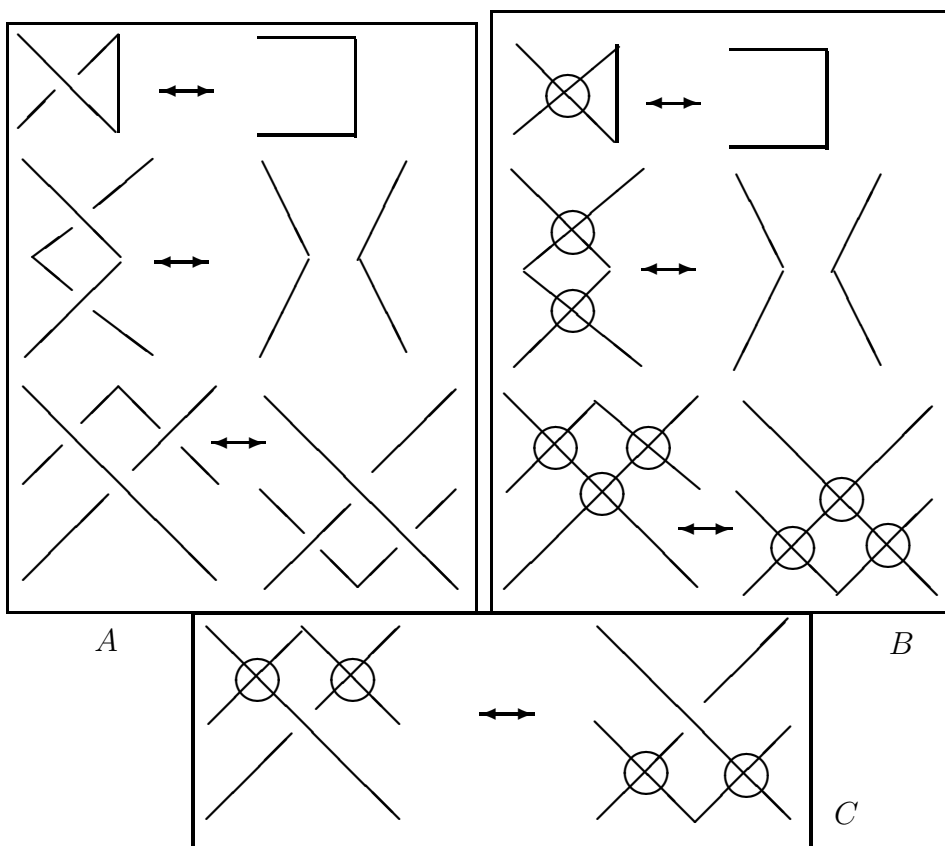


Figure 53 – Generalized Reidemeister Moves for Virtuals

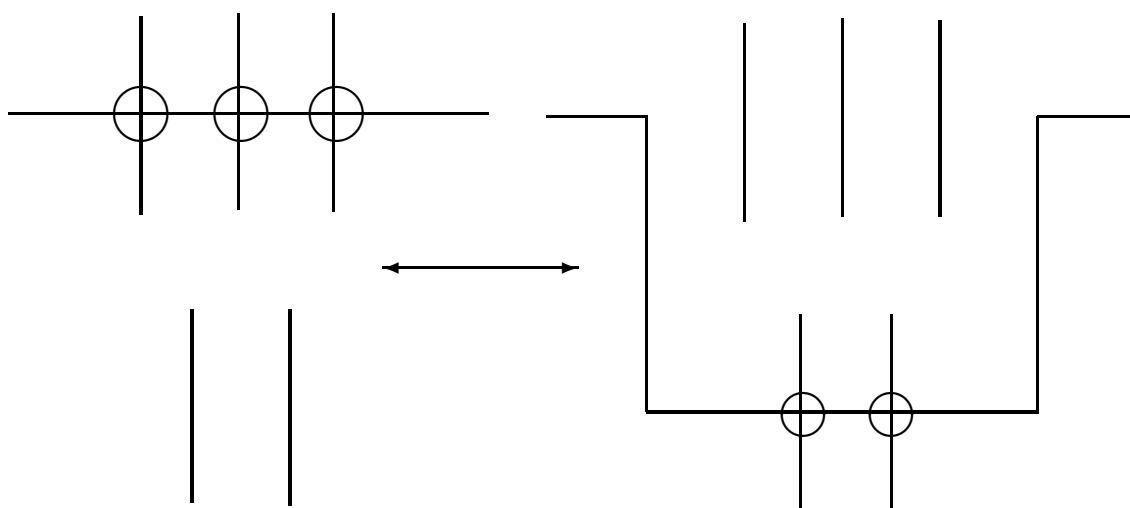


Figure 53.1 – Detour Move

7.1 Flat Virtual Knots and Links

Every classical knot or link diagram can be regarded as a 4-regular plane graph with extra structure at the nodes. This extra structure is usually indicated by the overcrossing and undercrossing conventions that give instructions for constructing an embedding of the link in three-dimensional space from the diagram. If we take the diagram without this extra structure, it is the shadow of some link in three-dimensional space, but the weaving of that link is not specified. It is well known that if one is allowed to apply the Reidemeister moves to such a shadow (without regard to the types of crossing since they are not specified) then the shadow can be reduced to a disjoint union of circles. This reduction is no longer true for virtual links. More precisely, let a *flat virtual diagram* be a diagram with virtual crossings as we have described them and *flat crossings* consisting in undecorated nodes of the 4-regular plane graph. Virtual crossings are flat crossings that have been decorated by a small circle. Two flat virtual diagrams are *equivalent* if there is a sequence of generalized flat Reidemeister moves (as illustrated in Figure 53) taking one to the other. A generalized flat Reidemeister move is any move as shown in Figure 53, but one can ignore the overcrossing or undercrossing structure. Note that in studying flat virtuals the rules for changing virtual crossings among themselves and the rules for changing flat crossings among themselves are identical. However, detour moves as in Figure 53C are available for virtual crossings with respect to flat crossings and not the other way around.

We shall say that a virtual diagram *overlies* a flat diagram if the virtual diagram is obtained from the flat diagram by choosing a crossing type for each flat crossing in the virtual diagram. To each virtual diagram K there is an associated flat diagram $F(K)$ that is obtained by forgetting the extra structure at the classical crossings in K . Note that if K is equivalent to K' as virtual diagrams, then $F(K)$ is equivalent to $F(K')$ as flat virtual diagrams. Thus, if we can show that $F(K)$ is not reducible to a disjoint union of circles, then it will follow that K is a non-trivial virtual link.

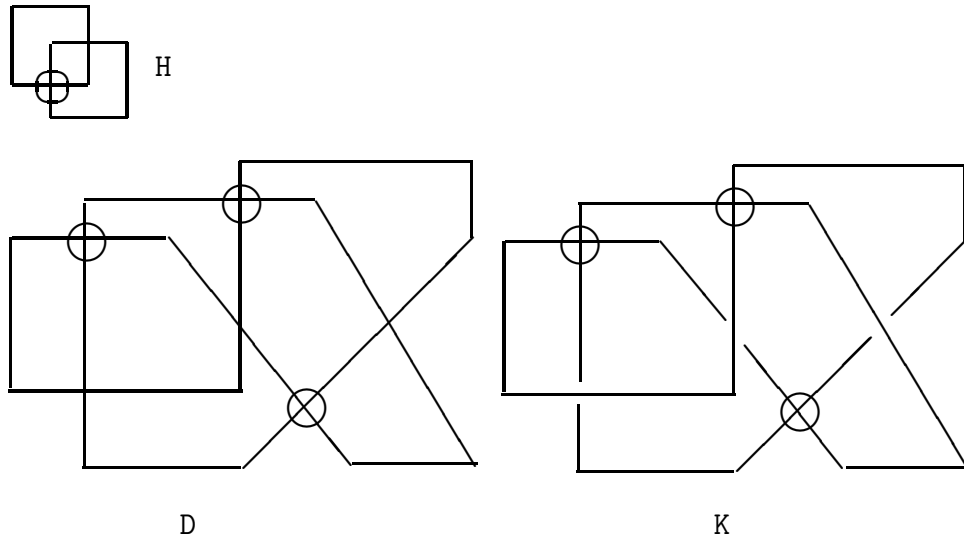


Figure 54 – Flats H and D , and the knot K .

Figure 54 illustrates an example of a flat virtual link H . This link cannot be undone in the flat category because it has an odd number of virtual crossings between its two components and each generalized Reidemeister move preserves the parity of the number of virtual crossings between components. Also illustrated in Figure 54 is a flat diagram D and a virtual knot K that overlies it. This example is given in [78]. The knot shown is undetectable by many invariants (fundamental group, Jones polynomial) but it is knotted and this can be seen either by using a generalization of the Alexander polynomial that we describe below, or by showing that the underlying diagram D is a non-trivial flat virtual knot using the filamentation invariant that is introduced in [47]. The filamentation invariant is a combinatorial method that is sometimes successful in indentifying irreducible flat virtuals. At this writing we know very few invariants of flat virtuals. The flat virtual diagrams present a strong challenge for the construction of new invariants. It is important to understand the structure of flat virtual knots and links. This structure lies at the heart of the comparison of classical and virtual links. We wish to be able to determine when a given virtual link is equivalent to a classical link. The reducibility or irreducibility of the underlying flat diagram is the first obstruction to such an equivalence.

7.2 Interpretation of Virtuals as Stable Classes of Links in Thickened Surfaces

There is a useful topological interpretation for this virtual theory in terms of embeddings of links in thickened surfaces. See [78, 80, 102]. Regard each virtual crossing as a shorthand for a detour of one of the arcs in the crossing through a 1-handle that has been attached to the 2-sphere of the original diagram. By interpreting each virtual crossing in this way, we obtain an embedding of a collection of circles into a thickened surface $S_g \times R$ where g is the number of virtual crossings in the original diagram L , S_g is a compact oriented surface of genus g and R denotes the real line. We say that two such surface embeddings are *stably equivalent* if one can be obtained from another by isotopy in the thickened surfaces, homeomorphisms of the surfaces and the addition or subtraction of empty handles. Then we have the

Theorem [78, 89, 102]. *Two virtual link diagrams are equivalent if and only if their correspondent surface embeddings are stably equivalent.*

Virtual knots and links give rise to a host of problems. As we saw in the previous section, there are non-trivial virtual knots with unit Jones polynomial. Moreover, there are non-trivial virtual knots with integer fundamental group and trivial Jones polynomial. (The fundamental group is defined combinatorially by generalizing the Wirtinger presentation.) These phenomena underline the question of how planarity is involved in the way the Jones polynomial appears to detect classical knots, and that the relationship of the fundamental group (and peripheral system) is a much deeper one than the surface combinatorics for

classical knots. It is possible to take the connected sum of two trivial virtual diagrams and obtain a non-trivial virtual knot (the Kishino knot).

Here long knots (or, equivalently $1 - 1$ tangles) come into play. Having a knot, we can break it at some point and take its ends to infinity (say, in a way that they coincide with the horizontal axis line in the plane). One can study isotopy classes of such knots. A well-known theorem says that in the classical case, knot theory coincides with long knot theory. However, this is not the case for virtual knots. By breaking the same virtual knot at different points, one can obtain non-isotopic long knots [34]. Furthermore, even if the initial knot is trivial, the resulting long knot may not be trivial. The “connected sum” of two trivial virtual diagrams may not be trivial in the compact case. The phenomenon occurs because these two knot diagrams may be non-trivial in the long category. It is sometimes more convenient to consider long virtual knots rather than compact virtual knots, since connected sum is well-defined for long knots. It is important to construct long virtual knot invariants to see whether long knots are trivial and whether they are classical. One approach is to regard long knots as $1 - 1$ tangles and use extensions of standard invariants (fundamental group, quandle, biquandle, etc). Another approach is to distinguish two types of crossings: those having early undercrossing and those having later undercrossing with respect to the orientation of the long knot. The latter technique is described in [120].

Unlike classical knots, the connected sum of long knots is not commutative. Thus, if we show that two long knots K_1 and K_2 do not commute, then we see that they are different and both non-classical.

A typical example of such knots is the two parts of the Kishino knot, see Figure 54.1.

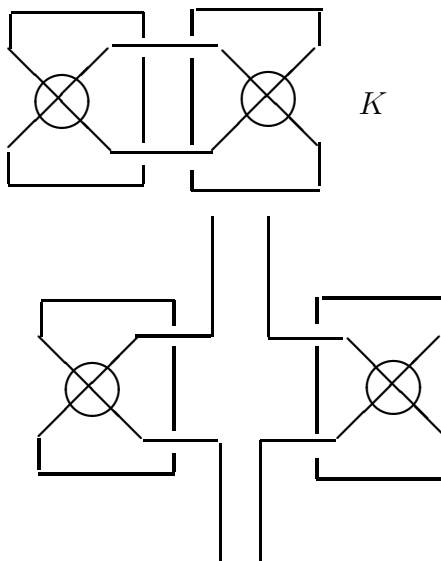


Figure 54.1 – Kishino and Parts

We have a natural map

$$\langle \text{Long virtual knots} \rangle \rightarrow \langle \text{Oriented compact virtual knots} \rangle,$$

obtained by taking two infinite ends of the long knots together to make a compact knot. This map is obviously well defined and allows one to construct (weak) long virtual knot invariants from classical invariants (by regarding compact knot invariants as long knot invariants). There is no well-defined inverse for this map. But, if we were able to construct the map from compact virtual knots to long virtual knots, we could apply the long techniques for the compact case. This map does have an inverse for classical knots. Thus, the long techniques are applicable to classical (long) knots. It would be interesting to obtain new classical invariants from it. The long category can also be applied in the case of flat virtuals, where all problems formulated above occur as well.

There are examples of virtual knots that are very difficult to prove knotted, and there are infinitely many flat virtual diagrams that appear to be irreducible, but we have no techniques to prove it. How can one tell whether a virtual knot is classical? One can ask: Are there non-trivial virtual knots whose connected sum is trivial? The latter question cannot be shown by classical techniques, but it can be analyzed by using the surface interpretation for virtuals. See [121].

In respect to virtual knots, we are in the same position as the compilers of the original knot tables. We are, in fact, developing tables. At Sussex, tables of virtual knots are being constructed, and tables will appear in a book being written by Kauffman and Manturov. The website “Knotilus” has tables as do websites developed by Zinn-Justin and Zuber. The theory of invariants of virtual knots, needs more development. Flat virtuals (whose study is a generalization of the classification of immersions) are a nearly unknown territory (but see [47, 151]). The flat virtuals provide the deepest challenge since we have very few invariants to detect them.

7.3 Jones Polynomial of Virtual Knots

We use a generalization of the bracket state summation model for the Jones polynomial to extend it to virtual knots and links. We call a diagram in the plane *purely virtual* if the only crossings in the diagram are virtual crossings. Each purely virtual diagram is equivalent by the virtual moves to a disjoint collection of circles in the plane.

Given a link diagram K , a state S of this diagram is obtained by choosing a smoothing for each crossing in the diagram and labelling that smoothing with either A or A^{-1} according to the convention that a counterclockwise rotation of the overcrossing line sweeps two regions labelled A , and that a smoothing that connects the A regions is labelled by the letter A . Then, given a state S , one has the evaluation $\langle K|S \rangle$ equal to the product of

the labels at the smoothings, and one has the evaluation $||S||$ equal to the number of loops in the state (the smoothings produce purely virtual diagrams). One then has the formula

$$\langle K \rangle = \sum_S \langle K|S \rangle d^{||S||-1}$$

where the summation runs over the states S of the diagram K , and $d = -A^2 - A^{-2}$. This state summation is invariant under all classical and virtual moves except the first Reidemeister move. The bracket polynomial is normalized to an invariant $f_K(A)$ of all the moves by the formula $f_K(A) = (-A^3)^{-w(K)} \langle K \rangle$ where $w(K)$ is the writhe of the (now) oriented diagram K . The writhe is the sum of the orientation signs (± 1) of the crossings of the diagram. The Jones polynomial, $V_K(t)$, is given in terms of this model by the formula

$$V_K(t) = f_K(t^{-1/4}).$$

The reader should note that this definition is a direct generalization to the virtual category of the state sum model for the original Jones polynomial [58]. It is straightforward to verify the invariances stated above. In this way one has the Jones polynomial for virtual knots and links.

In terms of the interpretation of virtual knots as stabilized classes of embeddings of circles into thickened surfaces, our definition coincides with the simplest version of the Jones polynomial for links in thickened surfaces. In that version one counts all the loops in a state the same way, with no regard for their isotopy class in the surface. It is this equal treatment that makes the invariance under handle stabilization work. With this generalized version of the Jones polynomial, one has again the problem of finding a geometric/topological interpretation of this invariant. There is no fully satisfactory topological interpretation of the original Jones polynomial and the problem is inherited by this generalization.

We have [80] the

Theorem. *To each non-trivial classical knot diagram of one component K there is a corresponding non-trivial virtual knot diagram $\text{Virt}(K)$ with unit Jones polynomial.*

This Theorem is a key ingredient in the problems involving virtual knots. Here is a sketch of its proof. The proof uses two invariants of classical knots and links that generalize to arbitrary virtual knots and links. These invariants are the *Jones polynomial* and the *involutory quandle* denoted by the notation $IQ(K)$ for a knot or link K .

Given a crossing i in a link diagram, we define $s(i)$ to be the result of *switching* that crossing so that the undercrossing arc becomes an overcrossing arc and vice versa. We also define the *virtualization* $v(i)$ of the crossing by the local replacement indicated in Figure 55. In this Figure we illustrate how in the virtualization of the crossing the original crossing is replaced by a crossing that is flanked by two virtual crossings.

Suppose that K is a (virtual or classical) diagram with a classical crossing labeled i . Let $K^{v(i)}$ be the diagram obtained from K by virtualizing the crossing i while leaving the

rest of the diagram just as before. Let $K^{s(i)}$ be the diagram obtained from K by switching the crossing i while leaving the rest of the diagram just as before. Then it follows directly from the definition of the Jones polynomial that

$$V_{K^{s(i)}}(t) = V_{K^{v(i)}}(t).$$

As far as the Jones polynomial is concerned, switching a crossing and virtualizing a crossing look the same.

The involutory quandle [64] is an algebraic invariant equivalent to the fundamental group of the double branched cover of a knot or link in the classical case. In this algebraic system one associates a generator of the algebra $IQ(K)$ to each arc of the diagram K and there is a relation of the form $c = ab$ at each crossing, where ab denotes the (non-associative) algebra product of a and b in $IQ(K)$. See Figure 56. In this Figure we have illustrated through the local relations the fact that

$$IQ(K^{v(i)}) = IQ(K).$$

As far the involutory quandle is concerned, the original crossing and the virtualized crossing look the same.

If a classical knot is actually knotted, then its involutory quandle is non-trivial [155]. Hence if we start with a non-trivial classical knot, we can virtualize any subset of its crossings to obtain a virtual knot that is still non-trivial. There is a subset A of the crossings of a classical knot K such that the knot SK obtained by switching these crossings is an unknot. Let $Virt(K)$ denote the virtual diagram obtained from A by virtualizing the crossings in the subset A . By the above discussion the Jones polynomial of $Virt(K)$ is the same as the Jones polynomial of SK , and this is 1 since SK is unknotted. On the other hand, the IQ of $Virt(K)$ is the same as the IQ of K , and hence if K is knotted, then so is $Virt(K)$. We have shown that $Virt(K)$ is a non-trivial virtual knot with unit Jones polynomial. This completes the proof of the Theorem.

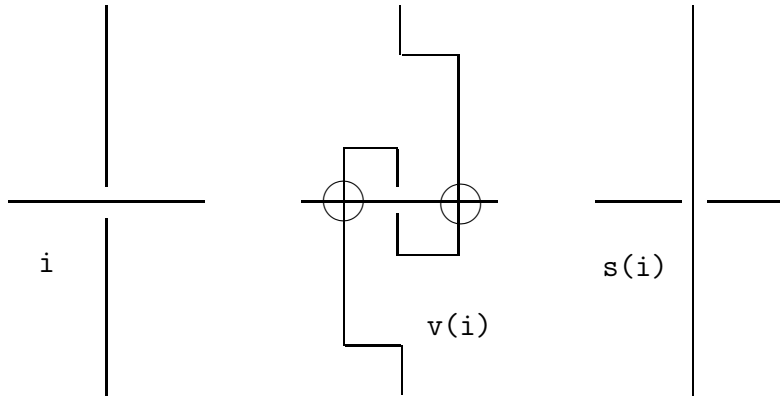


Figure 55 – Switching and Virtualizing a Crossing

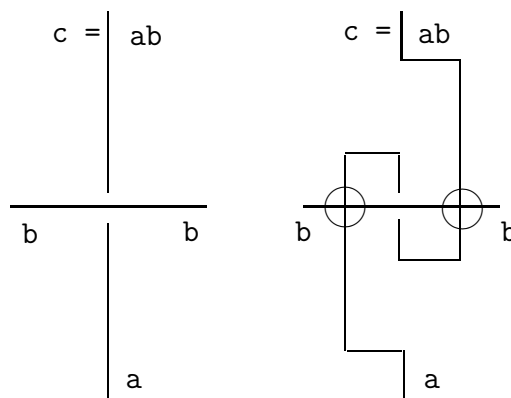


Figure 56 – $IQ(Virt(K)) = IQ(K)$

If there exists a classical knot with unit Jones polynomial, then one of the knots $Virt(K)$ produced by this theorem may be equivalent to a classical knot. It is an intricate task to verify that specific examples of $Virt(K)$ are not classical. This has led to an investigation of new invariants for virtual knots. In this investigation a number of issues appear. One can examine the combinatorial generalization of the fundamental group (or quandle) of the virtual knot and sometimes one can prove by pure algebra that the resulting group is not classical. This is related to observations by Silver and Williams [139], Manturov [112, 113] and by Satoh [135] showing that the fundamental group of a virtual knot can be interpreted as the fundamental group of the complement of a torus embedded in four-dimensional Euclidean space. A very fruitful line of new invariants comes about by examining a generalization of the fundamental group or quandle that we call the *biquandle* of the virtual knot. The biquandle is discussed in the next Section. Invariants of flat knots (when one has them) are useful in this regard. If we can verify that the flat knot $F(Virt(K))$ is non-trivial, then $Virt(K)$ is non-classical. In this way the search for classical knots with unit Jones polynomial expands to the exploration of the structure of the infinite collection of virtual knots with unit Jones polynomial.

Another way of putting this theorem is as follows: In the arena of knots in thickened surfaces there are many examples of knots with unit Jones polynomial. Might one of these be equivalent via handle stabilization to a classical knot? In [102] Kuperberg shows the uniqueness of the embedding of minimal genus in the stable class for a given virtual link. The minimal embedding genus can be strictly less than the number of virtual crossings in a diagram for the link. There are many problems associated with this phenomenon.

There is a generalization of the Jones polynomial that involves surface representation of virtual knots. See [29, 30, 114, 109]. These invariants essentially use the fact that the Jones polynomial can be extended to knots in thickened surfaces by keeping track of the isotopy classes of the loops in the state summation for this polynomial. In the approach of Dye and Kauffman, one uses this generalized polynomial directly. In the approach of Manturov, a polynomial invariant is defined using the stabilization description of the virtual knots.

7.4 Biquandles

In this section we give a sketch of some recent approaches to invariants of virtual knots and links.

A *biquandle* [17, 80, 34, 84, 8, 9] is an algebra with 4 binary operations written $a^b, a_b, a^{\bar{b}}, a_{\bar{b}}$ together with some relations which we will indicate below. The *fundamental* biquandle is associated with a link diagram and is invariant under the generalized Reidemeister moves for virtual knots and links. The operations in this algebra are motivated by the formation of labels for the edges of the diagram. View Figure 57. In this Figure we have shown the format for the operations in a biquandle. The overcrossing arc has two labels, one on each side of the crossing. There is an algebra element labeling each *edge* of the diagram. An edge of the diagram corresponds to an edge of the underlying plane graph of that diagram.

Let the edges oriented toward a crossing in a diagram be called the *input* edges for the crossing, and the edges oriented away from the crossing be called the *output* edges for the crossing. Let a and b be the input edges for a positive crossing, with a the label of the undercrossing input and b the label on the overcrossing input. In the biquandle, we label the undercrossing output by

$$c = a^b,$$

while the overcrossing output is labeled

$$d = b_a.$$

The labelling for the negative crossing is similar using the other two operations. To form the fundamental biquandle, $BQ(K)$, we take one generator for each edge of the diagram and two relations at each crossing (as described above).

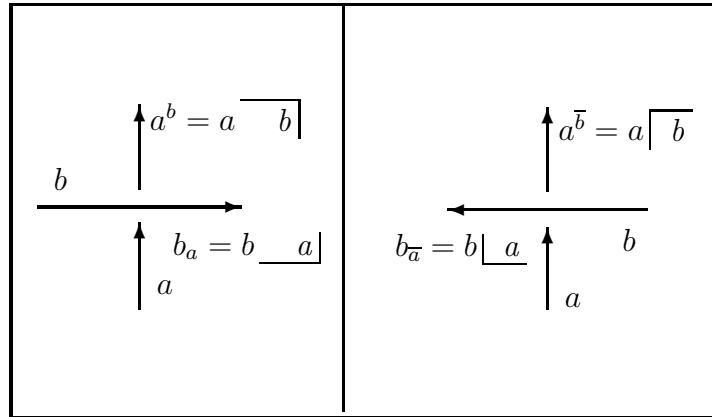


Figure 57 – Biquandle Relations at a Crossing

Another way to write this formalism for the biquandle is as follows:

$$\begin{aligned} a^b &= a \overline{} b \big] \\ a_b &= a \underline{} b \big] \\ a^{\bar{b}} &= a \big[\overline{} b \\ a_{\bar{b}} &= a \big[\underline{} b. \end{aligned}$$

We call this the *operator formalism* for the biquandle.

These considerations lead to the following definition.

Definition. A *biquandle* B is a set with four binary operations indicated above: $a^b, a^{\bar{b}}, a_b, a_{\bar{b}}$. We shall refer to the operations with barred variables as the *left* operations and the operations without barred variables as the *right* operations. The biquandle is closed under these operations and the following axioms are satisfied:

1. Given an element a in B , then there exists an x in the biquandle such that $x = a_x$ and $a = x^a$. There also exists a y in the biquandle such that $y = a^{\bar{y}}$ and $a = y_{\bar{a}}$.
2. For any elements a and b in B we have

$$a = a^{b\bar{b}_a} \quad \text{and} \quad b = b_{a\bar{a}^b} \quad \text{and}$$

$$a = a^{\bar{b}b_{\bar{a}}} \quad \text{and} \quad b = b_{\bar{a}\bar{a}^{\bar{b}}}.$$

3. Given elements a and b in B then there exist elements x, y, z, t such that $x_b = a$, $y^{\bar{a}} = b$, $b^x = y$, $a_{\bar{y}} = x$ and $t^a = b$, $a_t = z$, $z_{\bar{b}} = a$, $b^{\bar{z}} = t$. The biquandle is called *strong* if x, y, z, t are uniquely defined and we then write $x = a_{b^{-1}}$, $y = b^{\bar{a}^{-1}}$, $t = b^{a^{-1}}$, $z = a_{\bar{b}^{-1}}$, reflecting the inversive nature of the elements.
4. For any a, b, c in B the following equations hold and the same equations hold when all right operations are replaced in these equations by left operations.

$$a^{bc} = a^{c_b b^c}, \quad c_{ba} = c_{a^b b_a}, \quad (b_a)^{c_{ab}} = (b^c)_{a^{c_b}}.$$

These axioms are transcriptions of the Reidemeister moves. The first axiom transcribes the first Reidemeister move. The second axiom transcribes the directly oriented second Reidemeister move. The third axiom transcribes the reverse oriented Reidemeister move. The fourth axiom transcribes the third Reidemeister move. Much more work is needed in exploring these algebras and their applications to knot theory.

We may simplify the appearance of these conditions by defining

$$S(a, b) = (b_a, a^b), \quad \overline{S}(a, b) = (\overline{b^a}, \overline{a_b})$$

and in the case of a strong biquandle,

$$S_{-}^{+}(a, b) = (b^{a_{b^{-1}}}, a_{b^{-1}}), \quad S_{+}^{-}(a, b) = (b^{a^{-1}}, a_{b^{a^{-1}}})$$

and

$$\overline{S}_{-}^{+}(a, b) = (b_{\overline{a_{b^{-1}}}}, \overline{a^{b^{-1}}}) = (b_{\overline{a_{b^{a^{-1}}}}}, \overline{a^{b_{a^{-1}}}})$$

and

$$\overline{S}_{+}^{-}(a, b) = (b_{\overline{a^{-1}}}, \overline{a^{b_{a^{-1}}}}) = (b_{\overline{a_{b^{-1}}}}, \overline{a^{b_{a_{b^{-1}}}}})$$

which we call the *sideways* operators. The conditions then reduce to

$$S\overline{S} = \overline{S}S = 1,$$

$$(S \times 1)(1 \times S)(S \times 1) = (1 \times S)(S \times 1)(1 \times S)$$

$$\overline{S}_{+}^{-}S_{-}^{+} = S_{+}^{-}\overline{S}_{-}^{+} = 1$$

and finally all the sideways operators leave the diagonal

$$\Delta = \{(a, a) | a \in X\}$$

invariant.

7.5 The Alexander Biquandle

It is not hard to see that the following equations in a module over $Z[s, s^{-1}, t, t^{-1}]$ give a biquandle structure.

$$\begin{aligned} a^b &= a \overline{b} = ta + (1 - st)b, & a_b &= a \underline{b} = sa \\ a^{\overline{b}} &= a \overline{\overline{b}} = t^{-1}a + (1 - s^{-1}t^{-1})b, & a_{\overline{b}} &= a \underline{\underline{b}} = s^{-1}a. \end{aligned}$$

We shall refer to this structure, with the equations given above, as the *Alexander Biquandle*.

Just as one can define the Alexander Module of a classical knot, we have the Alexander Biquandle of a virtual knot or link, obtained by taking one generator for each *edge* of the projected graph of the knot diagram and taking the module relations in the above linear form. Let $ABQ(K)$ denote this module structure for an oriented link K . That is, $ABQ(K)$ is the module generated by the edges of the diagram, factored by the submodule generated by the relations. This module then has a biquandle structure specified by the operations defined above for an Alexander Biquandle.

The determinant of the matrix of relations obtained from the crossings of a diagram gives a polynomial invariant (up to multiplication by $\pm s^i t^j$ for integers i and j) of knots and links that we denote by $G_K(s, t)$ and call the *generalized Alexander polynomial*. **This polynomial vanishes on classical knots, but is remarkably successful at detecting virtual knots and links.** In fact $G_K(s, t)$ is the same as the polynomial invariant of virtuals of Sawollek [136] and defined by an alternative method by Silver and Williams [139]. It is a reformulation of the invariant for knots in surfaces due to the principal investigator, Jaeger and Saleur [66, 65].

We end this discussion of the Alexander Biquandle with two examples that show clearly its limitations. View Figure 58. In this Figure we illustrate two diagrams labeled K and KI . It is not hard to calculate that both $G_K(s, t)$ and $G_{KI}(s, t)$ are equal to zero. However, The Alexander Biquandle of K is non-trivial – it is isomorphic to the free module over $Z[s, s^{-1}, t, t^{-1}]$ generated by elements a and b subject to the relation $(s^{-1} - t - 1)(a - b) = 0$. Thus K represents a non-trivial virtual knot. This shows that it is possible for a non-trivial virtual diagram to be a connected sum of two trivial virtual diagrams. However, the diagram KI has a trivial Alexander Biquandle. In fact the diagram KI , discovered by Kishino [20], is now known to be knotted and its general biquandle is non-trivial. The Kishino diagram has been shown non-trivial by a calculation of the three-strand Jones polynomial [94], by the surface bracket polynomial of Dye and Kauffman [29, 30], by the Ξ -polynomial (the surface generalization of the Jones polynomial of Manturov [114], and its biquandle has been shown to be non-trivial by a quaternionic biquandle representation [8] of Fenn and Bartholomew which we will now briefly describe.

Referring back to the previous section define the linear biquandle by

$$S = \begin{pmatrix} 1+i & jt \\ -jt^{-1} & 1+i \end{pmatrix},$$

where i, j have their usual meanings as quaternions and t is a central variable. Let R denote the ring which they determine. Then as in the Alexander case considered above, for each diagram there is a square presentation of an R -module. We can take the (Study) determinant of the presentation matrix. In the case of the Kishino knot this is zero. However the greatest common divisor of the codimension 1 determinants is $2 + 5t^2 + 2t^4$ showing that this knot is not classical.

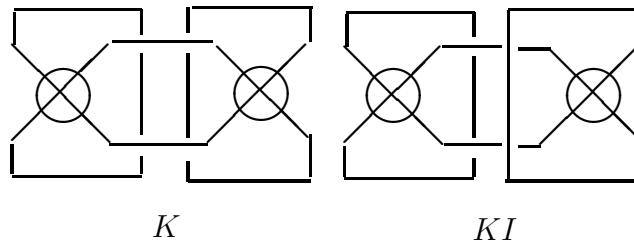


Figure 58 – The Knot K and the Kishino Diagram KI

7.5.1 Virtual quandles

There is another generalization of quandle [108] by means of which one can obtain the same polynomial as in [139, 136] from the other point of view [112, 113]. Namely, the formalism is the same as in the case of quandles at classical crossings but one adds a special structure at virtual crossings. The fact that these approaches give the same result in the linear case was proved recently by Roger Fenn and Andrew Bartholomew.

Virtual quandles (as well as biquandles) yield generalizations of the fundamental group and some other invariants. Also, virtual biquandles admit a generalization for multi-variable polynomials in the case of multicomponent links, see [112]. One can extend these definitions by bringing together the virtual quandle (at virtual crossings) and the biquandle (at classical crossings) to obtain what is called a *virtual biquandle*; this work is now in process, [90].

7.6 A Quantum Model for $G_K(s, t)$, Oriented and Bi-oriented Quantum Algebras

We can understand the structure of the invariant $G_K(s, t)$ by rewriting it as a quantum invariant and then analysing its state summation. The quantum model for this invariant is obtained in a fashion analogous to the construction of a quantum model of the Alexander polynomial in [65, 66]. The strategy in those papers was to take the basic two-dimensional matrix of the Burau representation, view it as a linear transformation $T : V \rightarrow V$ on a two-dimensional module V , and then take the induced linear transformation $\hat{T} : \Lambda^* V \rightarrow \Lambda^* V$ on the exterior algebra of V . This gives a transformation on a four-dimensional module that is a solution to the Yang-Baxter equation. This solution of the Yang-Baxter equation then becomes the building block for the corresponding quantum invariant. In the present instance, we have a generalization of the Burau representation, and this same procedure can be applied to it.

The normalized state summation $Z(K)$ obtained by the above process satisfies a skein relation that is just like that of the Conway polynomial: $Z(K_+) - Z(K_-) = zZ(K_0)$. The basic result behind the correspondence of $G_K(s, t)$ and $Z(K)$ is the

Theorem [84]. *For a (virtual) link K , the invariants $Z(K)(\sigma = \sqrt{s}, \tau = 1/\sqrt{t})$ and $G_K(s, t)$ are equal up to a multiple of $\pm s^n t^m$ for integers n and m (this being the well-definedness criterion for G).*

It is the purpose of this section to place our work with the generalized Alexander polynomial in a context of bi-oriented quantum algebras and to introduce the concept of an oriented quantum algebra. In [82, 83] Kauffman and Radford introduce the concept and show that *oriented quantum algebras encapsulate the notion of an oriented quantum link invariant*.

An *oriented quantum algebra* (A, ρ, D, U) is an abstract model for an oriented quantum invariant of classical links [82, 83]. This model is based on a solution to the Yang-Baxter equation. The definition of an oriented quantum algebra is as follows: We are given an algebra A over a base ring k , an invertible solution ρ in $A \otimes A$ of the Yang-Baxter equation (in the algebraic formulation of this equation – differing from a braiding operator by a transposition), and commuting automorphisms $U, D : A \longrightarrow A$ of the algebra, such that

$$(U \otimes U)\rho = \rho,$$

$$(D \otimes D)\rho = \rho,$$

$$[(1_A \otimes U)\rho][(D \otimes 1_{A^{op}})\rho^{-1}] = 1_{A \otimes A^{op}},$$

and

$$[(D \otimes 1_{A^{op}})\rho^{-1}][(1_A \otimes U)\rho] = 1_{A \otimes A^{op}}.$$

The last two equations say that $[(1_A \otimes U)\rho]$ and $[(D \otimes 1_{A^{op}})\rho^{-1}]$ are inverses in the algebra $A \otimes A^{op}$ where A^{op} denotes the opposite algebra.

When $U = D = T$, then A is said to be *balanced*. In the case where D is the identity mapping, we call the oriented quantum algebra *standard*. In [83] we show that *the invariants defined by Reshetikhin and Turaev (associated with a quasi-triangular Hopf algebra) arise from standard oriented quantum algebras*. It is an interesting structural feature of algebras that we have elsewhere [67] called *quantum algebras* (generalizations of quasi-triangular Hopf algebras) that they give rise to standard oriented quantum algebras. We are continuing research on the relationships of quantum link invariants and oriented quantum algebras. In particular we are working on the reformulation of existing invariants such as the Links-Gould invariant [76] that are admittedly powerful but need a deeper understanding both topologically and algebraically.

We now extend the concept of oriented quantum algebra by adding a second solution to the Yang-Baxter equation γ that will take the role of the virtual crossing.

Definition. A *bi-oriented quantum algebra* is a quintuple (A, ρ, γ, D, U) such that (A, ρ, D, U) and (A, γ, D, U) are oriented quantum algebras and γ satisfies the following properties:

1. $\gamma_{12}\gamma_{21} = 1_{A \otimes A}$. (This is the equivalent to the statement that the braiding operator corresponding to γ is its own inverse.)
2. Mixed identities involving ρ and γ are satisfied. These correspond to the braiding versions of the virtual detour move of type three that involves two virtual crossings and one real crossing. See [84] for the details.

By extending the methods of [83], it is not hard to see that *a bi-oriented quantum algebra will always give rise to invariants of virtual links up to the type one moves (framing and virtual framing)*.

In the case of the generalized Alexander polynomial, the state model $Z(K)$ translates directly into a specific example of a bi-oriented balanced quantum algebra (A, ρ, γ, T) . The main point about this bi-oriented quantum algebra is that the operator γ for the virtual crossing is *not* the identity operator; this non-triviality is crucial to the structure of the invariant. We will investigate bi-oriented quantum algebras and other examples of virtual invariants derived from them.

We have taken a path to explain not only the evolution of a theory of invariants of virtual knots and links, but also (in this subsection) a description of our oriented quantum algebra formulation of the whole class of quantum link invariants. Returning to the case of the original Jones polynomial, we want to understand its capabilities in terms of the oriented quantum algebra that generates the invariant.

7.7 Invariants of Three-Manifolds

As is well-known, invariants of three-manifolds can be formulated in terms of Hopf algebras and quantum algebras and spin recoupling networks. In formulating such invariants it is useful to represent the three-manifold via surgery on a framed link. Two framed links that are equivalent in the Kirby calculus of links represent the same three-manifold and conversely. To obtain invariants of three-manifolds one constructs invariants of framed links that are also invariant under the Kirby moves (handle sliding, blowing up and blowing down).

A classical three-manifold is mathematically the same as a Kirby equivalence class of a framed link. The fundamental group of the three-manifold associated with a link is equal to the fundamental group of the complement of the link modulo the subgroup generated by the framing longitudes for the link. We refer to the fundamental group of the three-manifold as the *three-manifold group*. If there is a counterexample to the classical Poincaré conjecture, then the counterexample would be represented by surgery on some link L whose three-manifold group is trivial, but L is not trivial in Kirby calculus (i.e. it cannot be reduced to nothing).

Kirby calculus can be generalized to the class of virtual knots and links. We define a *virtual three-manifold* to be a Kirby equivalence class of framed virtual links. The three-manifold group generalizes via the combinatorial fundamental group associated to the virtual link (the framing longitudes still exist for virtual links). The *Virtual Poincaré Conjecture* to virtuals would say that a virtual three-manifold with trivial fundamental group is trivial in Kirby calculus. However, **The virtual Poincaré conjecture is false** [31]. There exist virtual links whose three-manifold group is trivial that are nevertheless

not Kirby equivalent to nothing. The simplest example is the virtual knot in Figure 59 . We detect the non-triviality of the Kirby class of this knot by computing that it has an $SU(2)$ Witten invariant that is different from the standard three-sphere.

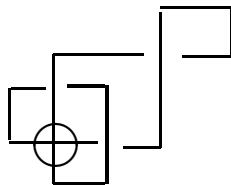


Figure 59 – A counterexample to the Poincaré Conjecture for Virtual Three-Manifolds

This counterexample to the Poincaré conjecture in the virtual domain shows how a classical counterexample might behave in the context of Kirby calculus. Virtual knot theory can be used to search for a counterexample to the classical Poincaré conjecture by searching for virtual counterexamples that are equivalent in Kirby calculus to classical knots and links. This is a new and exciting approach to the dark side of the classical Poincaré conjecture.

7.8 Gauss Diagrams and Vassiliev Invariants

The reader should recall the notion of a *Gauss diagram* for a knot. If K is a knot diagram, then $G(K)$, its Gauss diagram, is a circle comprising the Gauss code of the knot by arranging the traverse of the diagram from crossing to crossing along the circle and putting an arrow (in the form of a chord of the circle) between the two appearances of the crossing. The arrow points from the overcrossing segment to the undercrossing segment in the order of the traverse of the diagram. (Note: Turaev uses another convention, [151].) Each chord is endowed with a sign that is equal to the sign of the corresponding crossing in the knot diagram. At the level of the Gauss diagrams, a virtual crossing is simply the absence of a chord. That is, if we wish to transcribe a virtual knot diagram to a Gauss diagram, we ignore the virtual crossings. Reidemeister moves on Gauss diagrams are defined by translation from the corresponding diagrams from planar representation. Virtual knot theory is precisely the theory of *arbitrary Gauss diagrams*, up to the Gauss diagram Reidemeister moves. Note that an arbitrary Gauss diagram is any pattern of directed, signed chords on an oriented circle. When transcribed back into a planar knot diagram, such a Gauss diagram may require virtual crossings for its depiction.

In [128] Goussarov, Polyak and Viro initiate a very important program for producing Vassiliev invariants of finite type of virtual and classical knots. The gist of their program is as follows. They define the notion of a semi-virtual crossing, conceived as a dotted, oriented,

signed chord in a Gauss diagram for a knot. An *arrow diagram* is a Gauss diagram all of whose chords are dotted. Let \mathcal{A} denote the collection of all linear combinations of arrow diagrams with integer coefficients. Let \mathcal{G} denote the collection of all arbitrary Gauss diagrams (hence all representatives of virtual knots). Define a mapping

$$i : \mathcal{G} \longrightarrow \mathcal{A}$$

by expanding each chord of a Gauss diagram G into the sum of replacing the chord by a dotted chord and the removal of that chord. Thus

$$i(G) = \sum_{r \in R(G)} G^r$$

where $R(G)$ denotes all ways of replacing each chord in G either by a dotted chord, or by nothing; and G^r denotes that particular replacement applied to G .

Now let \mathcal{P} denote the quotient of \mathcal{A} by the subalgebra generated by the relations in \mathcal{A} corresponding to the Reidemeister moves. Each Reidemeister move is of the form $X = Y$ for certain diagrams, and this translates to the relation $i(X) - i(Y) = 0$ in \mathcal{P} , where $i(X)$ and $i(Y)$ are individually certain linear combinations in \mathcal{P} . Let

$$I : \mathcal{G} \longrightarrow \mathcal{P}$$

be the map induced by i . Then it is a formal fact that $I(G)$ is invariant under each of the Reidemeister moves, and hence that $I(G)$ is an invariant of the corresponding Gauss diagram (virtual knot) G . The algebra of relations that generate the image of the Reidemeister moves in \mathcal{P} is called the *Polyak algebra*.

So far, we have only described a tautological and not a computable invariant. The key to obtaining computable invariants is to truncate. Let \mathcal{P}_n denote \mathcal{P} modulo all arrow diagrams with more than n dotted arrows. Now \mathcal{P}_n is a finitely generated module over the integers, and the composed map

$$I_n : \mathcal{G} \longrightarrow \mathcal{P}_n$$

is also an invariant of virtual knots. Since we can choose a specific basis for \mathcal{P}_n , the invariant I_n is in principle computable, and it yields a large collection of Vassiliev invariants of virtual knots that are of finite type. The paper by Goussarov, Polyak and Viro investigates specific methods for finding and representing these invariants. They show that every Vassiliev invariant of finite type for classical knots can be written as a combinatorial state sum for long knots. They use the virtual knots as an intermediate in the construction.

By directly constructing Vassiliev invariants of virtual knots from known invariants of virtuals, we can construct invariants that are not of finite type in the above sense (See [78].) These invariants also deserve further investigation.

8 Other Invariants

The *Khovanov Categorification of the Jones polynomial* [6] is important for our concerns. This invariant is constructed by promoting the states in the bracket summation to tensor powers of a vector space V , where a single power of V corresponds to a single loop in the state. In this way a graded complex is constructed, whose graded Euler characteristic is equal to the original Jones polynomial, and the ranks of whose graded homology groups are themselves invariants of knots. It is now known that the information in the Khovanov construction exceeds that in the original Jones polynomial. It is an open problem whether a Khovanov type construction can generalize to virtual knots in the general case. The construction for the Khovanov polynomial for virtuals over \mathbf{Z}_2 was proposed in [110]. Recent work by other authors related to knots in thickened surfaces promises to shed light on this issue.

One of the more promising directions for relating Vassiliev invariants to our present concerns is the theory of gropes [21, 22], where one considers surfaces spanning a given knot, and then recursively the surfaces spanning curves embedded in the given surface. This hierarchical structure of curves and surfaces is likely to be a key to understanding the geometric underpinning of the original Jones polynomial. The same techniques in a new guise could elucidate invariants of virtual knots and links.

9 The Bracket Polynomial and The Jones Polynomial

It is an open problem whether there exist classical knots (single component loops) that are knotted and yet have unit Jones polynomial. In other words, it is an open problem whether the Jones polynomial can detect all knots. There do exist families of links whose linkedness is undetectable by the Jones polynomial [146, 147]. It is the purpose of this section of the paper to give a summary of some of the information that is known in this arena. We begin with a sketch of ways to calculate the bracket polynomial model of the Jones polynomial, and then discuss how to construct classical links that are undetectable by the Jones polynomial.

The formula for the bracket model of the Jones polynomial [58] can be indicated as follows: The letter chi, χ , denotes a crossing in a link diagram. The barred letter denotes the mirror image of this first crossing. A crossing in a diagram for the knot or link is expanded into two possible states by either smoothing (reconnecting) the crossing horizontally, \asymp , or vertically $><$. Any closed loop (without crossings) in the plane has value $\delta = -A^2 - A^{-2}$.

$$\chi = A\asymp + A^{-1}><$$

$$\overline{\chi} = A^{-1}\asymp + A><.$$

One useful consequence of these formulas is the following *switching formula*

$$A\chi - A^{-1}\overline{\chi} = (A^2 - A^{-2})\asymp.$$

Note that in these conventions the A -smoothing of χ is \asymp , while the A -smoothing of $\overline{\chi}$ is $\succ<$. Properly interpreted, the switching formula above says that you can switch a crossing and smooth it either way and obtain a three diagram relation. This is useful since some computations will simplify quite quickly with the proper choices of switching and smoothing. Remember that it is necessary to keep track of the diagrams up to regular isotopy (the equivalence relation generated by the second and third Reidemeister moves). Here is an example. View Figure 60.

You see in Figure 60, a trefoil diagram K , an unknot diagram U and another unknot diagram U' . Applying the switching formula, we have

$$A^{-1}K - AU = (A^{-2} - A^2)U'$$

and $U = -A^3$ and $U' = (-A^{-3})^2 = A^{-6}$. Thus

$$A^{-1}K - A(-A^3) = (A^{-2} - A^2)A^{-6}.$$

Hence

$$A^{-1}K = -A^4 + A^{-8} - A^{-4}.$$

Thus

$$K = -A^5 - A^{-3} + A^{-7}.$$

This is the bracket polynomial of the trefoil diagram K . We have used the same symbol for the diagram and for its polynomial.

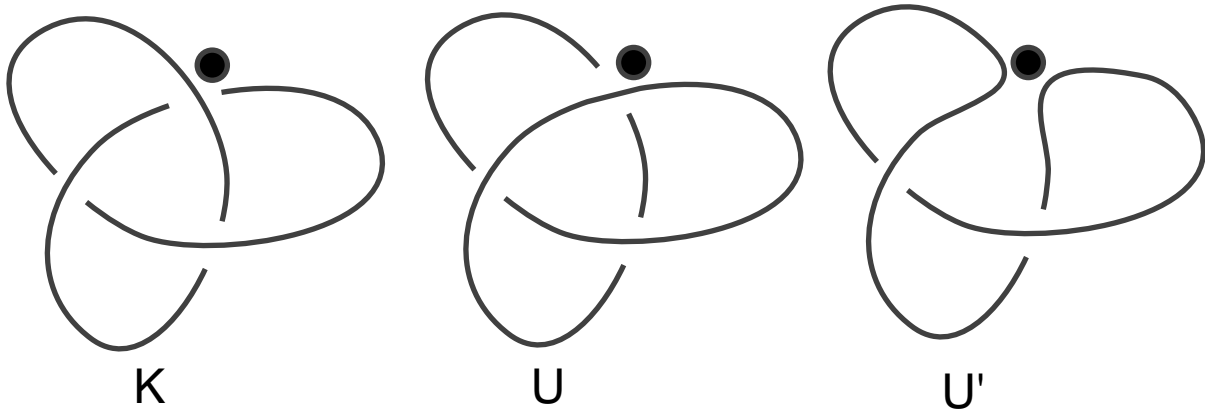


Figure 60 – Trefoil and Two Relatives

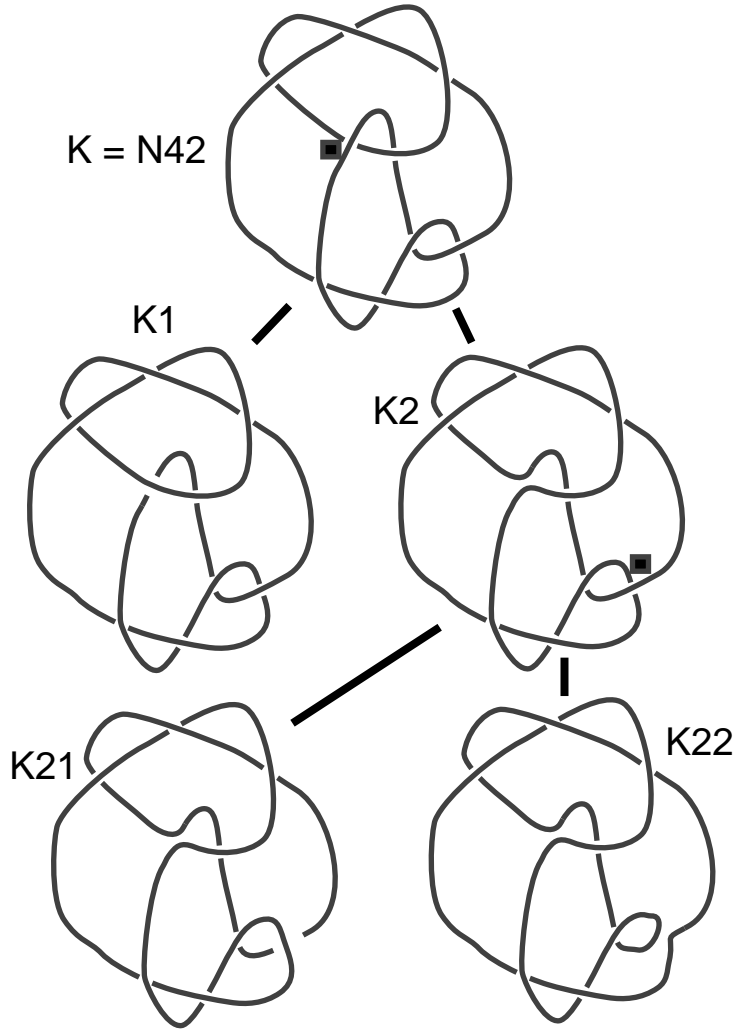


Figure 61 – Skein Tree for 9_{42}

Since the trefoil diagram K has writhe $w(K) = 3$, we have the normalized polynomial

$$f_K(A) = (-A^3)^{-3} \langle K \rangle = -A^{-9}(-A^5 - A^{-3} + A^{-7}) = A^{-4} + A^{-12} - A^{-16}.$$

The asymmetry of this polynomial under the interchange of A and A^{-1} proves that the trefoil knot is not ambient isotopic to its mirror image.

In Figure 61 you see the knot $K = N_{42} = 9_{42}$ (the latter being its standard name in the knot tables) and a skein tree for it via switching and smoothing. In Figure 62 we show simplified (via regular isotopy) representatives for the end diagrams in the skein tree.

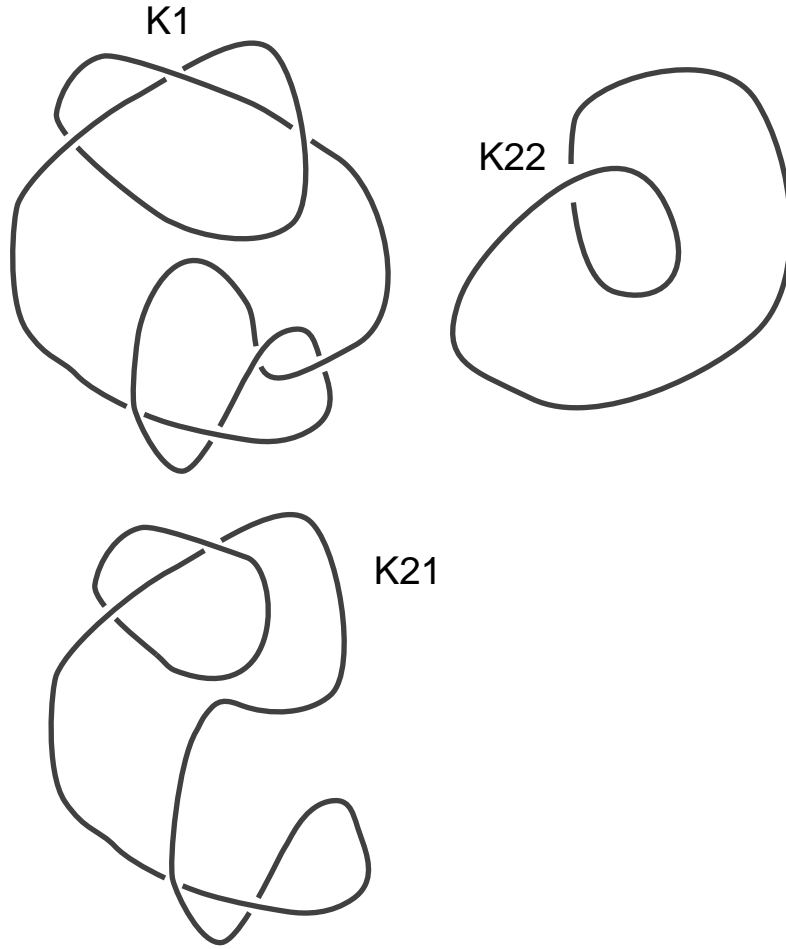


Figure 62 – Regular Isotopy Versions of Bottom of Skein Tree for 9_{42}

It follows from the switching formula that for $K = 9_{42}$,

$$A^{-1}K - AK_1 = (A^{-2} - A^2)K_2$$

$$AK_2 - A^{-1}K_{21} = (A^2 - A^{-2})K_{22}$$

and that K_1 is a connected sum of a right-handed trefoil diagram and a figure eight knot diagram, while K_{21} is a Hopf link (simple link of linking number one) with extra writhe of -2 while K_{22} is an unknot with writhe of 1. These formulas combine to give

$$\langle K_1 \rangle = -A^{-9} + A^{-5} - A^{-1} + A^3 - A^7 + A^{11} - A^{15}.$$

Since K has writhe one, we get

$$f_K = A^{-12} - A^{-8} + A^{-4} - 1 + A^4 - A^8 + A^{12}.$$

This shows that the normalized bracket polynomial does not distinguish 9_{42} from its mirror image. This knot is, in fact chiral (inequivalent to its mirror image), a fact that can be verified by other means. The knot 9_{42} is the first chiral knot whose chirality is undetected by the Jones polynomial.

Remark. In writing computer programs for calculating the bracket polynomial it is useful to use the coding method illustrated in Figure 63. In this method each edge from one classical crossing to another has a label. Virtual crossings do not appear in the code. Each classical crossing has a four letter code in the form $[abcd]$ connoting a clockwise encirclement of the crossing, starting at an overcrossing edge.

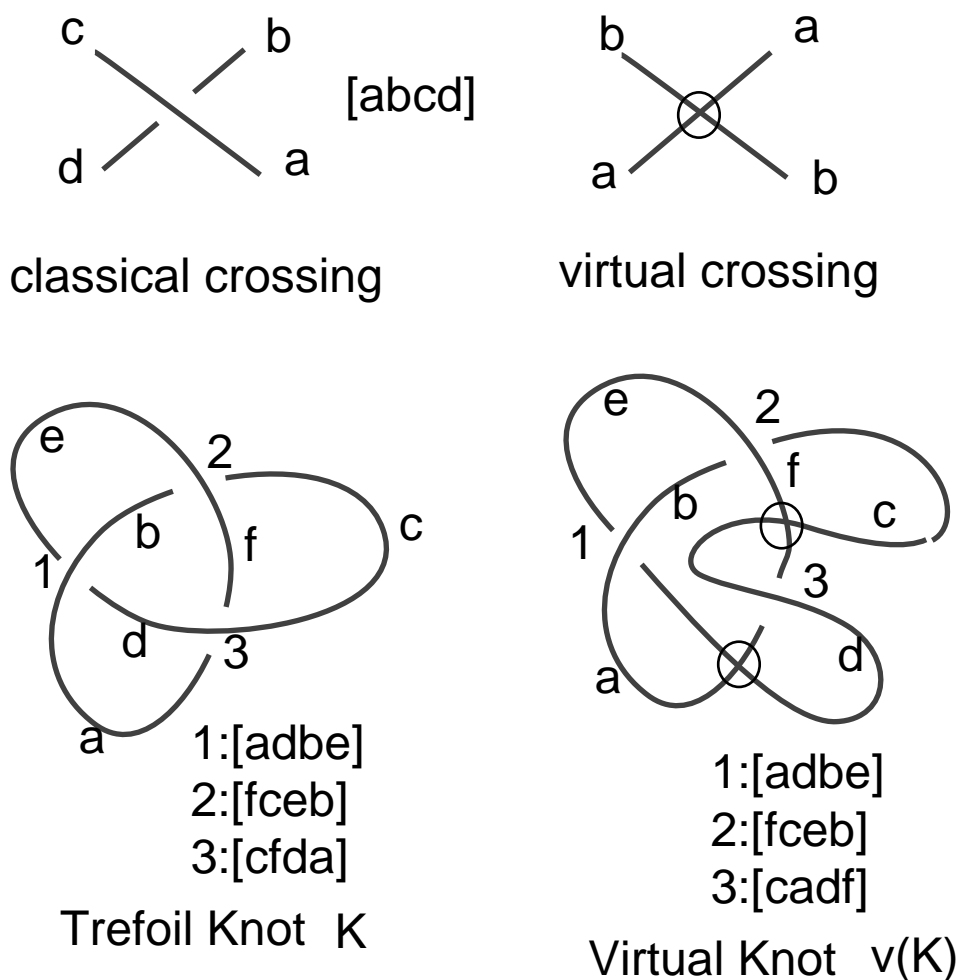


Figure 63 – Coding a Link Diagram

9.1 Thistlethwaite's Example

View Figure 64. Here we have a version of a link L discovered by Morwen Thistlethwaite [146] in December 2000. We discuss some theory behind this link in the next subsection. It is a link that is linked but whose linking is not detectable by the Jones polynomial. One can verify such properties by using a computer program, or by the algebraic techniques described below.

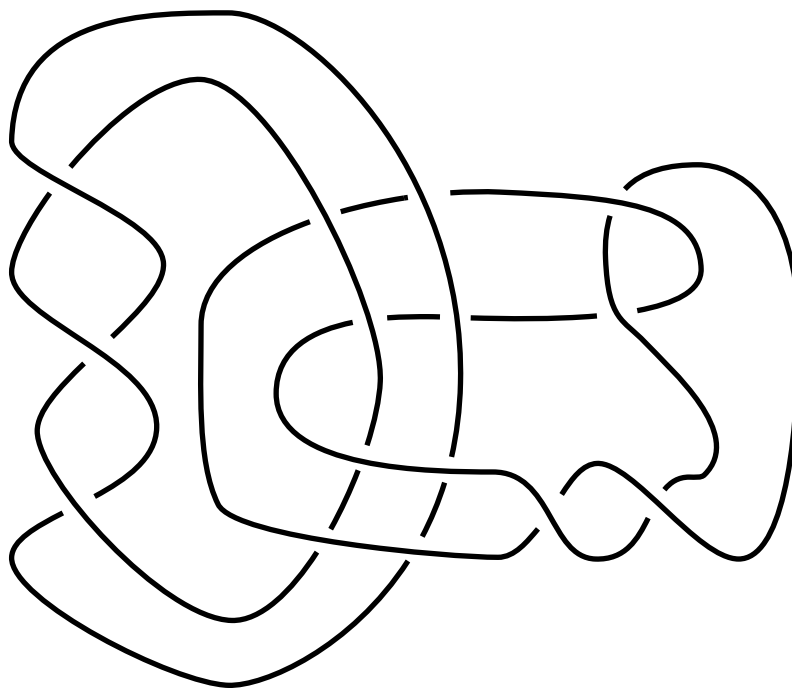


Figure 64 – Thistlethwaite's Link

9.2 Present Status of Links Not Detectable by the Jones Polynomial

In this section we give a quick review of the status of our work [147] producing infinite families of distinct links all evaluating as unlinks by the Jones polynomial.

A tangle (2-tangle) consists in an embedding of two arcs in a three-ball (and possibly some circles embedded in the interior of the three-ball) such that the endpoints of the arcs are on the boundary of the three-ball. One usually depicts the arcs as crossing the boundary transversely so that the tangle is seen as the embedding in the three-ball augmented by four segments emanating from the ball, each from the intersection of the arcs with the boundary. These four segments are the *exterior edges* of the tangle, and are used for operations that form new tangles and new knots and links from given tangles. Two tangles in a given

three-ball are said to be *topologically equivalent* if there is an ambient isotopy from one to the other in the given three-ball, fixing the intersections of the tangles with the boundary.

It is customary to illustrate tangles with a diagram that consists in a box (within which are the arcs of the tangle) and with the exterior edges emanating from the box in the NorthWest (NW), NorthEast (NE), SouthWest (SW) and SouthEast (SE) directions. Given tangles T and S , one defines the *sum*, denoted $T + S$ by placing the diagram for S to the right of the diagram for T and attaching the NE edge of T to the NW edge of S , and the SE edge of T to the SW edge of S . The resulting tangle $T + S$ has exterior edges corresponding to the NW and SW edges of T and the NE and SE edges of S . There are two ways to create links associated to a tangle T . The *numerator* T^N is obtained, by attaching the (top) NW and NE edges of T together and attaching the (bottom) SW and SE edges together. The denominator T^D is obtained, by attaching the (left side) NW and SW edges together and attaching the (right side) NE and SE edges together. We denote by $[0]$ the tangle with only unknotted arcs (no embedded circles) with one arc connecting, within the three-ball, the (top points) NW intersection point with the NE intersection point, and the other arc connecting the (bottom points) SW intersection point with the SE intersection point. A ninety degree turn of the tangle $[0]$ produces the tangle $[\infty]$ with connections between NW and SW and between NE and SE. One then can prove the basic formula for any tangle T

$$\langle T \rangle = \alpha_T \langle [0] \rangle + \beta_T \langle [\infty] \rangle$$

where α_T and β_T are well-defined polynomial invariants (of regular isotopy) of the tangle T . From this formula one can deduce that

$$\langle T^N \rangle = \alpha_T d + \beta_T$$

and

$$\langle T^D \rangle = \alpha_T + \beta_T d.$$

We define the *bracket vector* of T to be the ordered pair (α_T, β_T) and denote it by $br(T)$, viewing it as a column vector so that $br(T)^t = (\alpha_T, \beta_T)$ where v^t denotes the transpose of the vector v . With this notation the two formulas above for the evaluation for numerator and denominator of a tangle become the single matrix equation

$$\begin{bmatrix} \langle T^N \rangle \\ \langle T^D \rangle \end{bmatrix} = \begin{bmatrix} d & 1 \\ 1 & d \end{bmatrix} br(T).$$

We then use this formalism to express the bracket polynomial for our examples. The class of examples that we considered are each denoted by $H(T, U)$ where T and U are each tangles and $H(T, U)$ is a satellite of the Hopf link that conforms to the pattern shown in Figure 65, formed by clasping together the numerators of the tangles T and U . Our method is based on a transformation $H(T, U) \rightarrow H(T, U)^\omega$, whereby the tangles T and U are cut out and reglued by certain specific homeomorphisms of the tangle boundaries. This

transformation can be specified by a modification described by a specific rational tangle and its mirror image. Like mutation, the transformation ω preserves the bracket polynomial. However, it is more effective than mutation in generating examples, as a trivial link can be transformed to a prime link, and repeated application yields an infinite sequence of inequivalent links.

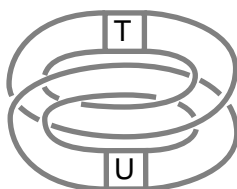


Figure 65 – Hopf Link Satellite $H(T,U)$

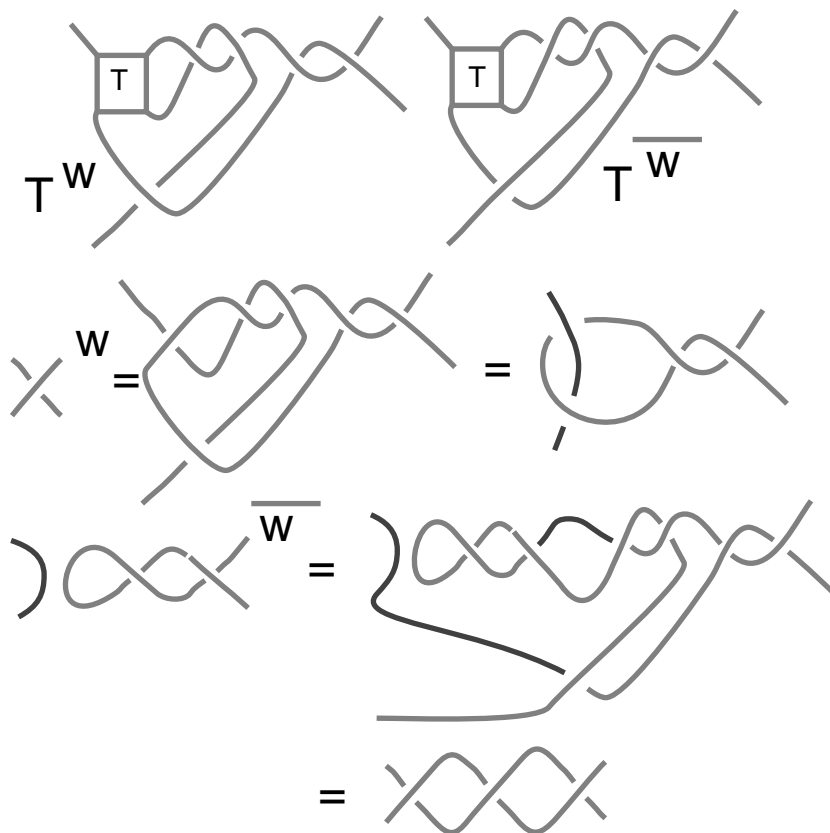


Figure 66 – The Omega Operations

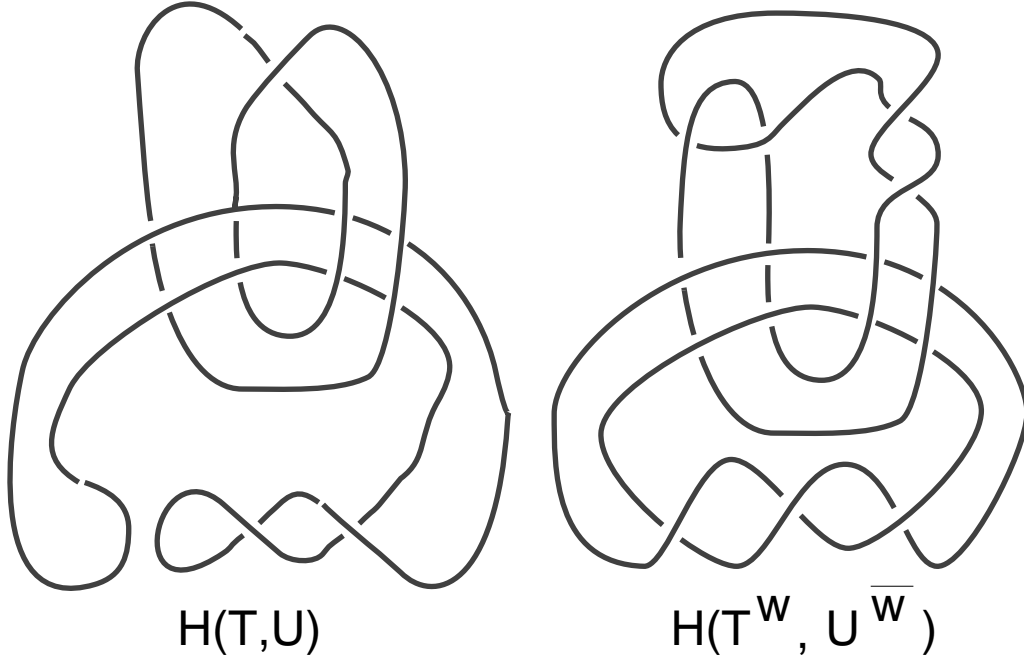


Figure 67 – Applying Omega Operations to an Unlink

Specifically, the transformation $H(T, U)^\omega$ is given by the formula

$$H(T, U)^\omega = H(T^\omega, U^{\bar{\omega}})$$

where the tangle operations T^ω and $U^{\bar{\omega}}$ are as shown in Figure 66. By direct calculation, there is a matrix M such that

$$\langle H(T, U) \rangle = br(T)^t M br(U)$$

and there is a matrix Ω such that

$$br(T^\omega) = \Omega br(T)$$

and

$$br(T^{\bar{\omega}}) = \Omega^{-1} br(T).$$

One verifies the identity

$$\Omega^t M \Omega^{-1} = M$$

from which it follows that $\langle H(T, U) \rangle^\omega = \langle H(T, U) \rangle$. This completes the sketch of our method for obtaining links that whose linking cannot be seen by the Jones polynomial. Note that the link constructed as $H(T^\omega, U^{\bar{\omega}})$ in Figure 67 has the same Jones polynomial as an unlink of two components. This shows how the first example found by Thistlethwaite fits into our construction.

9.3 Switching a Crossing

If in Figure 67, we start with T replaced by $Flip(T)$, switching the crossing, the resulting link $L = H(Flip(T)^\omega, U^{\bar{\omega}})$ will still have Jones polynomial the same as the unlink, but the link L will be distinct from the link $H(T^\omega, U^{\bar{\omega}})$ of Figure 67. We illustrate this process in Figure 68.

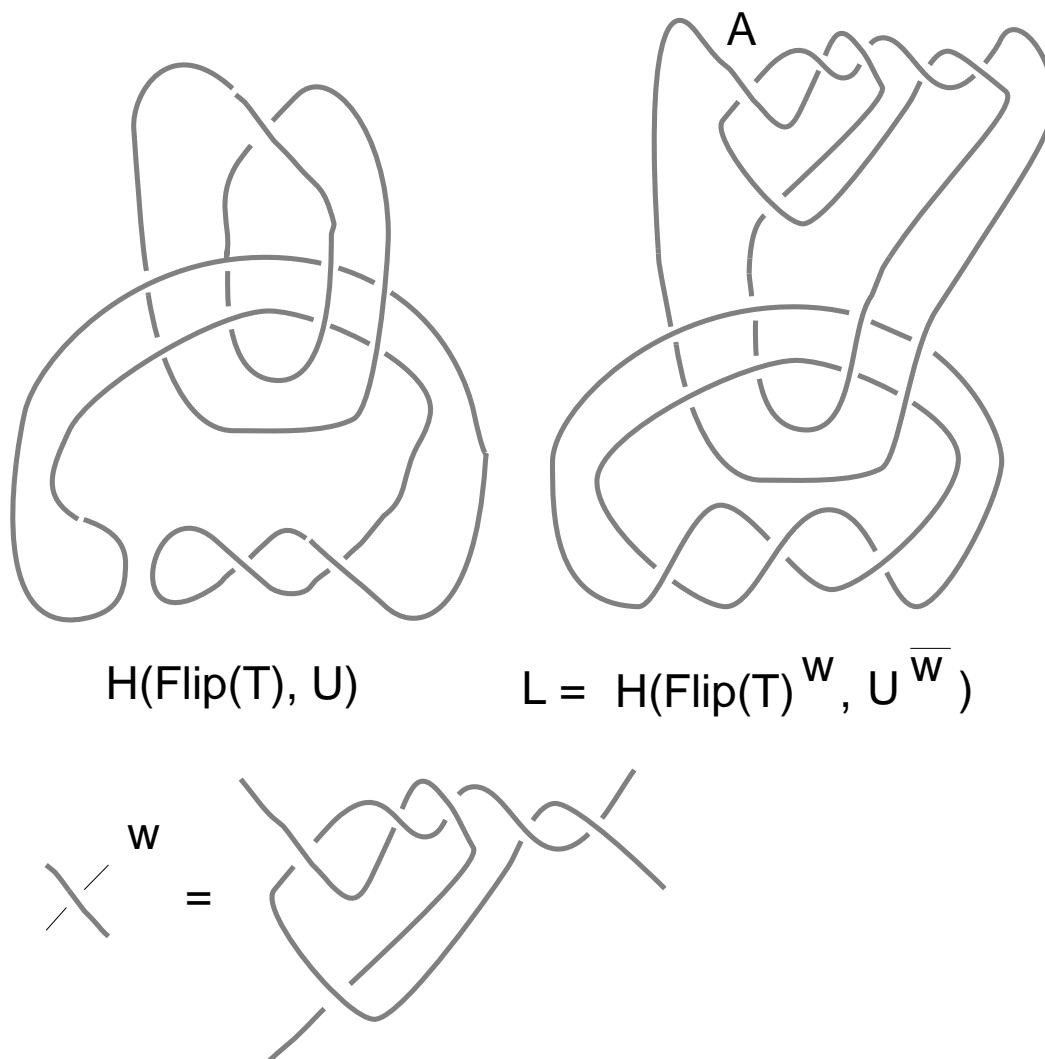


Figure 68 – Applying Omega Operations to an Unlink with Flipped Crossing

The link L has the remarkable property that both it and the link obtained from it by flipping the crossing labeled A in Figure 68 have Jones polynomial equal to the Jones polynomial of the unlink of two components. (We thank Alexander Stoimenow for pointing out the possibility of this sort of construction.)

Now let's think about a link L with the property that it has the same Jones polynomial as a link L' obtained from L by switching a single crossing. We can isolate the rest of the link that is not this crossing into a tangle S so that (without any loss of generality) $L = N(S + [1])$ and $L' = N(S + [-1])$. Let's assume that orientation assignment to L and L' is as shown in Figure 69.

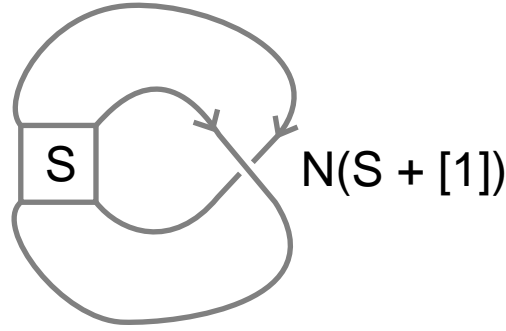


Figure 69 – $N(S + [1])$

Since we are told that L and L' have the same Jones polynomial, it follows that $\langle L \rangle = -A^{-3}\kappa$ and $\langle L' \rangle = -A^3\kappa$ for some non-zero Laurent polynomial κ . Now suppose that $\langle S \rangle = \alpha \langle [0] \rangle + \beta \langle [\infty] \rangle$. Then

$$\langle L \rangle = \alpha(-A^3) + \beta(-A^{-3})$$

and

$$\langle L' \rangle = \alpha(-A^{-3}) + \beta(-A^3).$$

From this it follows that

$$\kappa = \alpha A^6 + \beta$$

and

$$\kappa = \alpha A^{-6} + \beta.$$

Thus

$$\alpha = 0$$

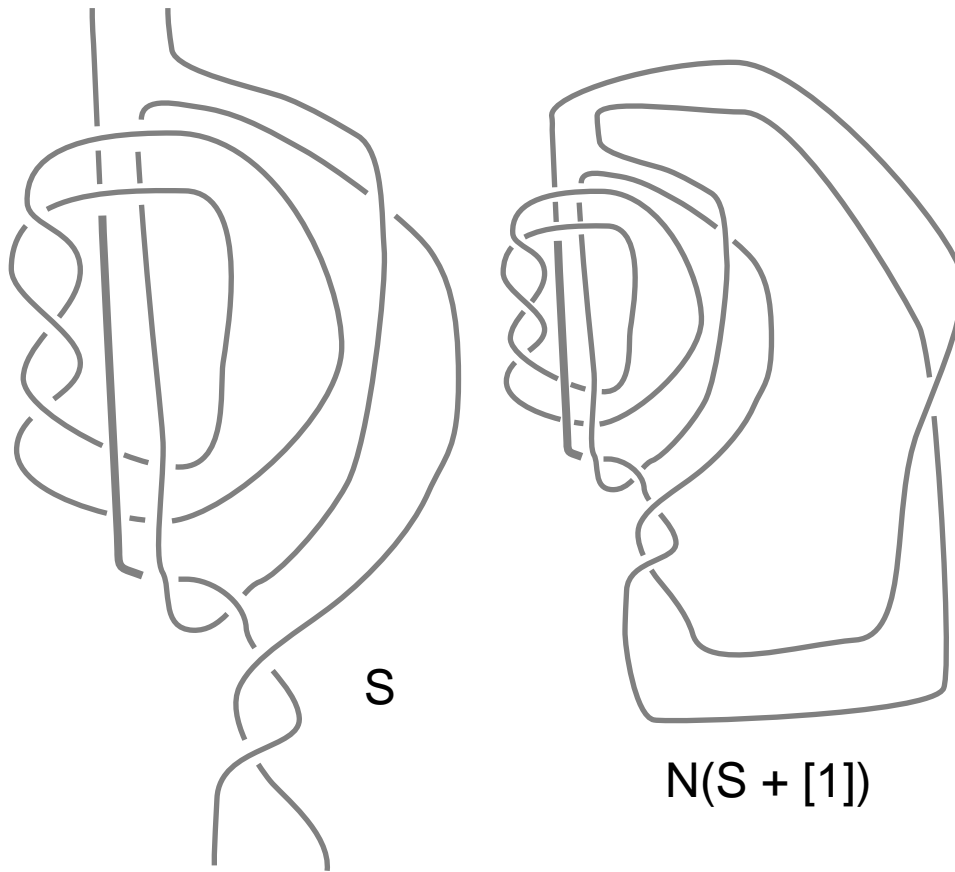
and

$$\beta = \kappa.$$

We have shown that

$$\langle S \rangle = \kappa \langle [\infty] \rangle.$$

This means that we can, by using the example described above, produce a tangle S that is not splittable and yet has the above property of having one of its bracket coefficients equal to zero. The example is shown in Figure 70.



$N(S + [1])$ and $N(S+[-1])$ both have Jones poly same as the unlink of two components.

Figure 70 – The Tangle S

Finally, in Figure 71 we show L and the link $v(L)$ obtained by virtualizing the crossing corresponding to $[1]$ in the decomposition $L = N(S + [1])$. The virtualized link $v(L)$ has the property that it also has Jones polynonial the same as an unlink of two components. We wish to prove that $v(L)$ is not isotopic to a classical link. The example has been designed so that surface bracket techniques will be difficult to apply.

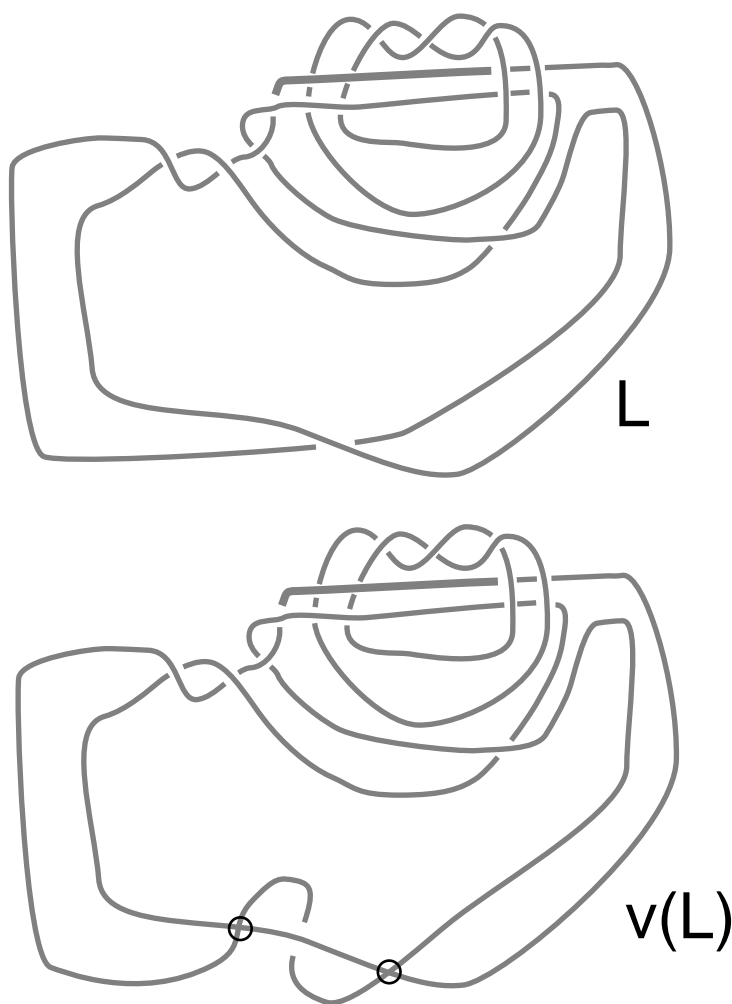


Figure 71 – The Virtual Link $v(L)$

References

- [1] D. Altshuler and L. Friedel, Vassiliev knot invariants and Chern-Simons perturbation theory to all orders. *Comm. Math. Phys.* 187 (1997), no. 2, 261–287.
- [2] M.F. Atiyah, *Geometry of Yang-Mills Fields*, Accademia Nazionale dei Lincei Scuola Superiore Lezioni Fermi, Pisa, 1979.
- [3] M.F. Atiyah, *The Geometry and Physics of Knots*, Cambridge University Press, 1990.
- [4] D. Bar-Natan, On the Vassiliev knot invariants, (to appear in *Topology*).
- [5] D. Bar-Natan, *Perturbative Aspects of the Chern-Simons Topological Quantum field Theory*, Ph. D. Thesis, Princeton University, June 1991.
- [6] D. Bar-Natan, On Khovanov’s categorification of the Jones polynomial. *Algebraic and Geometric Topology*, Vol. 2 (2002), pp. 337–370.
- [7] D. Bar-Natan, (private conversation).
- [8] A. Bartholomew and R. Fenn, Quaternionic invariants of virtual knots and links, www.maths.sussex.ac.uk/Staff/RAF/Maths/Current/Andy/equivalent.ps To appear in *JLMS*.
- [9] S. Budden and R. Fenn, The equation $[B, (A - 1)(A, B)] = 0$ and virtual knots and link, preprint available from R. Fenn’s website.
- [10] R.J. Baxter, *Exactly Solved Models in Statistical Mechanics*, Acad. Press, 1982.
- [11] J. Birman and X.S. Lin, Knot polynomials and Vassiliev’s invariants. *Invent. Math.* 111 (1993), no. 2, 225–270.
- [12] R. Bott and C. Taubes, On the self-linking of knots, *Jour. Math. Phys.* **35** (1994), pp. 5247–5287.
- [13] P. Cartier, Construction combinatoire des invariants de Vassiliev - Kontsevich des noeuds, *C. R. Acad. Sci. Paris* **316**, Série I, (1993), pp. 1205–1210.
- [14] J.S. Carter, D.E. Flath, M. Saito, *The Classical and Quantum 6j-Symbols*, Mathematical Notes 43, Princeton University Press (1995).
- [15] J.S. Carter, L.H. Kauffman, M. Saito, *Diagrammatics, Singularities and Their Algebraic Interpretations*. 10th Brazilian Topology Meeting (So Carlos, 1996). *Mat. Contemp.* 13 (1997), 21–115.
- [16] J.S. Carter, L.H. Kauffman, M. Saito, Structures and diagrammatics of four-dimensional topological lattice field theories. *Adv. Math.* 146 (1999), no. 1, 39–100.

- [17] J.S. Carter and M. Saito, Diagrammatic invariants of knotted curves and surfaces, (unpublished manuscript - 1992).
- [18] J.S. Carter and M. Saito, *Knotted Surfaces and Their Diagrams*. Mathematical Surveys and Monographs, 55. American Mathematical Society, Providence, RI, 1998.
- [19] J.S. Carter, S. Kamada, M. Saito, Geometric interpretations of quandle homology, *JKTR* **10**, No. 3 (2001), 345-386.
- [20] J.S. Carter and D. Silver (private conversation).
- [21] J. Conant and P. Teichner, Grope cobordism of classical knots. *Topology* 43 (2004), no. 1, 119–156.
- [22] J. Conant and P. Teichner, Grope cobordism and Feynman diagrams. *Math. Ann.* 328 (2004), no. 1-2, 135–171.
- [23] J.H. Conway, (private conversation)
- [24] J.H. Conway, An enumeration of knots and links and some of their algebraic properties, in *Computational Problems in Abstract Algebra*, Pergammon Press, N.Y., 1970, pp. 329-358.
- [25] L. Crane and I. Frenkel, Four-dimensional topological quantum field theory, Hopf categories and canonical bases, *J. Math. Physics*, No. 35 (1994), pp. 5136-5154.
- [26] L. Crane, L.H. Kauffman, D. Yetter, State sum invariants of 4-manifolds, *Journal of Knot Theory and Its Ramifications* 6 (1997), no. 2, 177–234.
- [27] J.W. Barrett, L. Crane, A Lorentzian signature model for quantum general relativity. *Classical Quantum Gravity* 17 (2000), no. 16, 3101–3118.
- [28] P. Dehornoy, “Braids and Self-Distributivity”, Progress in Math. vol. 192, Birkhauser (2000).
- [29] H. Dye, Characterizing Virtual Knots, Ph.D. Thesis (2002), UIC.
- [30] H. Dye and L.H. Kauffman, Minimal surface representations of virtual knots and links. *arXiv:math.AT/0401035 v1*, Jan. 2004.
- [31] H. Dye and L.H. Kauffman, VirtualThree-Manifolds, www.arxiv.org/math.GT/0407407, (to appear in JKTR).
- [32] I.A. Dynnikov, Arc presentations of links - Monotonic simplification, www.arxiv.org/math.GT/0208153 v2 8 Sept 2003.
- [33] R. Fenn, [www.maths.sussex.ac.uk//Staff/RAF/Maths/historyi.jpg], ($i = 1, 2, \dots$)

- [34] R. Fenn, M. Jordan and L.H. Kauffman, Biracks, Biquandles and Virtual Knots, to appear in *Topology and Its Applications*.
- [35] R. Fenn and C. Rourke, Racks and links in codimension two, *JKTR* No. 4, pp 343-406 (1992).
- [36] R. Fenn, C. Rourke and B. Sanderson, Trunks and classifying spaces, *Applied Categorical Structures* 3(1995) pp 321-356.
- [37] R. Fenn, C. Rourke and B. Sanderson, An introduction to species and the rack space, *Topics in Knot Theory*, Kluwer Acad. pp 33-55 (1993).
- [38] R. Fenn, R. Rimanyi and C. Rourke, The Braid Permutation Group, *Topology*, Vol. 36, No. 1 (1997), 123–135.
- [39] R. Fenn and P. Taylor, Introducing doodles, *Lect. Notes in Maths. LMS No. 722*, pp 37-43,
- [40] R. Fenn, “Techniques of Geometric Topology,” *LMS Lect. Notes Series* 57 (1983).
- [41] S. Garoufalidis, Applications of TQFT to invariants in low dimensional topology, (preprint 1993).
- [42] E. Guadagnini, M. Martellini and M. Mintchev, Chern-Simons model and new relations between the Homfly coefficients, *Physics Letters B*, Vol. 238, No. 4, Sept. 28 (1989), pp. 489-494.
- [43] D.S. Freed and R.E. Gompf, Computer calculation of Witten’s three-manifold invariant, *Commun. Math. Phys.*, No. 141, (1991), pp. 79-117.
- [44] M. Greene, “Some Results in Geometric Topology and Geometry”, Thesis submitted for the degree of PhD, Warwick Maths Institute, Sept. 1997.
- [45] B. Hasslacher and M.J. Perry, Spin networks are simplicial quantum gravity, *Phys. Lett.*, No. 103 B (1981).
- [46] M.A. Hennings, Hopf algebras and regular isotopy invariants for link diagrams, *Math. Proc. Camb. Phil. Soc.*, Vol. 109 (1991), pp. 59-77
- [47] D. Hrencecin, “On Filamentations and Virtual Knot Invariants” Ph.D Thesis, University of Illinois at Chicago (2001).
- [48] D. Hrencecin and L.H. Kauffman, “On Filamentations and Virtual Knots”, *Topology and Its Applications*, 134(2003), 23-52.
- [49] L.C. Jeffrey, Chern-Simons-Witten invariants of lens spaces and torus bundles, and the semi-classical approximation, *Commun. Math. Phys.*, No. 147, (1992), pp. 563-604.

- [50] V.F.R. Jones, A polynomial invariant of links via von Neumann algebras, *Bull. Amer. Math. Soc.*, 1985, No. 129, pp. 103-112.
- [51] V.F.R. Jones, Hecke algebra representations of braid groups and link polynomials, *Ann. of Math.*, Vol. 126, 1987, pp. 335-338.
- [52] V.F.R. Jones, On knot invariants related to some statistical mechanics models, *Pacific J. Math.*, Vol. 137, no. 2, 1989, pp. 311-334.
- [53] Kanenobu, T (2001), Forbidden moves unknot a virtual knot, *Journal of Knot Theory and Its Ramifications*, **10** (1), pp. 89-96.
- [54] M. Khovanov, Doodle groups, *Trans. Amer. Math. Soc.*, Vol. 349, No. 6, pp 2297-2315.
- [55] L.H. Kauffman, The Conway polynomial, *Topology*, **20** (1980), pp. 101-108.
- [56] L.H. Kauffman, *Formal Knot Theory*, Princeton University Press, Lecture Notes Series 30 (1983).
- [57] L.H. Kauffman, *On Knots*, Annals Study No. 115, *Princeton University Press* (1987)
- [58] L.H. Kauffman, State Models and the Jones Polynomial, *Topology*, Vol. 26, 1987, pp. 395-407.
- [59] L.H. Kauffman, Statistical mechanics and the Jones polynomial, *AMS Contemp. Math. Series*, Vol. 78, 1989, pp. 263-297.
- [60] L.H. Kauffman, Map coloring, q-deformed spin networks, and Turaev-Viro invariants for 3-manifolds, *Int. J. of Modern Phys. B*, Vol. 6, Nos. 11, 12 (1992), pp. 1765-1794.
- [61] L.H. Kauffman, An invariant of regular isotopy, *Trans. Amer. Math. Soc.*, Vol. 318, No. 2, 1990, pp. 417-471.
- [62] L.H. Kauffman, New invariants in the theory of knots, *Amer. Math. Monthly*, Vol. 95, No. 3, March 1988. pp 195-242.
- [63] L.H. Kauffman and P. Vogel, Link polynomials and a graphical calculus, *Journal of Knot Theory and Its Ramifications*, Vol. 1, No. 1, March 1992.
- [64] L.H. Kauffman, "Knots and Physics", World Scientific, Singapore/New Jersey/London/Hong Kong, 1991, 1994, 2001.
- [65] L.H. Kauffman and H. Saleur, Free fermions and the Alexander-Conway polynomial, *Comm. Math. Phys.* 141, 293-327 (1991).
- [66] F. Jaeger, L.H. Kauffman and H. Saleur, The Conway polynomial in R^3 and in thickened surfaces: A new determinant formulation, *J. Comb. Theory Ser. B* Vol. 61 (1994), 237-259.

- [67] L.H. Kauffman, Gauss Codes, quantum groups and ribbon Hopf algebras, *Reviews in Mathematical Physics* **5** (1993), 735-773. (Reprinted in [64], 551–596.
- [68] L.H. Kauffman and D. Radford, Invariants of 3-Manifolds derived from finite dimensional Hopf algebras, *Journal of Knot Theory and Its Ramifications*. Vol. 4, No. 1 (1995), 131-162.
- [69] L.H. Kauffman, Knots and Diagrams, in “Lectures at Knots 96”, ed. by Shin’ichi Suzuki (1997), World Scientific Pub. Co. pp. 123-194.
- [70] L.H. Kauffman, D. Radford and S. Sawin, Centrality and the KRH Invariant, *J. Knot Theory Ramifications* **7** (1998), no. 5, 571–624.
- [71] L.H. Kauffman, Hopf algebras and 3-Manifold invariants, *Journal of Pure and Applied Algebra*. Vol. 100 (1995), 73-92.
- [72] L.H. Kauffman, Spin Networks, Topology and Discrete Physics. in second edition of *Braid Group, Knot Theory and Statistical Mechanics*, ed. by Yang and Ge, World Sci. Pub. (1994))
- [73] L.H. Kauffman and S. L. Lins, *Temperley-Lieb Recoupling Theory and Invariants of 3- Manifolds*, Annals of Mathematics Study 114, Princeton Univ. Press, 1994.
- [74] L.H. Kauffman, Functional Integration and the theory of knots, *J. Math. Physics*, Vol. 36 (5), May 1995, pp. 2402 - 2429.
- [75] L.H. Kauffman, “Knots and Functional Integration” (in preparation).
- [76] L.H. Kauffman, D. De Wit and J. Links. On the Links-Gould Invariant of Links. *JKTR*, Vol. 8, No. 2 (1999), 165-199.
- [77] L.H. Kauffman, Knot theory and the heuristics of functional integration. *Physica A* **281** (2000) 173-200.
- [78] Louis H. Kauffman, Virtual Knot Theory , *European J. Comb.* (1999) Vol. 20, 663-690.
- [79] Louis H. Kauffman, A Survey of Virtual Knot Theory in *Proceedings of Knots in Hellas ’98*, World Sci. Pub. 2000 , pp. 143-202.
- [80] Louis H. Kauffman, Detecting Virtual Knots, in *Atti. Sem. Mat. Fis. Univ. Modena Supplemento al Vol. IL*, 241-282 (2001).
- [81] L.H. Kauffman, Right Integrals and Invariants of Three-Manifolds, *Proceedings of Conference in Honor of Robion Kirby’s 60th Birthday*, Geometry and Topology Monographs, Vol. 2 (1999), 215-232.
- [82] Louis H. Kauffman and David E. Radford, Oriented quantum algebras and invariants of knots and links, *Journal of Algebra*, Vol. 246, 253-291 (2001).

- [83] Louis H. Kauffman and David E. Radford, Oriented quantum algebras, categories and invariants of knots and links. *JKTR*, vol 10, No. 7 (2001), 1047-1084.
- [84] L.H. Kauffman and D.E. Radford, Bi-oriented Quantum Algebras, and a Generalized Alexander Polynomial for Virtual Links, in “Diagrammatic Morphisms and Applications” (San Francisco, CA, 2000), 113–140, Contemp. Math., 318, Amer. Math. Soc., Providence, RI, 2003.
- [85] L.H. Kauffman, S. Lambropoulou, On the classification of rational tangles. *Adv. in Appl. Math.* 33 (2004), no. 2, 199–237.
- [86] L.H. Kauffman, S. Lambropoulou, On the classification of rational knots. *L’Enseign. Math.* (2) 49 (2003), no. 3-4, 357–410.
- [87] L.H. Kauffman, S. Lambropoulou, Virtual Braids, www.arxiv.org/math.GT/0407349, (to appear in Fundamenta Mathematicae).
- [88] L.H. Kauffman, M. Saito, M. Sullivan, Quantum invariants of templates. *J. Knot Theory Ramifications* 12 (2003), no. 5, 653–681.
- [89] Louis H. Kauffman, Diagrammatic Knot Theory (in preparation).
- [90] L.H. Kauffman, V.O. Manturov, Virtual biquandles (to appear in Fundamenta Mathematicae)
- [91] L.H. Kauffman and S. J. Lomonaco, Quantum entanglement and topological entanglement. *New J. Phys.* 4 (2002), 73.1 - 73.18.
- [92] R. Kirby, A calculus for framed links in S^3 , *Invent. Math.*, **45**, (1978), pp. 35-56.
- [93] R. Kirby and P. Melvin, On the 3-manifold invariants of Reshetikhin-Turaev for $\mathfrak{sl}(2, \mathbb{C})$, *Invent. Math.* 105, 473-545, 1991.
- [94] T. Kishino and S. Satoh, A note on non-classical virtual knots, (to appear in JKTR).
- [95] T. Kishino, 6 kouten ika no kasou musubime no bunrui ni tsiuti (On classification of virtual links whose crossing number is less than or equal to 6), Master Thesis, Osaka City University, 2000.
- [96] T. Kadokami, Detecting non-triviality of virtual links, (to appear).
- [97] S. Kamada, Braid presentation of virtual knots and welded knots, (preprint, March 2000).
- [98] M. Kontsevich, Graphs, homotopical algebra and low dimensional topology, (preprint 1992).

- [99] T. Kohno, Linear representations of braid groups and classical Yang-Baxter equations, *Contemporary Mathematics*, Vol. 78, Amer. Math. Soc., 1988, pp. 339-364.
- [100] G. Kuperberg, Involutory Hopf algebras and 3-manifold invariants, *Int. J. Math.*, 1991, pp. 41-66.
- [101] G. Kuperberg, Non-involutive Hopf algebras and 3-manifold invariants, *Duke Math. J.* 84 (1996), no. 1, 83–129.
- [102] Greg Kuperberg, What is a virtual link? arXiv:math.GT / 0208039 v1 5 Aug 2002, *Algebraic and Geometric Topology*, 2003, **3**, 587-591.
- [103] T.Q.T. Le, J. Murakami, T. Ohtsuki, On a universal perturbative invariant of 3-manifolds. *Topology* 37 (1998), no. 3, 539–574.
- [104] R. Lawrence, Asymptotic expansions of Witten-Reshetikhin-Turaev invariants for some simple 3-manifolds. *J. Math. Phys.*, No. 36(11), November 1995, pp. 6106-6129.
- [105] W.B.R. Lickorish, The Temperley-Lieb Algebra and 3-manifold invariants, *Journal of Knot Theory and Its Ramifications*, Vol. 2,1993, pp. 171-194.
- [106] W.B.R. Lickorish and K.C. Millett, Some evaluations of link polynomials, *Comment. Math. Helvetici* **61** (1986), 349–359.
- [107] V.O. Manturov (2004), *Knot Theory*, CRC-Press, Chapman& Hall.
- [108] V.O. Manturov (2002), Invariants of Virtual Links, *Doklady Mathematics*, **384**(1), pp. 11-13.
- [109] V.O. Manturov (2003), Curves on Surfaces, Virtual Knots, and the Jones–Kauffman Polynomial, *Doklady Mathematics*, **390**(2), pp. 155-157 .
- [110] V.O. Manturov, The Khovanov polynomial for virtual knots, *Doklady Mathematics*, to appear.
- [111] V.O. Manturov (2003), Atoms and minimal diagrams of virtual links, *Doklady Mathematics*, **391** (2), pp.136-138
- [112] V.O. Manturov,(2002), Two–variable invariant polynomial for virtual links, *Russian Math. Surveys*,**5**, pp. 141–142.
- [113] V.O. Manturov (2003), Multivariable polynomial invariants for virtual knots and links, *Journal of Knot Theory and Its Ramifications*, **12**,(8), pp. 1131-1144
- [114] V.O. Manturov (2003), Kauffman–like polynomial and curves in 2–surfaces, *Journal of Knot Theory and Its Ramifications*, **12**,(8),pp.1145-1153.

- [115] V.O. Manturov, Vassiliev Invariants for Virtual Links, Curves on Surfaces, and the Jones-Kauffman polynomial, to appear in JKTR
- [116] V.O. Manturov (2002), On Invariants of Virtual Links, *Acta Applicandae Mathematicae*, **72** (3), pp. 295–309.
- [117] V.O. Manturov, Long virtual knots and their invariants, Journal of Knot Theory and its Ramifications, to appear.
- [118] V.O. Manturov (2003)., O raspoznavanii virtual'nyh kos (On the recognition of virtual braids), POMI Scientific Seminars. Geometry and Topology.8. Saint-Petersburg, pp. 267-286.
- [119] V.O. Manturov (2003), Atoms and Minimal Diagrams of Virtual Links, *Doklady Mathematics*, **68**, (1), pp. 37-39.
- [120] V.O. Manturov, Long virtual knots and their invariants, (to appear in JKTR). .
- [121] V.O. Manturov, (in preparation).
- [122] J. Mathias, *Ph.D. Thesis*, University of Illinois at Chicago, 1996.
- [123] K. Murasugi, The Jones polynomial and classical conjectures in knot theory, *Topology* **26** (1987), 187–194.
- [124] S. Nelson, Unknotting virtual knots with Gauss diagram forbidden moves. *JKTR* 10 (2001), no. 6,931-935.
- [125] R. Penrose, Angular momentum: An approach to Combinatorial Spacetime, In *Quantum Theory and Beyond*, edited by T. Bastin, Cambridge University Press (1969).
- [126] R. Penrose, Applications of negative dimensional tensors, In *Combinatorial Mathematics and Its Applications*, edited by D. J. A. Welsh, Academic Press (1971).
- [127] Michael Polyak and Oleg Viro, Gauss diagram formulas for Vassiliev invariants, *Intl. Math. Res. Notices*, No. 11, (1994) pp. 445-453.
- [128] Mikhail Goussarov, Michael Polyak and Oleg Viro (2000), Finite type invariants of classical and virtual knots, *Topology* **39**, pp. 1045–1068.
- [129] P. Cotta-Ramusino, E.Guadagnini, M.Martellini, M.Mintchev, Quantum field theory and link invariants, (preprint 1990)
- [130] G. Ponzano and T. Regge, Semiclassical limit of Racah coefficients, In *Spectroscopic and Group Theoretical Methods in Theoretical Physics*, (1968) North Holland, Amsterdam.

- [131] K. Reidemeister, *Knotentheorie*, Chelsea Pub. Co., New York, 1948, Copyright 1932, Julius Springer, Berlin.
- [132] N.Y. Reshetikhin, Quantized universal enveloping algebras, the Yang-Baxter equation and invariants of links, I and II, *LOMI reprints E-4-87 and E-17-87*, Steklov Institute, Leningrad, USSR.
- [133] N.Y. Reshetikhin and V. Turaev, Invariants of Three-Manifolds via link polynomials and quantum groups, *Invent. Math.*, Vol.103, 1991, pp. 547-597.
- [134] L. Rozansky, Witten's invariant of 3-dimensional manifolds: loop expansion and surgery calculus, In *Knots and Applications*, edited by L. Kauffman, (1995), World Scientific Pub. Co.
- [135] S. Satoh, Virtual knot presentation of ribbon torus-knots, *JKTR*, Vol. 9 No. 4 (2000), pp. 531-542.
- [136] J. Sawollek, On Alexander-Conway polynomials for virtual knots and links, *arXiv : math.GT/9912173*, 21 Dec 1999.
- [137] J. Sawollek, An orientation-sensitive Vassiliev invariant for virtual knots, 2002, *arXiv : math.GT/0203123v3*,
- [138] L. Siebenmann and F. Bonahon, (Unpublished Manuscript)
- [139] D. S. Silver and S. G. Williams, Alexander Groups and Virtual Links, *JKTR*, vol. 10, (2001), 151-160.
- [140] L. Smolin, Link polynomials and critical points of the Chern-Simons path integrals, *Mod. Phys. Lett. A*, Vol. 4, No. 12, 1989, pp. 1091-1112.
- [141] L. Smolin, The physics of spin networks. The geometric universe (Oxford, 1996), 291–304, Oxford Univ. Press, Oxford, 1998.
- [142] T. Stanford, Finite-type invariants of knots, links and graphs, (preprint 1992).
- [143] H. Trotter, Non-invertible knots exist, *Topology*, Vol.2, 1964, pp. 275-280.
- [144] W. Menasco and M.B. Thistlethwaite, The classification of alternating links, *Ann. of Math.* **138** (1993), 113–171.
- [145] M.B. Thistlethwaite, A spanning tree expansion of the Jones polynomial, *Topology* **26** no. 3 (1987), 297–309.
- [146] M.B. Thistlethwaite, Links with trivial Jones polynomial, *JKTR*, Vol. 10, No. 4 (2001), 641-643.

- [147] S. Eliahou, L. Kauffman and M.B. Thistlethwaite, Infinite families of links with trivial Jones polynomial, *Topology*, **42**, pp. 155–169.
- [148] V.G. Turaev, The Yang-Baxter equations and invariants of links, LOMI preprint E-3-87, Steklov Institute, Leningrad, USSR., *Inventiones Math.*, Vol. 92, Fasc.3, pp. 527-553.
- [149] V.G. Turaev and O.Y. Viro, State sum invariants of 3-manifolds and quantum 6j symbols, *Topology* 31, (1992), pp. 865-902.
- [150] V.G. Turaev and H. Wenzl, Quantum invariants of 3-manifolds associated with classical simple Lie algebras, *International J. of Math.*, Vol. 4, No. 2, 1993, pp. 323-358.
- [151] V. Turaev, Virtual strings and their cobordisms, math.GT/0311185.
- [152] V. Vassiliev, Cohomology of knot spaces, In *Theory of Singularities and Its Applications*, V.I. Arnold, ed., Amer. Math. Soc., 1990, pp. 23-69.
- [153] K. Walker, On Witten's 3-Manifold Invariants, (preprint 1991).
- [154] J.H. White, Self-linking and the Gauss integral in higher dimensions. *Amer. J. Math.*, **91** (1969), pp. 693-728.
- [155] S. Winker. PhD. Thesis, University of Illinois at Chicago (1984).
- [156] Edward Witten, Quantum field Theory and the Jones Polynomial, *Commun. Math. Phys.*, vol. 121, 1989, pp. 351-399.
- [157] D. Yetter, Quantum groups and representations on monoidal categories. *Math. Proc. Camb. Phil. Soc.*, Vol. 108 (1990), pp. 197-229.
- [158] P. Zinn-Justin and J.B. Zuber, Matrix integrals and the generation and counting of virtual tangles and links, *J. Knot Theory Ramifications* 13 (2004), no. 3, 325–355.